

DISSERTATION

**USE OF REMOTE SENSING TO ESTIMATE SOIL SALINITY AND
EVAPOTRANSPIRATION IN AGRICULTURAL FIELDS**

Submitted by

Aymn Elhaddad

Department of Civil and Environmental Engineering

In partial fulfillment of the requirements

For the Degree of Doctor of Philosophy

Colorado State University

Fort Collins, Colorado


Summer 2007

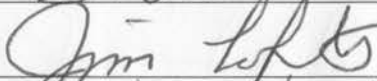
COLORADO STATE UNIVERSITY


July 10, 2007


WE HEREBY RECOMMEND THAT THE DISSERTATION
PREPARED UNDER OUR SUPERVISION BY AYMN ELHADDAD
ENTITLED USE OF REMOTE SENSING TO ESTIMATE SOIL
SALINITY AND EVAPOTRANSPIRATION IN AGRICULTURAL
FIELDS BE ACCEPTED AS FULFILLING IN PART THE
REQUIREMENTS FOR THE DEGREE OF DOCTOR OF
PHILOSOPHY.


Committee on Graduate work

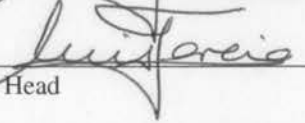










Adviser


Department Head

ABSTRACT OF DISSERTATION

USE OF REMOTE SENSING TO ESTIMATE SOIL SALINITY AND EVAPOTRANSPIRATION IN AGRICULTURAL FIELDS

In recent years, methods for detecting soil salinity have improved greatly. This research describes methods to detect soil salinity levels in agricultural lands based on crop conditions and evapotranspiration (ET) using satellite imagery.

Elevated levels of soil salinity affect the growth of most crops as well as their appearance. For this research, satellite images of the study area, the Arkansas River Basin in Colorado, are used to classify the condition of the crops being grown in fields according to their different reflectance values. Using spatially referenced ground data collected in the study area, each class in the satellite image is related to a level of soil salinity. These classes are then used to create a signature file to classify other areas within the same image having the same crop.

For the purpose of detecting soil salinity in this study, two satellite scenes were used: a multi-spectral Ikonos image from July 27, 2001 and a Landsat 7 image from July 8, 2001. While the Ikonos image provides more details, the results of this study indicate that the Landsat imagery also performed remarkably well.

Evapotranspiration (ET) is one of the processes that are affected by soil salinity. Reliable estimates of evapotranspiration from vegetation are needed for investigations of

the relationship between soil salinity and ET. Satellite-derived information has been found useful for estimation of aerial ET. For this purpose, a surface energy balance-based model (RESET) was developed using remotely sensed data from satellite imagery. The RESET model takes into consideration the spatial variability in weather. Moreover, the model implements a spatiotemporal interpolation methodology in order to obtain ET information between satellite scenes.

The RESET model was applied to estimate ET values in the study area. A geographic information system (GIS) was used to spatially relate the ET values to soil salinity data. The ET values were regressed against the spatially corresponding soil salinity values to develop a relationship between ET and soil salinity. The ET values were found to correlate well with the soil salinity levels in the study area, with correlation coefficients of up to 0.92.

Aymn Elhaddad
Department of Civil Engineering
Colorado State University
Fort Collins, CO 80523
Summer 2007

ACKNOWLEDGEMENT

All praise is due to Allah and salutations upon the Prophet Muhammad (P.B.U.H). I am grateful to Allah who has given me the wisdom, guidance and courage to have completed this research. This dissertation could not have been written without the support of My Parents that encouraged me to accomplish it. I thank my father who started me on this path. I am in debt to my mother who provided me with her unconditional support throughout all my life. I would like also to extend my thanks to Dr. Luis Garcia who not only served as my supervisor but also encouraged and challenged me throughout my academic program. He and my other committee members patiently guided me through the dissertation process, never accepting less than my best efforts. I thank them all.

July 3rd, 2007

DEDICATION

This dissertation is dedicated to my son Shehab Elhaddad who in his little voice I feel all the warmness and whom I wish all the best for.

TABLE OF CONTENTS

LIST OF TABLES	IX
LIST OF FIGURES	X
1. INTRODUCTION.....	1
1.1 GENERAL.....	1
1.1.1 Overview.....	1
1.1.2 Research Objectives.....	3
1.1.3 Defining Soil Salinity	4
1.1.4 Causes of Soil Salinity.....	6
1.1.5 Defining Irrigation Salinity.....	7
1.1.6 The Effects of Salinity	7
1.1.7 Estimating the Extent and Severity of Soil Salinity	8
1.1.8 Location and Signs of Salinization	8
1.1.9 Signs of Soil Salinity	9
1.1.10 Effects of Salinization.....	9
1.1.11 Responses	10
1.1.12 Scope of the Research.....	10
1.2 LITERATURE REVIEW	10
1.2.1 Introduction.....	10
1.2.2 Approaches for Mapping Soil Salinity	14
1.2.2.1 Methods Currently Used for Soil Salinity Mapping.....	14
1.2.3 Testing Remote-Sensing Techniques	15
1.3. REMOTE SENSING	16
1.3.1 Introduction.....	16
1.3.2 Advantages of Using Satellite Images	17
1.3.3 How Satellites Acquire Images	17
1.3.4 Interpreting Image Displays	19

1.3.5 How the Remote Sensing Information is being used.....	20
1.3.5.1 Remote sensing in agriculture.....	21
2. USING REMOTE SENSING AND GIS TO DETECT SOIL SALINITY LEVELS IN THE ARKANSAS RIVER BASIN IN COLORADO	22
2.1 ABSTRACT.....	22
2.2 INTRODUCTION	23
2.2.1 Previous work	24
2.2.2 Study area	25
2.3 METHODOLOGY	26
2.3.1 Image processing and overlaying	27
2.3.2 Methods for Calibration and Validation	29
2.3.2.1 Ikonos.....	30
2.3.2.2 Landsat 7.....	37
2.3.2.3 Using Principal Component Analysis.....	41
2.3.3 Sources of Error.....	49
2.3.4 Advantages and Disadvantages of Methods Used to Detect Soil Salinity Traditional Method.....	51
2.4 CONCLUSIONS.....	54
3. SURFACE ENERGY BALANCE-BASED MODEL FOR ESTIMATING EVAPOTRANSPIRATION TAKING INTO ACCOUNT SPATIAL VARIABILITY IN WEATHER	56
3.1 ABSTRACT.....	56
3.2 INTRODUCTION	56
3.3 MODEL DEVELOPMENT.....	59
3.4 MATERIALS AND METHODS.....	63
3.4.1 Study Areas.....	63
3.4.2 Satellite Imagery for the Lower Arkansas Study Region	63
3.5 RESET MODEL ENHANCEMENTS	64
3.5.1 Spatial Interpolation Between Weather Stations	65
3.5.2 Temporal Interpolation Between Scenes	65
3.6 DATA PREPARATION.....	66
3.7 GIS MODEL INTERFACE.....	67

3.8 APPLICATION OF THE RESET MODEL	70
3.9 EVALUATING THE IMPACT OF REDUCING THE NUMBER OF WEATHER STATIONS	78
3.10 CONCLUSIONS.....	80
4. A REMOTE SENSING - GIS APPROACH TO EVALUATE THE EFFECTS OF SOIL SALINITY ON EVAPOTRANSPIRATION.....	81
4.1 ABSTRACT.....	81
4.2 INTRODUCTION	81
4.3 METHODOLOGY	84
4.3.1 Selecting Fields to Study	84
4.3.2 Estimating Evapotranspiration.....	85
4.3.2.1 Energy Balance and Microclimatological Methods.....	86
4.3.3 Soil Salinity Data.....	87
4.3.4 Combining the ET Surface and Soil Salinity Points.....	88
4.4 RESULTS AND DISCUSSION.....	88
4.5 CONCLUSIONS.....	96
5. SUMMARY AND CONCLUSIONS	98
5.1 SUMMARY OF WORK.....	98
5.2 UNIQUE CONTRIBUTIONS	99
6. RECOMENDATIONS FOR FURTHER WORK	102
6.1 DETECTING SOIL SALINITY.....	102
6.2 RESET MODEL.....	102
6.3 SOIL SALINITY AND ET.....	103
7. REFERENCES.....	104

LIST OF TABLES

Table 1. The sixteen reflectance/salinity classes obtained from the calibrated field.....	32
Table 2. Cross validation of the classes in the calibration field.....	33
Table 3. Predicted soil salinity values versus the measured values for the validation in field RR*.....	36
Table 4. Soil salinity classes extracted from Landsat 7.....	40
Table 5. Soil salinity classes (dS/m) extracted from field 80 using the PCA image.....	43
Table 6. Extent of soil salinity in field 23.....	45
Table 7. Extent of soil salinity in field 6.....	47
Table 8. Extent of soil salinity in field 77.....	48

LIST OF FIGURES

Figure 1. Map of the study area.	26
Figure 2. Relationship between actual soil salinity values and EM-38 readings..	30
Figure 3. Calibration field.....	30
Figure 4. Expected yield loss in corn due to soil salinity in relation to the sixteen classes in the calibration field.....	33
Figure 6. Soil salinity points in the RR field (validation field)	35
Figure 7. Measured soil salinity values versus predicted values in the validation field (RR).	35
Figure 8. Predicted (a) and measured (b) salinity levels using the Ikonos image.	37
Figure 9. Spectral profile for field 80	38
Figure 10 (a) Original versus (b) PCA Landsat scenes.....	42
Figure 11. Soil salinity classes and the corresponding salinity levels extracted from the original (a) and PCA (b) scenes.....	44
Figure 12. Soil salinity levels in field 23	45
Figure 13. Spread of two levels of salinity in field 23.....	46
Figure 14. Soil salinity levels in field 6.	46
Figure 15. Spread of two levels of soil salinity in field 6.....	47
Figure 16. Soil salinity levels in field 77	48
Figure 17. Spread of two levels of soil salinity in field 77	49
Figure 18. Soil salinity points falling in between classes	51
Figure 19. The lower Arkansas River Basin study region in Colorado	63
Figure 20. Estimated ET for a portion of the lower Arkansas River Basin in Colorado.....	66

Figure 21. The satellite imagery for the study area on 6/22/2001.	71
Figure 22. Colorado's Arkansas River Valley ET Grid Using a Single Weather Station on 6/22/2001.	71
Figure 23. Colorado's Arkansas River Valley ET Grid Using Multiple Weather Stations on (6/22/2001).	72
Figure 24. Spatial distribution of the wind in the study area on 6/22/2001.	72
Figure 25. The difference in daily ReSET ET ($ET_{mws} - ET_{sws}$) for the whole study area and a zoomed area.	73
Figure 26. ET estimated at the CoAgMet CSU Rocky Ford weather station.	75
Figure 27. Cumulative ET calculated using ReSET and calculated using simple averaging.	76
Figure 28. Difference in cumulative ET between ReSET and average.	77
Figure 29. Variability in ETr at the Brush weather station over the interpolation period.	78
Figure 30. Cumulative ET using 6 and 3 weather stations.	79
Figure 31. Difference in Accumulative ET when using 6 weather stations versus 3 weather stations.	79
Figure 33. Plan view of field 80 from two different satellite scenes.	90
Figure 34. Soil salinity levels versus ET values in field 80 (zones to points).	91
Figure 35. Soil salinity levels versus ET values in field 80 (pixel to point).	92
Figure 36. Plan view and soil salinity distribution in field RR.	93
Figure 37. Soil salinity levels versus ET values for field RR.	93
Figure 38. Soil salinity versus ET for field 40.	94
Figure 39. Plan view and soil salinity distribution in field 23.	95
Figure 40. Soil salinity versus ET for field 23.	95
Figure 41. Soil salinity versus ET for individual grids as well as for whole fields.	96

1. INTRODUCTION

1.1 GENERAL

1.1.1 Overview

About 30 percent of the land in the western United States has a moderate to severe potential for salinity problems (Nation Research Council, 1996). Where salinity problems occur, the productivity and sustainability of agricultural communities are diminished (Western Water Policy Review Commission, 1997). This problem is not limited to the US. The threat to global crop production is serious (Postel, 1999) and losses, when measured in economic terms, can be very significant. Ghassemi et al. (1995) estimated that worldwide productivity loss was valued at about \$10 billion per year. In the Arkansas Valley in Colorado alone it is estimated that over 40,500 ha (100,000 acres) are irrigated with water having salinity concentrations greater than 1,500 mg/L (Gates et al. 2006). This value represents the second highest classification for salinity hazard according to the US Salinity Laboratory. Soil salinity is a main component in salinity problems related to agricultural production.

Mapping soil salinity is the first step in dealing with this problem. Saline soils may be delineated by taking soil samples to a lab for analysis or by using Electro Magnetic (EM) devices to estimate salinity in the field. Both techniques can generate estimates of soil salinity, but they are time consuming, especially when covering large areas and the results are for sample locations rather than areal values.

Satellite imagery can be used to evaluate the areal extent and severity of soil salinity and its impact on yield. Since soil salinity has a direct impact on the crop condition, the biomass of the crop can be classified and used to quantify the impact of soil salinity. Soil salinity can also be indirectly estimated from crop evapotranspiration (ET). The presence of salts in the soil affects the crop ET. Therefore, ET estimates derived from satellite imagery can be used to develop relationships between soil salinity and ET.

Satellite-derived information for estimating soil salinity and ET has been a focus of ongoing research. A number of studies have used information derived from satellite imagery to estimate soil salinity in bare soils (Taylor and Dehaan, 2000; Ben-Dor, 2002; Dehaan and Taylor, 2003). Recently, a number of studies have used an energy balance approach derived from satellite imagery by calculating the difference between the net radiation inflow and the net energy outflow to estimate ET (Bastiaanssen et al., 1998; Hafeez et al., 2002; and Savige et al., 2005).

1.1.2 Research Objectives

Satellite imagery can provide useful information for monitoring the spatial distribution and magnitude of soil salinity in agricultural fields. However, there has been very little research conducted in this area. Consequently, the main purpose of this research is to investigate the effectiveness of using satellite-derived information to monitor and evaluate the areal extent and severity of regional soil salinity and its impact on yield. The specific objectives are:

- 1) To develop a methodology that uses information about crop condition derived from satellite imagery to quantify soil salinity in agricultural fields.

- 2) To conduct a ground-based experiment for establishing the feasibility of quantifying the relationship between soil salinity and satellite-derived information.
- 3) To develop a model to estimate ET using information derived from satellite imagery based on an energy balance between the net radiation inflow and the net energy outflow. The energy balance model will provide a valuable tool to evaluate actual evapotranspiration in field conditions using minimum ground data, the model will be a valuable tool for irrigation management by identifying areas with low evapotranspiration the might be caused by low irrigation efficiency or lack of irrigation water (quantity and quality), the model can also be used to develop or verify water budgets and pumping records.
- 4) To develop a relationship between soil salinity levels and ET values under actual field conditions, this relationship will quantify the decrease in evapotranspiration due to the existence of different soil salinity levels, this will have two benefits:
 1. Ability to map and quantify areas of high soil salinity in order to start dealing with the salinity problems either by leaching or modifying the irrigation practices used in the identified areas or planting different crop types which have a higher tolerance to soil salinity,
 2. Monitor the impact of any remediation being done to salt affected areas to evaluate the success of any remediation activities.

1.1.3 Defining Soil Salinity

Soil salinity is a term that refers to a condition of the soil in which water-soluble salts are present. Properties and characteristics of saline soils are determined by

chemistry and concentration of soluble salts. Generally increases in soil salinity will occur after introducing irrigated agriculture, excessive irrigation slowly start to cause the water table to rise to the level that up flux starts to draw moisture towards the upper layer of soil surface. From this moisture, water will either evaporate and salts in that water will accumulate close to the soil surface, or plants will use water then salts accumulate in the root zone. Another source of salts can be the soil parent material or deeper geologic deposits; however, they have to start accumulating near the soil surface before high soil salinity becomes an obvious problem.

Another cause of soil salinity problems is groundwater movement through the soil from higher elevation recharge areas to lower elevation discharge areas. When water infiltrates the soil toward lower lying areas, existing salts are dissolved and carried by the groundwater. The distance between the recharge zone (infiltration of water) and the discharge zone can vary greatly from many kilometers to only a few meters. High water table can also be a source of high soil salinity spatially in fine textured soils.

There is no quick or easy remedy to decreasing soil salinity. Early detection of salt-affected areas is critical so as to allow as much time as possible to implement remediation strategies, and if possible, stop and reverse the accumulation of soil salinity. A field assessment of the severity of soil salinity, using soil sampling and analysis techniques, generally produces accurate results, but it is a time consuming and slow process if the targeted area is large. Alternatively, soil salinity maps obtained from remotely sensed data, such as satellite scenes or sensors mounted on airplanes, can provide a much faster and economical way for mapping soil salinity for large areas.

Howari (2003) concluded that remote sensing has a potential application for rapid and large scale mapping of salt affected lands.

1.1.4 Causes of Soil Salinity

Other land management practices other than irrigation and clearing for agriculture may also contribute to elevated watertables and saline seepage in many areas. Such practices include over watering of lawns and gardens, deforestation as a result of urban development, irrigation applied to public recreation areas, septic and sewage systems that are poorly designed, and the development of roads, bridges, railway and flood control banks, all this interfere with the natural surface drainage patterns and cause ponding of surface water (EPA, 1995).

Recently, Dehaan and Taylor (2002) stated that soil salinization is caused by a number of factors, the most significant of which is the rise of saline groundwater to where it approaches the ground surface.

Land salinity is closely related to other land degradation processes such as soil erosion, acidification and structural decline. Grossly salt-affected land, where vegetation has been reduced or lost, is more prone to erosion. Erosion of topsoil can also hasten the expression of land salinity by exposing saline under-soil. Preventive and remedial measures are much more difficult when land is affected by more than one form of land degradation (EPA, 1995). These linkages highlight the need for integrated catchment management so that all land users and the wider community participates in developing and implementing appropriate management practices to mitigate the underlying processes.

1.1.5 Defining Irrigation Salinity

The areas affected by irrigation salinity can be determined by two criteria:

- Areas where the ground water elevation is within a couple of meters from the land surface.
- Areas where soil salt levels, measured as electrical conductivity, exceed 2 dS/m. However, if gypsum (Calcium Sulfate) is present this number might be as high as 4 dS/m.

Detrimental effects on plant growth and crop yield have been noted when electrical conductivity levels in the top 30 cm or so of the soil exceed 2 dS/m (Calm, 1993). When the watertable rises to a critical depth -- around a couple of meters below the land surface -- evaporation and capillarity at the surface can result in the upward movement of water, carrying dissolved salts into the plant root zone where they accumulate and damage vegetation.

1.1.6 The Effects of Salinity

The negative impacts of salinity on soil properties and plant growth include:

- Ion toxicity, which can occur at certain thresholds;
- Osmotic effects hinders the water uptake for the crops and cause drought-like symptoms in them as they are unable to extract water from the soil;
- In instances when high ground water table is present and accompanies soil salinity it contributes to decreasing oxygen needed by the plant which cases additional plant stress;
- Denitrification in saline soils leads to low nitrogen levels and cases of nutrient deficiency;

- All the previous impacts will result in poor plant growth which reduces the ground cover and exposes the ground surface increasing the likelihood of soil erosion, which further reduces nutrient levels, such as phosphate levels and decreases soil organic matter which leads to reduced cation exchange capacity;
- Soil stability is reduced.

1.1.7 Estimating the Extent and Severity of Soil Salinity

Saline soils are present in many areas of the world. Moderate to severe salinity, which is more or less visible in the landscape, reduces the annual yields of most crops. Yield reduction varies depending on the salt tolerance of the individual crops. Researchers have tried over the years to record the type, extent, severity, and rate of change of soil salinity. These assessments differed in approach and have produced varying estimates of lands having high soil salinity levels (Eilers, 1991). In this study, a new methodology to map soil salinity is presented. This methodology is applied to determine the extent and severity of soil salinity in parts of the lower Arkansas River Basin in Colorado.

1.1.8 Location and Signs of Salinization

Salinization occurs where the following conditions occur simultaneously:

- Soluble salts are present of in the soil.
- Groundwater table is high.
- A combination of a high rate of evaporation with low precipitation amounts occurs (water evaporates from the soil surface rapidly depositing salted in the soil and leaching due to rainfall is limited).

1.1.9 Signs of Soil Salinity

Saline soils can be identified before they become seriously affected. The early signs of soil salinity include:

- Increased soil water content, to the point that the area becomes inaccessible.
- Salt-tolerant weeds, such as kochia, *Kochia scoparia*, and Schrad, *Eragrostis curvula*, starts to grow among the crop.

With the increase in soil salinity levels, signs become more obvious. They include:

- Fields show irregular crop growth patterns and lack of plant vigor.
- A white surface crusting starts to be spotted in the affected area.
- Broken-ring pattern of salts is detected adjacent to a water body.
- White spots and streaks in the soil are noticed, with or without surface crusting.
- Existence of naturally growing, salt-tolerant vegetation, such as red samphire.

1.1.10 Effects of Salinization

High levels of salt in the soil have a similar effect as drought since it makes water less available for uptake by plant roots (increases the osmotic potential). This effect is caused by the difference in salt concentrations between the plant and the soil: the *osmotic gradient* created between the soil and plant interferes with the process by which water is absorbed by the roots and, if the soil salinity is high enough, it can cause water to be drawn out of the roots. Depending on the degree of salinity, this effect reduces the soil's ability to produce crops and lowers annual crop yields. Because few plants grow well on saline soils, the farmer's cropping options start to be limited by the increasing levels of soil salinity.

1.1.11 Responses

Salinization is a long-term problem and is difficult to reverse. Management strategies require a whole-catchment approach (EPA, 1995). Consequently, salinity mapping and evaluation techniques that cover large areas or whole catchments would be of great benefit to large scale efforts to deal with the soil salinization problem.

1.1.12 Scope of the Research

The scope of this research is to develop a new methodology based on remotely sensed data (satellite imagery) to detect and quantify soil salinity in irrigated lands, and to develop a surface energy balance model (ReSET) that evaluates evapotranspiration using satellite imagery. Soil salinity will be evaluated through a direct approach, using crop reflectance, and an indirect approach, using evapotranspiration (ET), as indicators of the presence and the severity of soil salinization.

1.2 LITERATURE REVIEW

1.2.1 Introduction

It is estimated that half to two-thirds of the increase in food production needed in the future will have to come from irrigated lands, which are currently contributing about 40 percent of the world's food requirement (Serageldin, 1995). The global irrigation scenario, however, is characterized by poor performance, increased demand for higher agricultural productivity, decreased availability of water for agriculture, and increased soil salinity. In addition, the possible effects of global climate change and the changing role of the public-sector may negatively impact food production on irrigated lands.

Clearly, soil salinity is a serious problem that affects agriculture and causes substantial crop loss. Soil salinity is detrimental to the growth of vegetation in general (Csillag et al., 1993), and is considered to be a major cause of reduced crop production in many areas. Globally, it was estimated that 955 million ha of land were affected by salinity and sodicity (Szabolcs, 1992). Saline soils affect the physiological characteristics of the plants and the spectral reflectance of crops (Krimes and Kirchner, 1983). When the concentration of water-soluble salts in the root zone of plants reduces their growth, the soils are termed saline or salt-affected (Richards, 1954). Dissolved salts create an osmotic stress that adds to any existing matric stress (Thomas and Wiegand, 1970), which can stunt plant growth. When salt concentrations exceed the tolerance of seeds for germination, the land is barren. The salts also sometimes contain trace elements and ions, such as boron and chloride, in concentrations that are themselves toxic to plants (Wiegand, 1990). Soil salinity in agricultural areas has reached a level of great concern after a very brief period of human intervention, through irrigation (Abuzar et al., 2001).

In order to optimize the utilization of these salt-affected lands for sustainable agriculture, information on the nature, extent, magnitude, spatial distribution, and temporal behavior of salinity is of paramount importance. Improved irrigation management and informed decision making calls for the adoption of new tools such as satellite remote sensing and geographic information systems to provide the necessary spatial and temporal information on different subsystems and for different user groups (Thiruvengadachari, 1996). Until recently, such information has been generated through traditional soil surveys using topographical sheets and cadastral maps. This process is tedious, time-consuming, and can be cost-prohibitive (Dwivedi and Sreenivas, 1997).

Although remote sensing was identified as a tool for assessing salinity in the late 1980's (Abernethy and Pearce, 1987), it has been applied infrequently.

In order to take corrective and protective measures, it is essential to have accurate information about saline-prone areas in the form of maps. Common surveys cannot be depended upon for mapping soil salinity because farmer-based surveys are likely to underestimate the problem. For instance, Ferdowsian and Grenham (1992) estimated that more than 12% of the Upper Denmark catchment was salt-affected, while farmers in the area estimated that no salinity was present (Joshi, 1992). Detection and mapping of saline soils are the first steps in ameliorating the problem (Ghabour and Daels, 1993).

Evans and Caccetta (1995) presented a report showing maps of areas historically and presently affected by salinity and maps showing areas at risk in the future. These types of maps may be produced using remotely sensed data integrated with several computer derived terrain attributes. These terrain attributes can be easily derived from digital elevation data.

Using conventional ground methods, mapping of large areas is difficult, time consuming, expensive, laborious, and affected by weather (Rao et al., 1998). Until recently salinity information had been obtained from traditional soil surveys. Traditionally, the distribution of saline soils was mapped by combining aerial photos with field surveys (Mongkolsawat and Thirangoon, 1991). Early applications focused on mapping irrigated croplands (Huston and Titus, 1975; Draeger, 1976; Wall, 1979; and Thiruvengadachari, 1981).

In recent years, methods for studying soil salinization have improved greatly. Techniques have evolved from using geographical analysis alone to using remote sensing

analysis and visual interpretation of satellite scenes combined with computer processing of satellite scenes. Moreover single-source satellite scenes have been combined with remote sensing data and with non-remote sensing data. In particular, it is becoming increasingly popular to combine a remote sensing method with geographic information systems to solve complex problems (Peng, 1998). Hence, as part of this research, an attempt has been made to use remote sensing techniques for the purpose of preparing maps for fields around the study area in the lower Arkansas River Basin in Colorado. Steven (1993) discussed the logistic requirements of remote-sensing applications for agricultural management. Peng (1998) concluded that the analysis of soil salinity using multi-source data combining remote sensing and non-remote sensing is sufficiently scientific and accurate in terms of the theory of genesis of soil. Myers et al. (1966) noted that aerial photography was the first remote sensing technique used to study salt-affected soil and vegetation. Availability of aerial photographs in the early-1960s improved the pace of mapping soils and categorizing salt-affected soils (Karale and Venugopal, 1970; and Nagar and Singh, 1979) and ushered in a new era in inventorying natural resources and monitoring environmental hazards. Remote sensing has repeatedly been used as a promising tool to obtain information regarding soil properties and land degradation processes (De Jong, 1994; Dehaan and Taylor, 2002; and Van der Meer et al., 1999).

Ghabour and Daels (1993) concluded that detection of soil degradation by means of conventional soil survey requires a great deal of time. However, remote sensing data and techniques offer the possibility for more quickly mapping and monitoring soil salinity.

1.2.2 Approaches for Mapping Soil Salinity

1.2.2.1 Methods Currently Used for Soil Salinity Mapping

a) Sample Collection

Soil paste EC has been used to assess soil salinity (Rhoades et al., 1989) by collecting samples from the field and analyzing them in the laboratory using suitable equipment such as the Salinity Appraisal Laboratory for Soil and Irrigation Water (SIW) Kit. This kit works by determining the electrical conductivity of a soil 'saturation extract' (a solution obtained by saturating a soil sample with water). The electrical conductivity increases with salinity because of the greater presence of ions (usually sodium and chlorine ions). Electrical conductivity is often expressed in units such as deciSeimens per meter (dS/m). Rainwater, for example, has a conductivity of 0.02-0.05 dS/m, while seawater has a conductivity of 50-60 dS/m. Ground water becomes saline at about 6-8 dS/m. The sample collection and processing is time consuming,

b) Electrical Conductivity

Soil salinity can be measured by using an electromagnetic device (EM-38) that measures electrical conductivity. When a voltage is applied across a substance an electric current will flow if the substance conducts electricity. When salts dissolve in water, ions are formed, and the solution will conduct electricity. As a general rule, the higher the concentration of ions in solution, the better the solution conducts electricity. Temporal variability and measurement error can affect EC stability, but the collection of a large amount of data can override these problems (P.C. Robert et al. ed., 2000). EC readings can be combined with information from a GPS receiver, and geo-referenced maps can be generated since coordinates for each soil salinity measurement are collected. Although

this method is more convenient than taking soil samples back to the laboratory for analysis, it is still time consuming since measurements need to be taken on a grid covering the study area. It usually takes 3 to 4 hours for 2 people to collect the geo-referenced EM-38 data for 60 to 80 points. The EM-38 method has been used as part of this research to collect soil salinity data for fields that were used for calibration and validation of the proposed methodology.

1.2.3 Testing Remote-Sensing Techniques

Scientists may peer at satellite scenes or process them using high-powered computers, but the only way to assess their accuracy is to go out into the field and measure the soil salinity at ground level. A recent study by scientists at CSIRO Mathematical and Information Sciences tested a remote sensing technique in three study areas in Western Australia. They analyzed a series of Landsat scenes, which they combined with information on contours, the location of roads and farm boundaries, and farm management histories. They then compared the results of these analyses with the locations of known salt-affected and changing sites, as supplied by farmers, field officers from Agriculture Western Australia and from previous salinity mapping exercises. Results were very encouraging. At one study site, salt-affected land was mapped remotely at an accuracy of almost 100 percent. However, accuracy was lower at other sites.

1.3. REMOTE SENSING

1.3.1 Introduction

Remote sensing is one of a suite of tools now available to scientists that can provide up-to-date, detailed and recurrent information about land conditions. Remote sensing techniques have been found to be useful tools in diagnosing and predicting salt-related crop productivity problems (Rahman et al., 1994). Remote sensing techniques are widely used as a rapid method for delineating soil boundaries and characterizing soil units (Ghabour and Daels, 1993). Remote sensing uses instruments mounted on satellites or in airplanes to produce scenes of the earth's surface. Remote sensing and geographic information systems (GIS) are suitable techniques for environmental monitoring and data processing (Yamamoto, 2000). Remotely sensed scenes can be used in many applications, for example for mineral exploration, monitoring ocean currents, land use planning and monitoring the condition of forests and agricultural areas. The use of advanced technology such as satellite remote sensing, geographic information systems (GIS), and hydrologic modeling can greatly help improve irrigation management (Thiruvengadachari, 1996).

Satellite remote sensing has the ability to show large land areas and to detect specific features. Satellite and aerial imagery has been used by many researchers to detect salt-affected soils (Abdel-hamid 1992; Peng 1998; and Myers et al., 1966). Data from satellite scenes can show larger areas than aerial survey data, and since a satellite regularly passes over the same plot of land capturing new data each time, changes in the land use and condition can be monitored. The uniqueness of satellite remote sensing lies

in its ability to show large land areas and to detect features at electromagnetic wavelengths, which are not visible to the human eye.

In the Arkansas River Basin project, satellite scenes are being used to provide information on crop condition, specifically related to salinity, and the status of the crops. This information is intended to help farmers, environmental managers and planners better manage the land. For the last four years data has been collected for three geo-referenced soil salinity data sets per year for several fields in the lower Arkansas River basin in Colorado. One of the outcomes of the Arkansas River Basin project is an estimate of soil salinity in the selected fields. To validate the estimate, satellite scenes are combined with ground data.

1.3.2 Advantages of Using Satellite Images

The main advantages of using satellite scenes for monitoring and evaluation of large areas and features that change over time are that satellite scenes:

- show large areas of land in a single scene,
- detect features at wavelengths not visible to the human eye,
- are regularly and routinely acquired and archived, and
- can be very cost-effective for monitoring change over large areas.

1.3.3 How Satellites Acquire Images

Satellite sensors measure the intensity of electromagnetic radiation reflected from the earth at several wavelengths. A portion of the energy emitted from the sun is reflected by objects, the rest is absorbed. The amount of energy reflected depends on the object's emissivity. Remote sensing uses the different reflectance of earth objects to create a

signature that relates each spectrum of reflectance to a group of ground objects. For example Grass looks green, because it reflects green light and absorbs other visible wavelengths. The infrared portion of the spectrum shows that grass reflects even more strongly. Such thing can't be detected by the human eye.

Scanners mounted on satellites detect and measure the energy that has been reflected. The sensors of the satellite acquire energy in defined ranges of wavelengths, called 'bands'. The intensity of the reflected energy is measured and recorded as a number between 0 and 255.

Satellite systems differs based on three features, first the number and range of bands at which they measure the reflected energy. The Ikonos satellite, which provided some of the data that was used for this research, has bands in the blue, green and red wavelengths in the visible part of the spectrum and one band in the near infrared part of the spectrum.

The second feature that characterizes each satellite system is its footprint or pixel size. Which is the smallest area on the ground for which it can record the reflected energy. For every 4m by 4m plot of land, the Ikonos scanner records a number for each of the four bands, which is the average intensity of the reflected energy for the features in that plot of land.

The third feature that characterizes a satellite system is the time it takes to revisits a particular location. The Landsat 5 and 7 satellites revisit the same location every 16 days. Theoretically, a site can be viewed every 16 days to detect changes in land use or condition. But not all these scenes are unusable because the satellite sensors cannot see

through clouds. For the Arkansas River Basin project, one Ikonos image was purchased for two growing seasons and multiple Landsat scenes were purchased as well.

1.3.4 Interpreting Image Displays

The satellite scenes, as recorded by either Ikonos or Landsat, consist of numbers, which are the measurements of the amount of energy that has been reflected from the different objects on the earth's surface, these reflectances are displayed in different wavelength bands. Some of these bands, such as the infrared bands contain higher volume of information regarding vegetation growth and crop condition; the infrared portion can not be seen with the human eye. Therefore, those scenes can be displayed either using true colors or using false colors, on a computer screen these scenes if displayed in true color they would look like aerial imagery since they indicate the true colors of objects such as green trees and grass and brown soil. False-color imagery is formed by assigning mixtures of the visible and infrared bands to the red, green and blue colors on the computer screen. In these scenes different intensities in the wavelength bands shows up as different colors on the computer screen. Studies have shown that the human eye distinguishes changes in the red color better than in blue or green (American Society of Photogrammetry, 1983). Therefore, the band mostly strongly related to the feature of interest should be assigned to the red color on the screen.

Satellite records intensities between 0 and 255, but usually the actual intensities associated with our interest of the ground covers occupy a much smaller portion of values. This small portion can be stretched over the whole range, this is called 'image enhancement'.

Several image enhancements can be used to emphasize different details in an image. For example to show information over the whole image we assign the minimum image intensity to color level 0 and the maximum image intensity to color level 255. This distribution maximizes the number of colors on the computer screen that displays the image and shows information over the whole image. If the user only has interest in certain features in the image, such as vegetation, then the intensities of the corresponding vegetations is to be assigned to the 256 color levels, by this technique we highlight all the details in the vegetated areas in the image, but in the same time not showing the rest of the features of the image.

1.3.5 How the Remote Sensing Information is being used

The information obtained from remotely sensed scenes is used in a number of ways depending on the purposes to which it is being put. The information is usually combined with information from other data sources and with on-the-ground observations, called 'ground truth,' to get a more complete picture of what is happening.

Remotely sensed scenes have been used to monitor changes in land condition as well as changes in productivity. This is done by monitoring several factors that affect the land condition such as wind erosion and waterlogging, other usages for remotely sensed data are crop yield mapping and monitoring (El Kady and Mack, 1994) as well as monitoring rangeland conditions. Remote sensing is also increasingly being used for large-scale environmental monitoring because it is able to offer large-scale monitoring in a very cost-effective way and fairly easily, and can provide a baseline for future monitoring.

One of the uses of remote sensing is the satellite derived estimates of crop evapotranspiration (ET) which have become increasingly popular. ET is the most crucial information in water balance studies. A large body of literature is available on potential, reference, and actual ET and their modeling methods (FAO-24, 1977; Doorenbos et al., 1977; ASCE-Manual-70, 1990; and FAO-56, 1998). The energy-balance equation can be expressed as:

$$R_n = ET + H + G \quad (1.1)$$

Where R_n = the net radiant energy exchange at the earth surface, called net radiation; ET = the evapotranspiration expressed as latent heat flux density; H = the net surface-atmosphere flux of sensible heat; G = the soil heat flux density. At the present time, information about these energy-balance parameters is provided for the different satellites. A number of studies have applied the energy-balance equation using satellite imagery for the estimation of ET (Vidal and Perrier, 1989; Bastiaanssen et al., 1998; Hafeez et al., 2002; and Savige et al., 2005).

1.3.5.1 Remote sensing in agriculture

In the next chapters several applications of remote sensing and GIS in agriculture will be introduced. The second chapter illustrates a methodology for mapping soil salinity in agricultural fields using different types of satellite imagery integrated with ground data. Chapter three discusses the enhancement of a model based on the surface energy balance equation for calculating evapotranspiration. Chapter four assesses the relation between evapotranspiration and soil salinity and Chapter five provides conclusions and area for future research.

2. USING REMOTE SENSING AND GIS TO DETECT SOIL SALINITY LEVELS IN THE ARKANSAS RIVER BASIN IN COLORADO

2.1 ABSTRACT

In recent years, methods for detecting soil salinity have improved greatly. This chapter describes a methodology to detect soil salinity levels in agricultural lands based on crop reflectance using satellite imagery. Elevated levels of soil salinity affect the growth of most crops as well as their appearance. In the methodology described in this chapter, we classify the image and separate the crop condition into several classes. Then using spatially referenced ground data collected at a study area in the lower Arkansas Valley in Colorado, each class in the satellite image is related to a level of soil salinity. These classes are used to create a signature file to classify (supervised classification) other areas within the same scene having the same crop. For this study we used two satellite scenes. The first scene is a multi-spectral image from Ikonos (2001) which is composed of four bands (red, green, blue and near infrared) with 4 m spatial resolution. The second scene is a Landsat 7 (2001) image which is composed of eight bands with 30 m spatial resolution. The methodology is applied to several agricultural fields in the lower Arkansas River Basin in Colorado. While the Ikonos scene provides more spatial resolution, it was found that the Landsat scene performed remarkably well.

2.2 INTRODUCTION

Soil salinity is a problem that affects agriculture and reduces crop yields. Mapping soil salinity is the first step in identifying the magnitude of the problem. In recent years, methods for studying soil salinization have improved greatly. Techniques have evolved from using geographical analysis alone to using remote sensing analysis and visual interpretation of satellite scenes combined with computer processing of satellite scenes. Remote sensing has been used as a promising and convenient tool for extracting information regarding soil properties and land degradation processes (De Jong, 1994; Dehaan and Taylor, 2002; and Van der Meer et al., 1999). Moreover, it is becoming increasingly popular to combine a remote sensing method with geographic information systems to solve complex problems (Peng, 1998). This research attempts to use remote sensing techniques for the purpose of preparing a map of the extent and magnitude of salt-affected lands. The methodology is applied to a study area around La Junta, in the Arkansas Valley in Colorado. Although remote sensing techniques have been used to diagnose general salinity problems (Everitt et al., 1977; and Ripple et al., 1986), only limited attempts have been made to evaluate their effectiveness in identifying soils where the primary inhibitor of plant growth is nutrient deficiency induced by either alkalinity or salinity (Weigand et al., 1993). Ghabour and Daels (1993) concluded that detection of soil degradation by means of a conventional soil survey requires a great deal of time, but remote sensing data and techniques offer the possibility for mapping and monitoring these processes faster and more economically. However, to assess the accuracy of the ability of satellite scenes to map and monitor salinity, it is necessary to compare them with field measurements of salinity. Elevated levels of soil salinity affect

the growth of most crops as well as their appearance. The main objective of this study is to develop a methodology to detect soil salinity levels in agricultural lands based on crop appearance using satellite imagery.

2.2.1 Previous work

Remote sensing has been used for identifying and mapping saline areas in several countries, including Australia, Bolivia, China, Egypt, India, Iran, and USA. Works by Csillag et al. (1993), Epema (1990), Evans and Caccetta (2000), Everitt et al. (1988), Kalra and Joshi (1996), Metternicht (1996), Metternicht and Zinck (1996), Mougenot et al. (1993), eldiery (2006), Mulders (1987), Rao et al. (1995), Srivastava, Tripathi, and Gokhale (1997), and Verma, Saxena, Barthwal, and Deskmukh (1994) show illustrative application examples. These studies have been successful in discriminating between two surface types, namely, saline and nonsaline (Evans & Caccetta, 2000).

Previous attempts at mapping soil salinity showed the potentialities of hyperspectral imagery in salinity studies (Taylor and Dehaan, 2000; Ben-Dor, 2002; and Dehaan and Taylor, 2003). Several previous studies have focused on mapping soil salinity for bare soil. These studies used a method which identifies diagnostic absorption bands in the spectrum of evaporate minerals and salt crust either in the field or in the laboratory (e.g., Hunt et al., 1971, 1972; Hunt and Salisbury, 1971; Gaffey, 1987; Crowley, 1991a,b; Dark, 1995; and Howari et al., 2002). The information obtained was then used to produce a relationship between the spectral properties of salt-affected soils and the presence of high salinity levels in the soil (Farifteh et al., 2004). These studies were successful in detecting soil organic matter, soil moisture and salt-affected areas with different degrees of severity. However, there are drawbacks to mapping the soil salinity

from bare soil. For instance, Metternicht and Zinck, (2003) report that lack of specific absorption bands of some salt types, such as halite (NaCl), affect the mapping accuracy. Another problem is that the actual mapping is only done for the top soil layer, even though a much deeper soil profile affects plants and therefore should be evaluated. This shows the necessity of using other data and techniques, in combination with remote sensing, to map soil salinity (Farifteh et al., 2005).

Most of the published investigations based on remote sensing distinguish only three to four classes of soil salinity (Abd-Elwahed, 2005). In this study, the target is to produce a detailed soil salinity map that can detect between 9 and 16 levels of soil salinity. Farifteh et al. (2005) concluded that most of the remote sensing studies have concentrated on detecting severely saline soils and not paid enough attention to slightly affected areas, giving an incomplete map for the targeted area.

2.2.2 Study area

The methodology developed to detect soil salinity was applied to several corn fields in the lower Arkansas River Basin in Colorado. This region of the Arkansas River Basin is a highly agricultural area. The segment of the river covered by the study area (33 kilometers) spans from approximately the town of Manzanola on the west to the town of La Junta on the east. Although this region has salinity problems, a variety of crops are still grown there, including corn, alfalfa, melons, and onions.

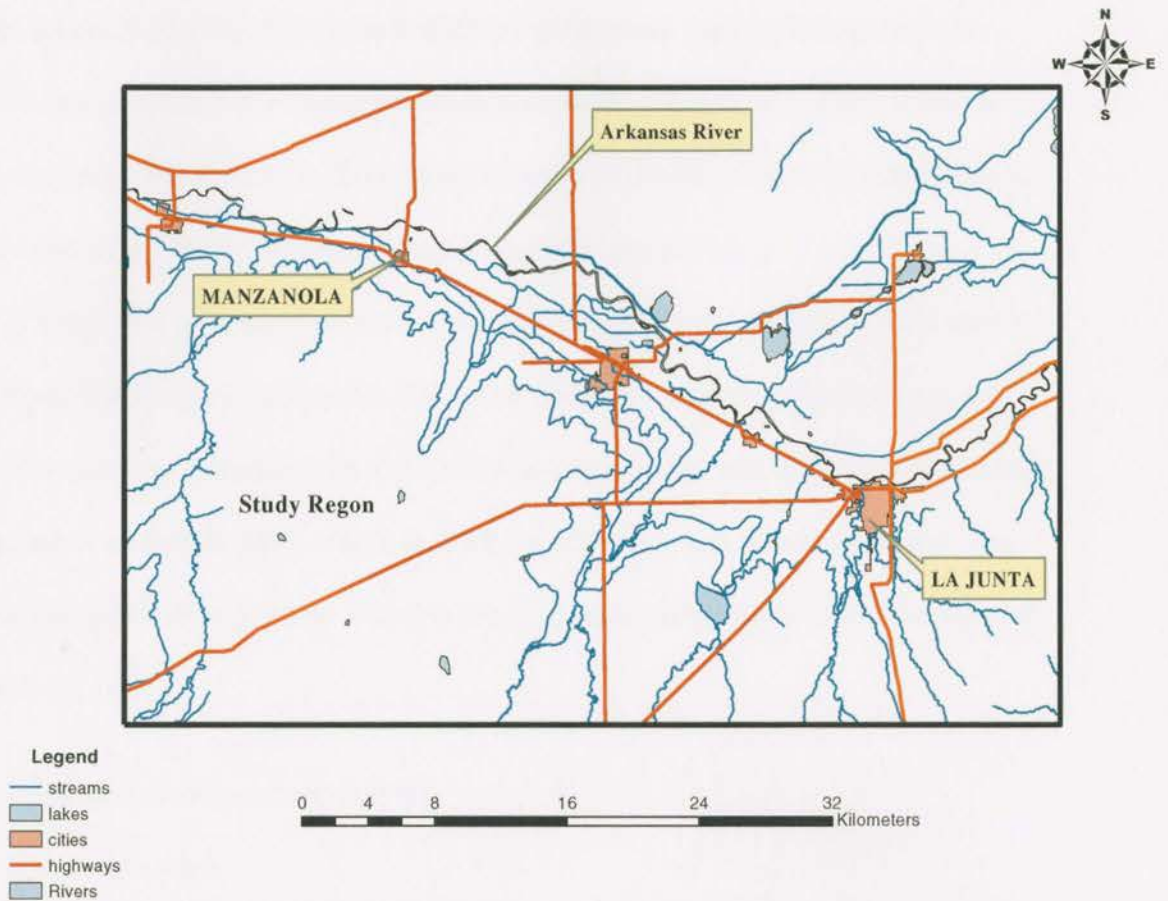


Figure 1. Map of the study area.

2.3 METHODOLOGY

In this study, crop condition is used as the main indicator of the presence and severity of soil salinity. Bastiaanssen et al. (2000) and Steven et al. (1992) have discussed using indirect indicators such as crop growth performance and leaf angle orientation (leaf roll), as indicators of the existence of soil salinity, and in this study focuses on crop condition as a indicator of soil salinity and therefore it is used to produce soil salinity maps.

Crop condition can be detected remotely using satellite imagery. In this research, after acquiring a satellite image of the study area, the condition of the crops being grown

in fields is classified according to their different reflectance values. Using spatially referenced ground data collected in the study area, each class in the satellite image is related to a level of soil salinity. These classes are then used to create a signature file to classify other areas within the same image having the same crop.

For this research, two satellite scenes are used. The first image is a multi-spectral image from Ikonos taken on July 27, 2001. The image is composed of four bands (red, green, blue and near infrared) with 4 m spatial resolution. The second scene is a Landsat 7 image taken on July 8, 2001, which is made up of eight bands (blue, green, red, near infrared, two mid infrared bands, a thermal and a panchromatic band) with 30 m spatial resolution.

2.3.1 Image processing and overlaying

Image Georectification

The scenes were georectified using polynomial and rubber sheeting models. Ground-control points (GCPs), such as road intersections, canals, and field boundaries were needed for the georectification, and these points were provided by geographic information system shapefiles and GPS points. The polynomial model was used for the initial georectification. This level of accuracy was all that was needed for rectifying the Landsat 7 image. For the higher resolution Ikonos image, a higher level of accuracy was targeted, and the rubber sheeting model that uses differentially corrected GPS points around the fields of interest as GCPs was employed.

Image Classification

The ERDAS 8.7 software was used to obtain spectral classes for crops from each image by using unsupervised classification techniques in this technique pixels with

similar spectral characteristics are clustered together , each cluster is called class all these classes is contained into a parametric signature that is based on statistical parameters such as mean and covariant matrix of the pixels that falls in each class, when using unsupervised classification classes are determined by spectral distinctions that are inherent in the data itself then later on those classes can be related to soil salinity classes. These spectral classes show different crop conditions. The spectral classes in the output image were then converted from raster to vector (polygons). Each set of polygons with the same grid-ID code was converted to a unique class. The spectral classes were identified based on information from satellite imagery and field surveys.

Overlaying

Using GIS (ArcMap 9), the polygons generated from the processed scenes were overlaid on a point coverage of soil salinity sample locations inside the study area. The combination of the polygons and the point coverage provided the capability of relating the soil salinity values within each field to its corresponding class. Each polygon was then assigned the average soil salinity value of the points falling within it. This was done by using a tool (polystat) developed in ArcMap 9 for this purpose. The tool estimates statistics (mean and standard deviation) of any point coverage (in this case soil salinity values) and automatically assigns them to the corresponding polygon. Then each set of polygons that have the same average salinity value was reclassified as one class. Following this procedure, up to sixteen classes of soil salinity were developed from the reflectance information extracted from the scenes.

2.3.2 Methods for Calibration and Validation

The methodology described above was calibrated using a field selected for that purpose before being applied to other fields covered by the image for validation. Ground soil salinity data was collected in the calibration field using both an EM-38 probe and the SIW Kit. The calibration was conducted in the middle of the summer, from July 1st to August 10th 2001, when the crop was fully developed. Both scenes (the Ikonos image from 7/27/01 and the Landsat 7 image from 7/8/2001) were calibrated in this way.

Several authors have demonstrated the advantage of combining data from remote sensing with detailed information observed on the ground (Bishop and McBratney, 2001; and Carré and Girard, 2002). For this study, over 100 soil samples were collected with each sampling point being comprised of 4 sub-samples collected at 4 depths (30, 60, 90, and 120 cms). In order to convert the EM-38 readings into actual soil salinity values (dS/m), several relationships were evaluated using regression techniques. After multiple iterations the following relationship was developed:

$$Y = 0.0877X - 1.8303 \quad (2.1)$$

Where Y: is the actual soil salinity value in dS/m

X: is the EM-38 readings (EM_{vc})

$$EM_{vc} = EM_v * SST_c \quad (2.2)$$

Where: EM_v = EM-38 vertical reading

$$SST_c = A * SS_{temp} \quad (2.3)$$

Where: SST_c = temperature correction factor)

$$A = 1 - .203462F - 0.038223(F^2) - 0.005554(F^3) \quad (2.4)$$

SS_{temp} = temperature of soil sample measured in deg C

$$F = \frac{(SS_{temp} - 25)}{10} \quad (2.5)$$

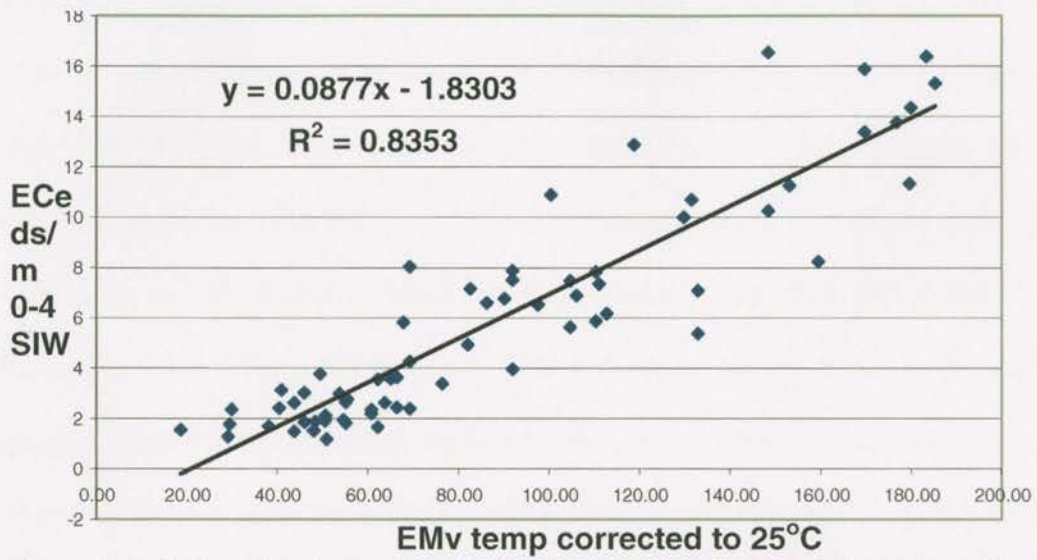


Figure 2. Relationship between actual soil salinity values and EM-38 readings.

2.3.2.1 Ikonos

Calibration field



Figure 3. Calibration field

Figure 3 shows the field that was selected (field 80) for calibration of the Ikonos image. The calibration field needed to have a wide range of soil salinity values, ranging from less than 1 dS/m, which causes no crop loss, to over 7.5 dS/m, which inflicts severe crop loss on corn. This wide range allowed for the assignment of reflectance ranges to sixteen different salinity levels in this calibration field. To separate these levels, the satellite image was spatially linked with the soil salinity data collected from points inside the field using an EM-38 sensor. The points were spatially located using a global positioning system. Using a combination of the blue, green and red bands in the satellite image, several pixels were selected, with each one corresponding to a different soil salinity level. Reflectance values ranged from 200-800, with high salinity points clustered around the 700 reflectance value, moderate salinity points clustered around the 400-500 reflectance value and the low salinity points around the 200 reflectance value. The classified image was re-coded based on the soil salinity points obtained using the EM-38 sensor. This re-coding process was accomplished by spatially matching each reflectance class in the image with the soil salinity values. The sixteen reflectance classes are shown in Table 1.

A subset of the data points collected with the EM-38 sensor was used to calibrate the methodology. The subset was selected using the ArcMap 9 “create subset” tool that randomly selects 50% of the points. For this subset of points a similar procedure as that conducted for the whole set of points was performed. An average value of soil salinity for the subset of points that were inside each of the polygons for the sixteen reflectance classes was calculated. To validate the methodology within the calibration field, the methodology was applied to predict soil salinity classes using another subset of measured

Table 1. The sixteen reflectance/salinity classes obtained from the calibrated field.

Class Number	Number of Points	Minimum Value	Maximum Value	Mean (dS/m)	Standard Deviation
1	7	0.0	1.3	0.8	0.40
2	24	1.8	6.0	3.3	1.24
3	35	1.0	6.6	3.1	1.24
4	59	1.3	9.7	3.8	1.50
5	61	1.7	6.7	4.5	0.94
6	36	1.4	7.0	5.2	0.97
7	32	3.5	7.7	5.5	1.12
8	19	3.1	7.3	5.7	1.15
9	27	3.2	7.4	6.0	0.97
10	25	3.8	9.2	6.2	1.22
11	15	2.3	8.0	6.2	1.46
12	15	4.3	10.4	6.6	1.31
13	25	1.3	10.1	6.7	1.98
14	48	4.7	10.6	7.4	1.19
15	56	4.3	11.0	8.1	1.37
16	18	7.2	11.4	8.8	1.24

ground data. The error between the measured and predicted soil salinity values for each class was calculated and is shown in Table 2.

Table 2 shows that the maximum error was 1.1 dS/m and it occurred in 8 -10 dS/m category where the crop experiences extreme loss. Areas that correspond to this category are bare soil meaning that vegetation, our primary indicator of the presence of soil salinity, is not present. Other values of errors between the predicted soil salinity and the actual soil salinity were 10% or less as can be seen from the prediction errors in table 2, which range from 0 dS/m to 1.1 dS/m over the range of 11 dS/m.

Figure 4 shows the expected yield loss in corn due to soil salinity in relation to the sixteen classes in the calibration field.

Table 2. Cross validation of the classes in the calibration field.

Training					Testing				Prediction Error (dS/m)
Class Num.	Points	Min. (dS/m)	Max. (dS/m)	Mean (dS/m)	Points	Min. (dS/m)	Max. (dS/m)	Mean (dS/m)	
16	6	8	10	8.7	5	8	11	9.8	1.10
15	16	6	11	8.0	31	4	11	7.9	-0.07
14	21	6	10	7.5	16	6	11	7.6	0.06
13	6	6	9	7.7	13	5	10	6.8	-0.86
12	3	6	7	6.7	4	6	7	6.5	-0.16
11	5	5	8	6.0	7	6	10	7.0	1.00
10	15	4	8	6.0	8	5	7	6.0	0.00
9	8	4	6	6.0	10	5	8	6.0	0.00
8	10	4	8	5.7	15	5	10	6.0	0.30
7	10	4	7	5.7	8	4	7	5.7	0.00
6	20	4	10	5.4	16	3	9	5.5	0.10
5	29	3	6	4.3	28	2	9	4.8	0.50
4	26	1	6	3.4	26	1	6	3.5	0.10
3	22	1	7	3.1	13	2	5	3.1	0.00
2	16	2	4	2.8	11	3	4	3.0	0.20
1	4	1	1	1.0	2	1	1	1.0	0.00



Figure 4. Expected yield loss in corn due to soil salinity in relation to the sixteen classes in the calibration field.

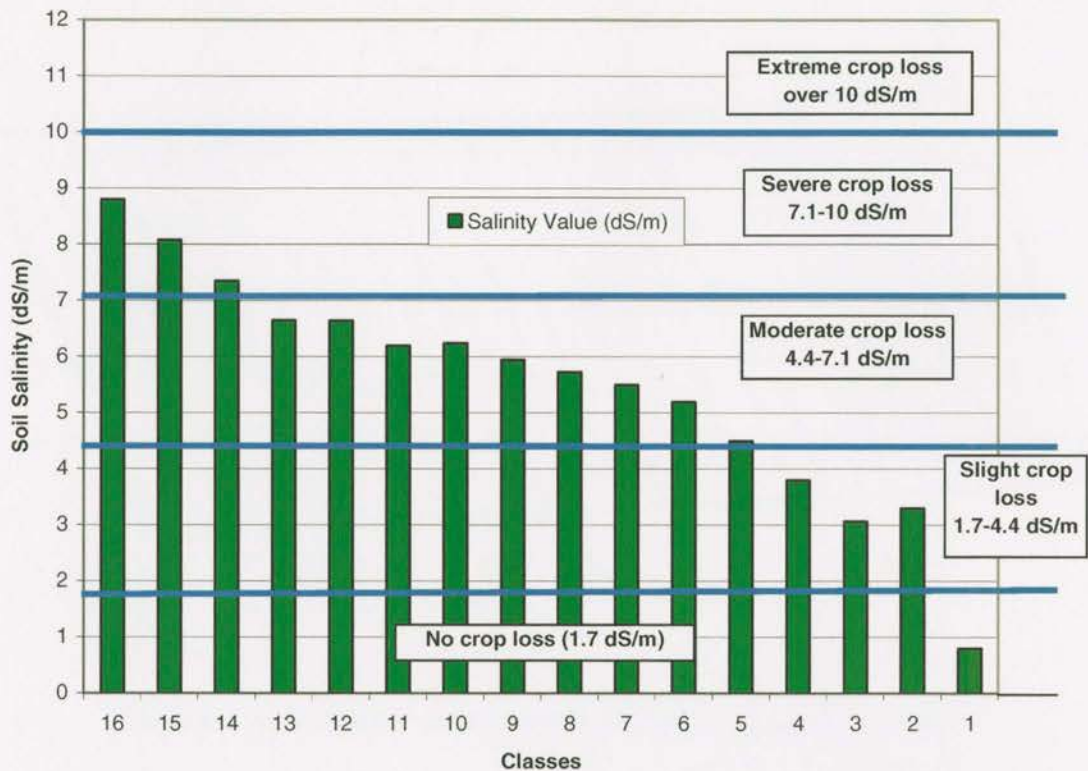


Figure 5. Mean values for the sixteen reflectance classes and their respective estimated yield losses in the calibration field.

Validation fields

Field RR

To validate the methodology, the EM-38 sensor was used to map soil salinity in another corn field, known as the RR field (Figure 6). This field is within the Ikonos image. In this validation field, EM-38 sensor soil salinity measurements were taken using a differential GPS. The points were then overlaid on the classified image, and each class was compared to its mean value to assess the prediction accuracy. Figure 7 shows predicted and measured salinity levels in the validation field.

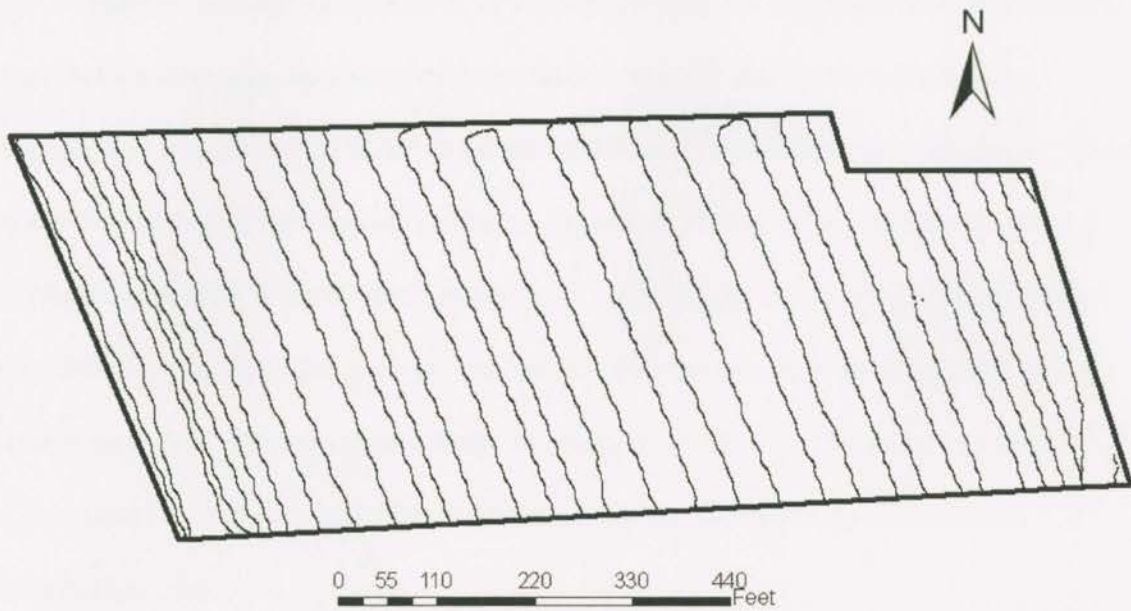


Figure 6. Soil salinity points in the RR field (validation field)

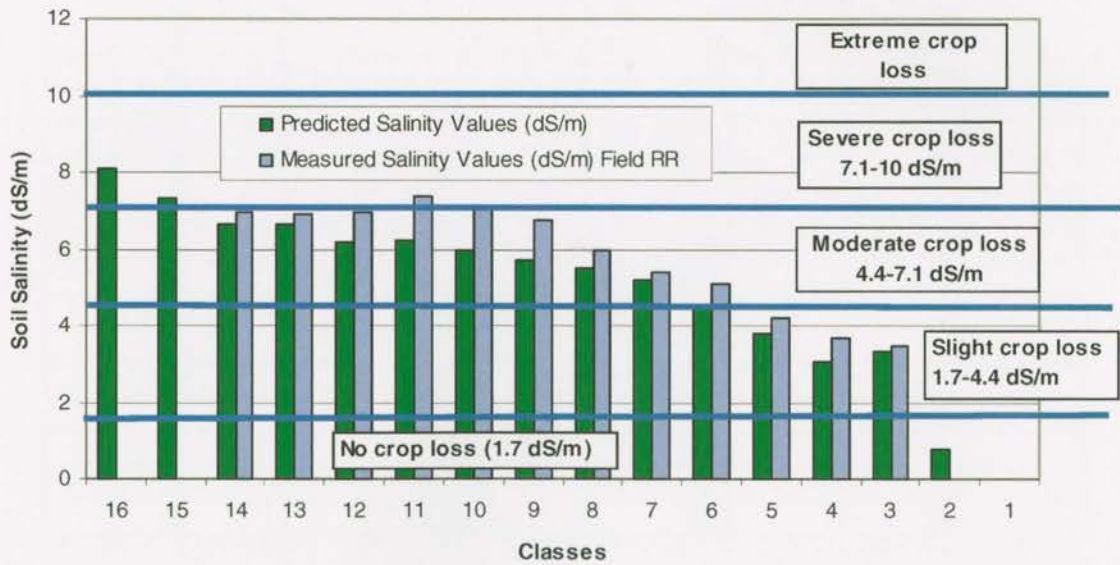


Figure 7. Measured soil salinity values versus predicted values in the validation field (RR).

Figure 7 shows that classes 1, 2, 15, and 16 were not represented in the RR field, therefore the detection accuracy for these classes was not able to be evaluated. Fortunately these four classes are in the no crop loss or severe crop loss categories. These categories are usually not important during salinity evaluation since categories 1 and 2 represent no salinity impact while categories 15 and 16 represent severe crop loss and very little vegetation might grow in these areas. The model was able to separate and predict the other 12 classes with a range of errors from 1% to 12% and an average error of less than 5%. The accuracy level and error achieved in predicting each class is presented in table 3.

Table 3. Predicted soil salinity values versus measured values for the validation field RR*.

Class Number	Predicted Value (dS/m)	Measured Value (dS/m)	Error (dS/m)
1	0.80	NA	NA
2	3.30	NA	NA
3	3.07	3.50	0.43
4	3.80	3.67	-0.13
5	4.50	4.20	-0.30
6	5.20	5.10	-0.10
7	5.50	5.40	-0.10
8	5.73	6.00	0.27
9	5.95	6.77	0.82
10	6.24	7.11	0.87
11	6.20	7.38	1.18
12	6.64	6.95	0.31
13	6.65	6.91	0.26
14	7.35	6.95	-0.4
15	8.08	NA	NA
16	8.80	NA	NA

Field # 23

Field 23 is a corn field with uniformly low soil salinity. When measured with an EM-38, most of the soil salinity measurements were between 3 and 4 dS/m. Using the re-coded Ikonos image to classify this field, it was determined that most of the field falls in the region of classes 1 and 2. These classes represent soil salinity values of 0.8 dS/m to

3.3 dS/m, which match very well with the actual soil salinity values obtained from the EM-38 measurements. Taking into consideration that the methodology is not able to differentiate between very low soil salinity levels, we can still see the compatibility of the soil salinity distribution in the ground data and satellite imagery estimates. Figure 8 shows (a) soil salinity levels detected from the Ikonos satellite image and (b) soil salinity measured in field 23.

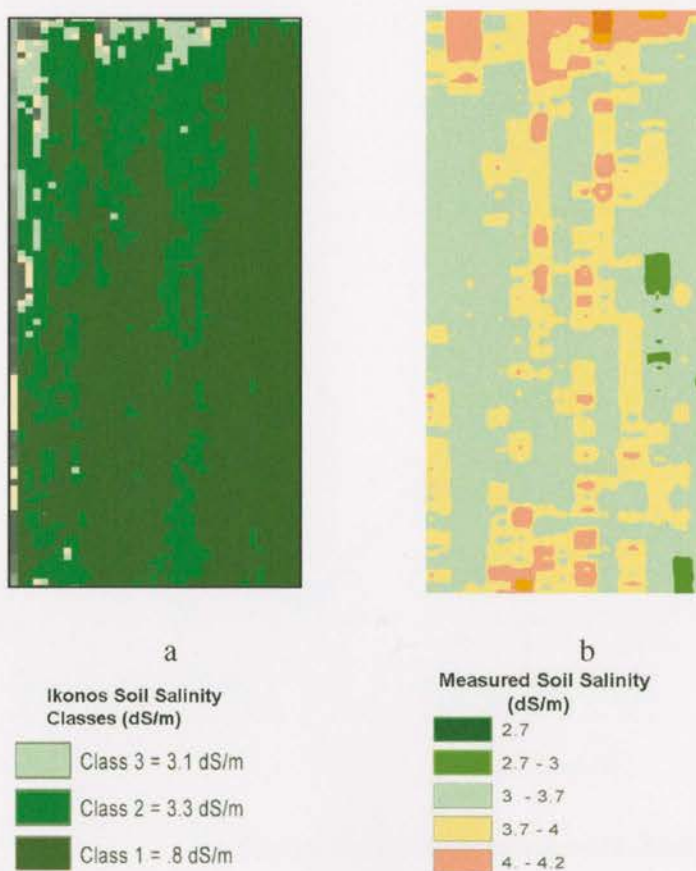


Figure 8. Soil salinity stimated using the Ikonos image (a) and measured (b).

2.3.2.2 Landsat 7

Landsat 7 scenes have 8 bands covering the visible range as well as the near and far infrared bands, a thermal infrared band, and a panchromatic band. The resolution of

the bands is 30 m by 30 m, except for the thermal band that is 60 m by 60 m and the panchromatic band which has a resolution of 15 m by 15 m.

Enhanced Thematic Mapper Plus (ETM+)	Landsat 7	Wavelength (micrometers)	Resolution (meters)
	Band 1	0.45-0.52	30
	Band 2	0.53-0.61	30
	Band 3	0.63-0.69	30
	Band 4	0.78-0.90	30
	Band 5	1.55-1.75	30
	Band 6	10.40-12.50	60
	Band 7	2.09-2.35	30
	Band 8	0.52-0.90	15

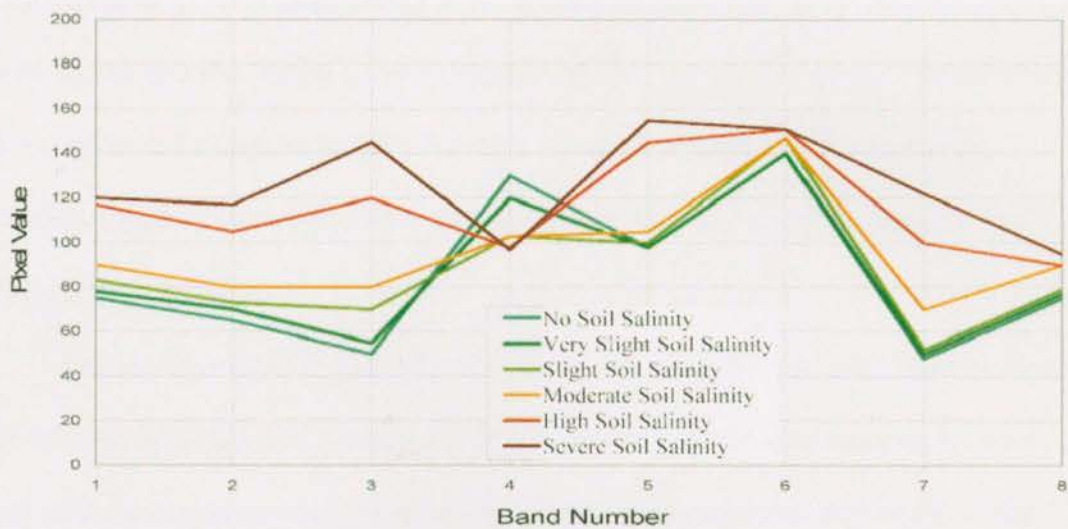


Figure 9. Spectral profile for field 80

When looking at the spectral profile of the Landsat scene for field 80 (Figure 9), in the context of targeting areas with different soil salinity levels, the spectral profile shows a reasonable separation in the reflectance of the bands. This means that regions with different soil salinity levels can be successfully separated into classes, where each class represents a range of soil salinity values. The clearest separation is in band 3. This

separation is obvious in the severe crop loss category, shown with the brown line. Areas of high, moderate, and slight crop loss are also easily separated. However, the separation between the categories of very slight crop loss and no crop loss is very small. For these classes, the difference in the reflectance for band 4 is minimal, but larger in band 3 which is expected since band 3 is the red chlorophyll absorption band of healthy vegetation, this proves that there is a significant difference in the crop condition that can be detected by band 3 meanwhile band 4 did not show a lot of variation between locations with different soil salinity levels and this could be because band 4 which is the reflective infra red is responsive to the amount of vegetation biomass but not sensitive to crop condition which in this case should vary significantly since it is affected greatly by soil salinity. From analyzing the spectral profile it can be concluded that a good soil salinity classification can be performed using the Landsat imagery. Several soil salinity classes can be identified, enabling the whole study area to be classified and therefore identify the salinity affected lands.

Testing the results of using the methodology on the Ikonos scene against the same methodology applied to the Landsat scene is valuable because Landsat scenes cover larger areas at a much lower cost per scene, which encourages the application of the methodology to different areas at different times. The main limitation of the Landsat 7 scenes is their spatial resolution. As mentioned previously Landsat 7 bands have 15m, 30m and 60m resolution for different bands and the detection technique used in this research depends on the bands with the 30m resolution, therefore detection of variability in salinity using Landsat scenes has a limitation on how small an area can be evaluated.

The same methodology that was applied using the Ikonos scene was applied to field 80 using the Landsat scene. The Landsat scene was georectified to preserve the geometric integrity of the field. Then, using the unsupervised classification technique in ERDAS Imagine 8.7 with the 16 classes, a classified map was generated for the targeted field. For field 80, nine classes were detected that can be clearly separated in the range between 0 dS/m and 9.96 dS/m. These classes are shown in Table 4. The first class represents areas with a mean soil salinity value of 4.2dS/m, and the ninth class represents areas with a mean soil salinity value of 9.96 dS/m. This classification allowed for the identification of one class in the no/slight crop loss zone which is class 1. Class 2 (5 dS/m) represents areas with moderate crop loss. Classes 3 and 4 indicate areas with high crop loss, and classes 5 to 9 fall in the category of severe crop loss.

Table 4. Soil salinity classes extracted from Landsat 7

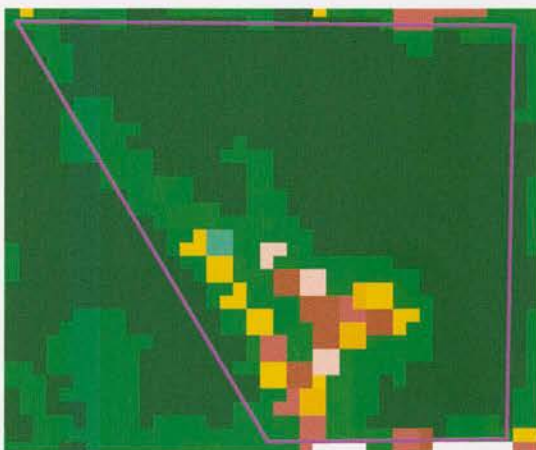
Class	Training	Testing
1	4.21	4.57
2	5.1	5.31
3	6.19	6.58
4	6.68	5.75
5	8.04	6.84
6	8.42	8.11
7	8.78	8.94
8	9.57	9.68
9	9.96	9.62

When using Landsat 7 imagery all but the no crop loss category was identified. The Landsat 7 scenes only compromise the classification to the extent that two classes (no crop loss, slight crop loss) were merged into one. Therefore, depending on what level of soil salinity impact researchers are trying to determine they may decide that it is to their benefit to use the lower resolution but less expensive Landsat 7 imagery.

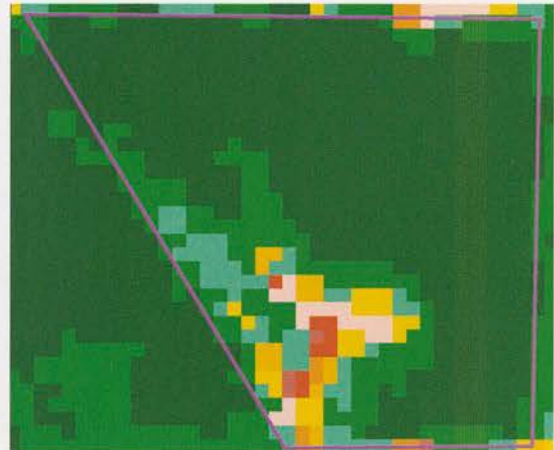
2.3.2.3 Using Principal Component Analysis

Images can usually be enhanced to improve their appearance for subsequent analysis. In this study the principal components analysis (PCA) technique was applied to improve the Landsat 7 image's appearance. PCA has proved to be of value in the analysis of multispectral remotely sensed data (Press et al., 1992). Applying PCA to an image can result in a new image that may be more interpretable than the original image (Singh and Harrison, 1985), moreover Principal Component Analysis is a method of data compression that computes redundant data into fewer bands, the bands of the PCA are noncorrelated and independent, PCA gives better interpretation more than the source data (Jensen, 1996; Faust, 1998). To compute PCA a linear transformation is applied to the data that re-computes the coordinates of each pixel into a new coordinate system. In this new coordinate system the highest variance by any projection of the data lies as the first coordinate. Figure 10(a) shows the original and the PCA classified (unsupervised) Landsat 7 scenes. Figure 10(b) shows the number of classes that could be extracted from the PCA image compared to the original scene.

Original Image (16 Classes)



PCA Image (16 Classes)



Number of classes in 7 band image

Number of classes in PCA image

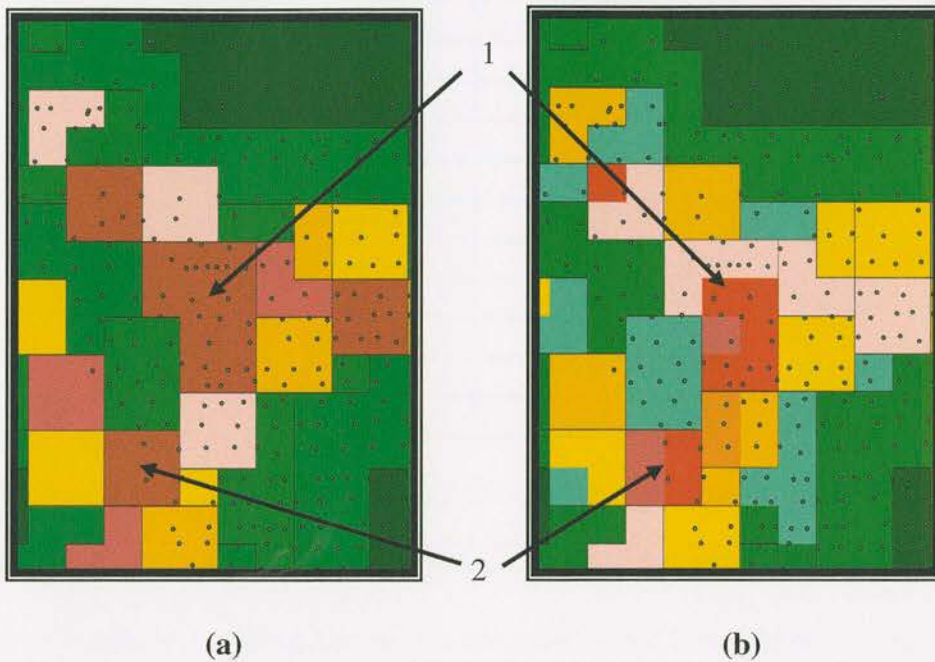


Figure 10 (a) Original versus (b) PCA Landsat scene

Using principal component analysis before classifying an image increases the accuracy of detecting the soil salinity by generating a better separation of bands as shown in Figure 10. Group 1 arrows point to one class in the original image that was separated into 3 classes in the PCA image; group 2 arrows point to one class in the original image that was separated into 2 classes in the PCA image. Figure 11 compares the salinity classes and the corresponding salinity levels extracted from field 80 during the calibration (training) and testing phases using the original and PCA scenes respectively.

As shown in Figure 11, using PCA one class was added to the classification, noting that the classes extracted from the original and PCA scene classification are not identical due to the change of the soil salinity points falling within each class; however, they should be close. Table 5 shows the number of classes that were extracted from field 80 using the PCA image.

Table 5. Soil salinity classes (dS/m) extracted from field 80 using the PCA image

Class	Training	Testing
1	4.2	4.55
2	5.01	5.4
3	6.68	7.14
4	7.47	7.65
5	8.91	7.82
6	8.91	8.38
7	9.98	10.07
8	10.07	9.14
9	10.17	9.62
10	11.88	10.93

The PCA technique was also applied to detect soil salinity on several corn fields. For example, Figure 12 shows the soil salinity levels detected in field 23 using the PCA image in comparison to soil salinity levels measured in the field. Table 6 presents a comparison between the extent (spread) of soil salinity that was detected by the PCA image and that measured in field 23. Table 6 presents a comparison between the extent (spread) of soil salinity that was detected by the PCA image and that measured in field 23. The ground data presented in Table 6 shows that soil salinity in the range of 1- 4 dS/m is spread over 87% of the field area, but the PCA image detected that this level of salinity was spread over only 83% of the field, meaning that there was a detection error of 4%. Salinity in the range of 4- 5 dS/m is spread over 17% of the field area according to the ground data but using the PCA image this level of salinity was only detected on 13% of the field area. The PCA image thus had a detection error of -4% for this salinity range. These results are shown in Figure 13.

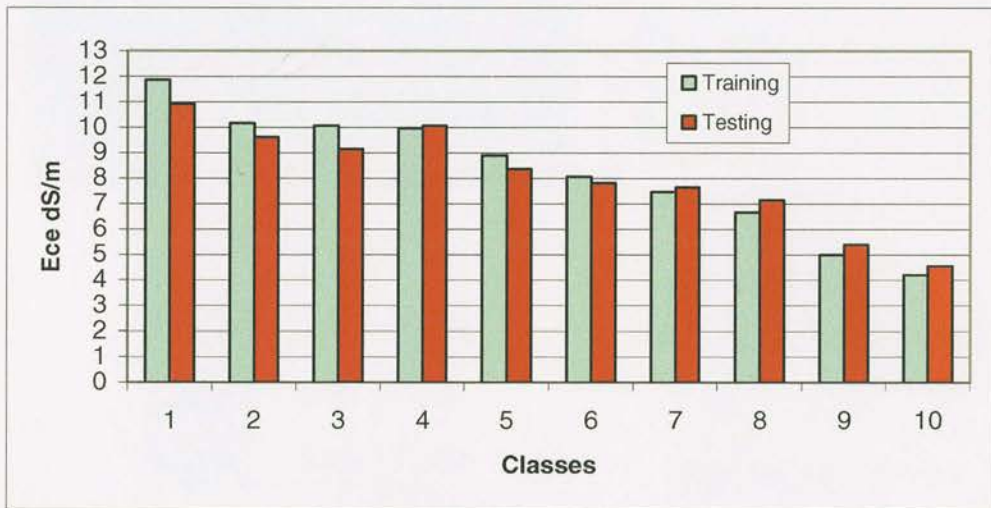
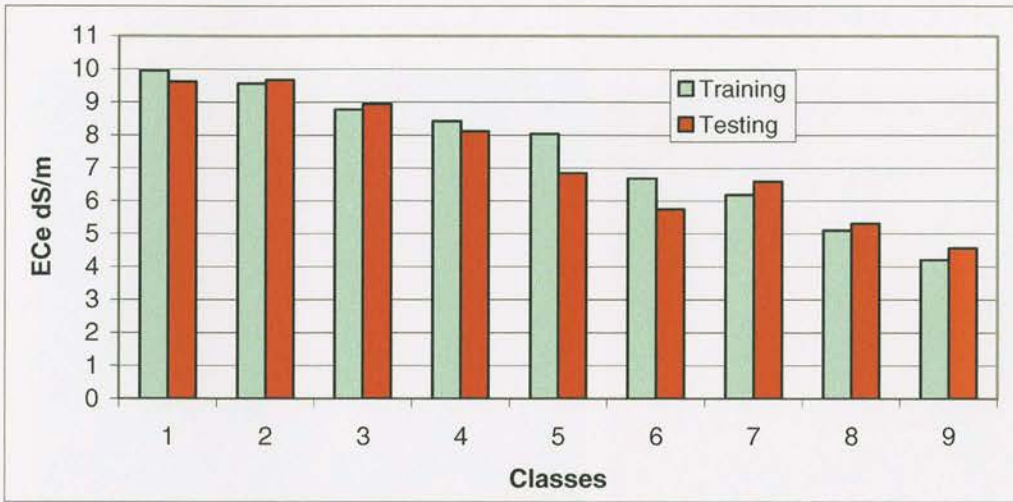


Figure 11. Soil salinity classes and the corresponding salinity levels extracted from the original (a) and PCA (b) scenes

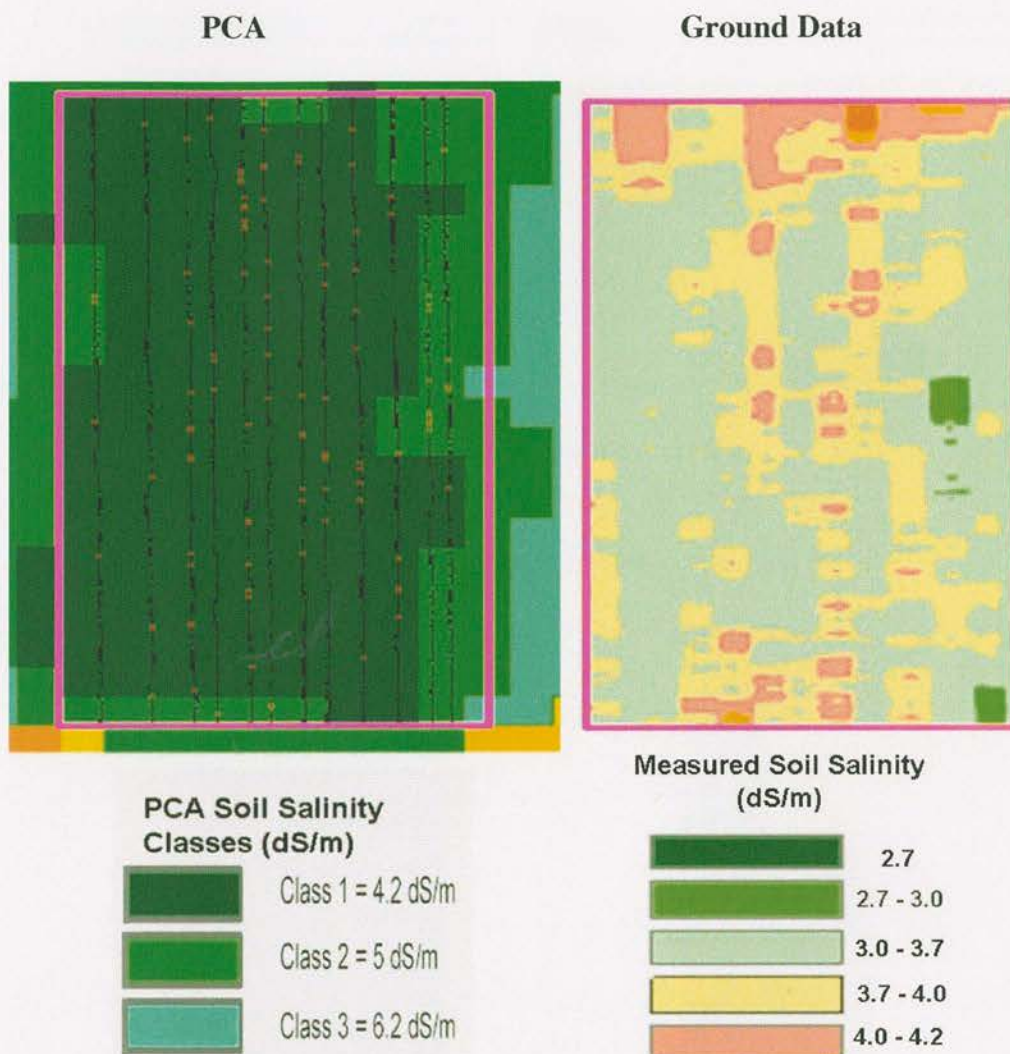


Figure 12. Soil salinity levels in field 23

Table 6. Extent of soil salinity in field 23

Soil Salinity	Image	Ground	Error
1-4 dS/m	83%	87%	4%
4-5 dS/m	17%	13%	-4%

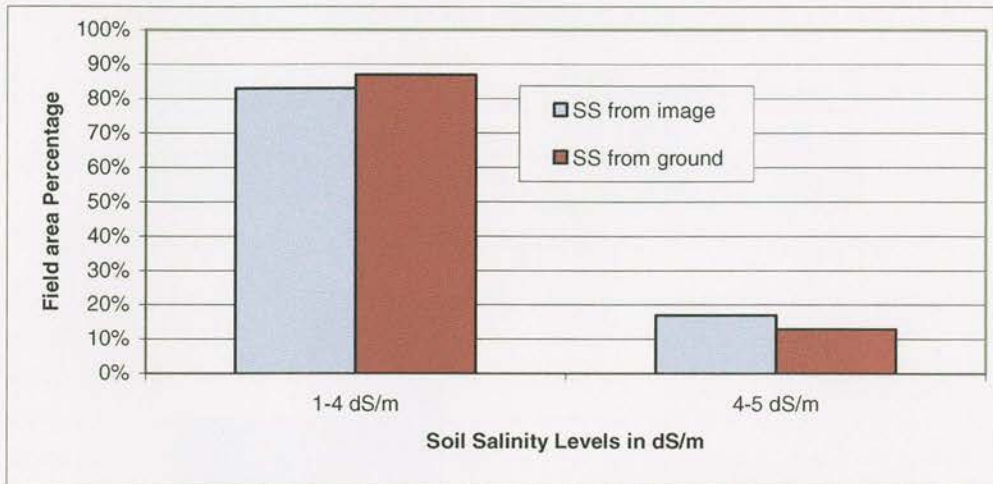


Figure 13. Spread of two levels of salinity in field 23

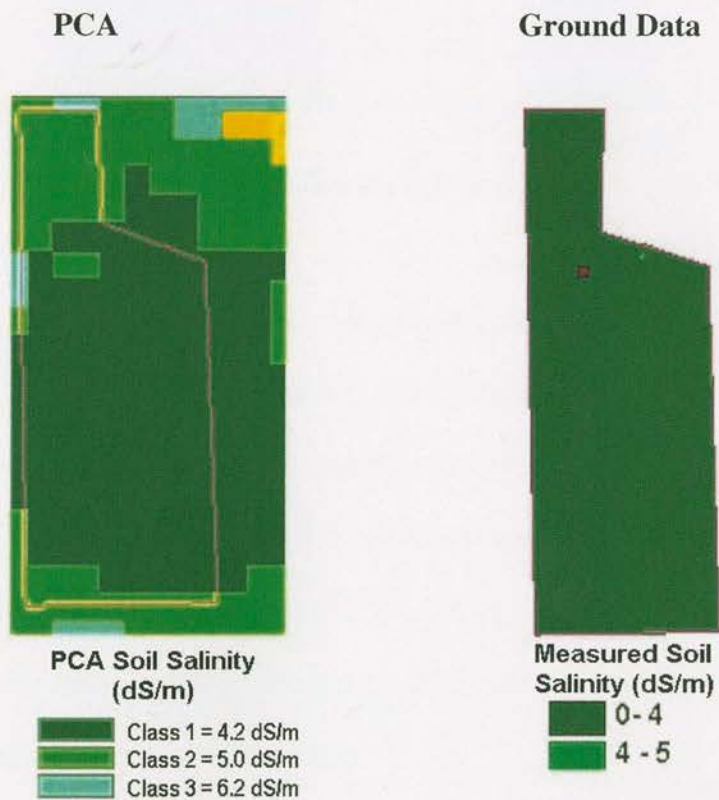


Figure 14. Soil salinity levels in field 6. Figure 14, table 7, and figure 15 present the extent (spread) of soil salinity in field 6.

Table 7. Extent of soil salinity in field 6

Soil Salinity	Image	Ground	Error
1-4 dS/m	83%	87%	4%
4-5 dS/m	17%	13%	-4%

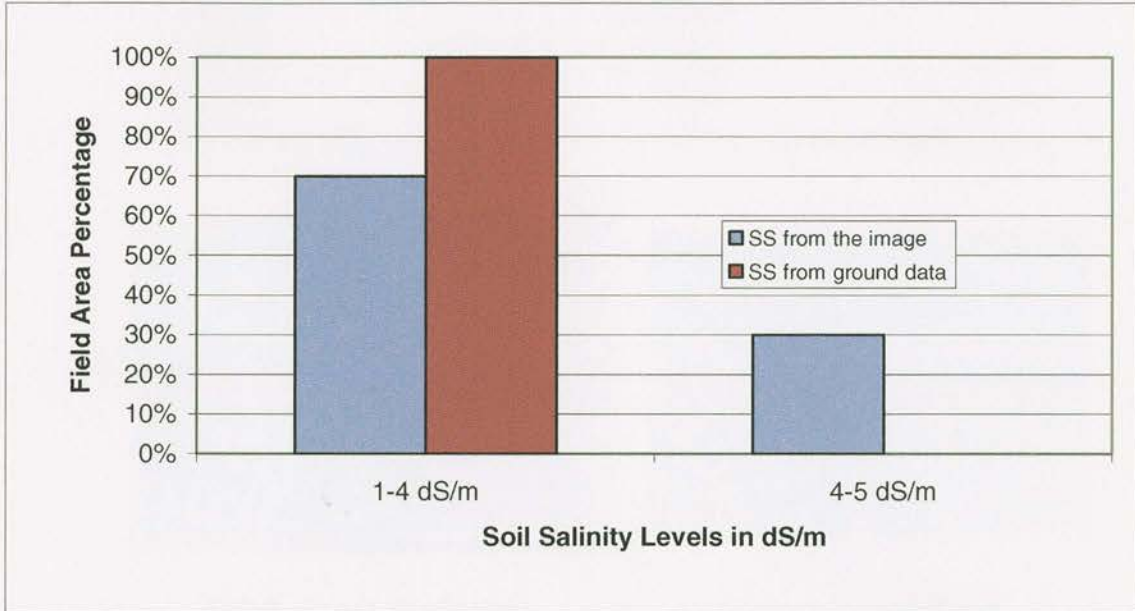


Figure 15. Spread of two levels of soil salinity in field 6

The source of error is in the top portion of the field, which was misclassified because of the presence of shill rocks that hinder the crop's growth causing the biomass to be stressed. However, this inhibition of crop growth is not due to soil salinity but due to soil properties. Such situations show some of the limitations of the methodology. Yet, the difference between the two classes was only 1 dS/m, which means that soil salinity in 30% of the field was over estimated by 1 dS/m.

Figure16, table 8, and figure 17 show the extent (spread) of soil salinity in field 77. Field 77 contains very low soil salinity levels. Ground measurements of soil salinity were in the range of 1.8 to 4.1 dS/m; such levels of soil salinity have minimal impacts on corn. In the satellite image most of this field was classified as low salinity except the

areas near to the field boundary that contain some mixed pixels. These mixed pixels introduce an error of misclassification of the bare soil around the field which results in an overestimation of soil salinity. This overestimation was about 1 dS/m in the range of 4-5 dS/m (20% of the field) and 2.2 dS/m in the range of 5-6.2 dS/m (20% of the field).

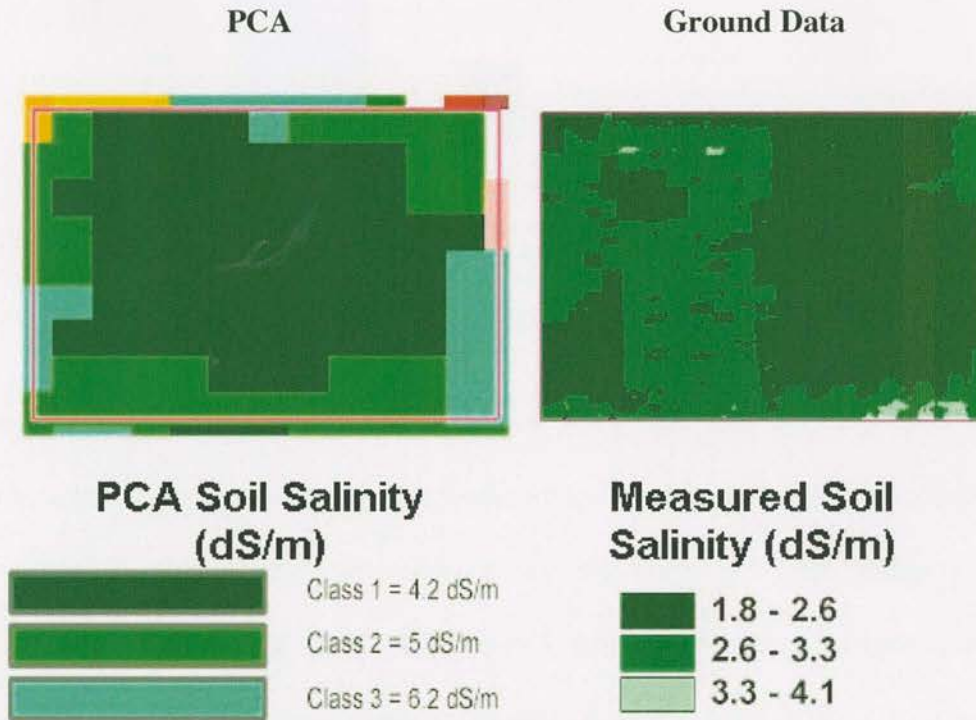


Figure 16. Soil salinity levels in field 77

Table 8. Extent of soil salinity in field 77

Soil Salinity	Image	Ground	Error
1-4 dS/m	60%	100%	40%
4-5 dS/m	20%	0%	-20%
5-6.2 dS/m	20%	0%	-20%

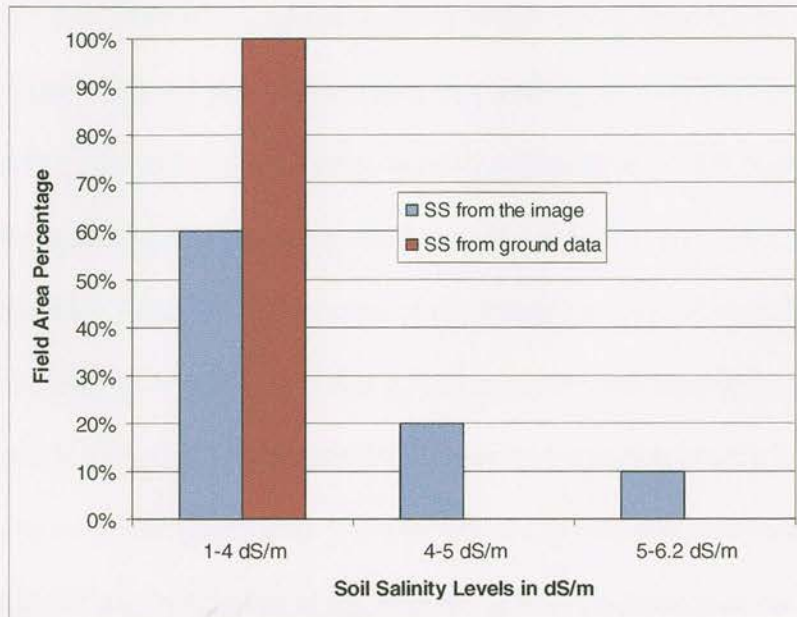


Figure 17. Distribution of two levels of soil salinity in field 77

2.3.3 Sources of Error

The sources of error in the applied methodology could be either from the satellite imagery or from the soil salinity ground data, errors from the imagery can be due to inaccuracy in the georectifying of the image that happens either because of inaccurate reference points used to rectify the image or because of inaccuracies in the georeferencing process, this errors can be reduced by obtaining a sufficient number of high accuracy reference points that adequately cover the area of interest in the image, the minimum value for this error will at lease be the size of the largest pixel size of the bands used which is 4 m when using the Ikonos image and 30 m when using Landsat 7 without the thermal band and goes up to 60 m if the thermal band is used, the second error that can be introduced from the imagery is the existence of cloud cover which can affect the image classification process, this can be reduced by using imagery that has no cloud cover or for which cloud have been masked in order to exclude cloud cover areas, the

third error that can be introduced by the imagery is the atmospheric effects which are not really an error since they are part of the signal received by the satellite, however this can be corrected using atmospheric correction techniques, finally the fourth source of possible error from the satellite imagery is the resolution of the image which is not as much an error than it is a limitation, if the resolution of the image (pixel size) is larger than the resolution of the ground soil salinity point grid then several soil salinity points will fall within one pixel in the image, those points falling within one pixel in the image might vary in value, to relate the pixel value to the points, the points will be averaged to one value, instead if a higher resolution image was being used that matched the ground data resolution, then each ground soil salinity point would be represented by one pixel in the image, this would give more details in the soil salinity prediction. The other source of errors is caused by ground data collection which could be from GPS errors that cause points with certain soil salinity values to be placed away from their actual locations causing soil salinity values to be related with image pixels that do not actually fall over those points, this error can be eliminated by using high quality GPS receivers that have errors smaller than the satellite image pixel size (4m in the case of Ikonos images and 30m in the case of Landsat images) or by using differentially corrected GPS which reduces the position to less than a meter, the second error that can be caused by ground data are errors of the soil salinity ground surveying device (the EM-38 in this case), the EM-38 can produce wrong readings due to either being not correctly calibrated or because of the field conditions, this errors can be avoided by performing the right calibration on the EM-38 and by doing the survey on the field when the field conditions are suitable for conducting soil salinity surveys (not too wet or too dry). One last source

of errors on the ground are no crop areas such as area covered with trees, weeds, bare soil, burned areas, houses, roads, etc. As an example of these errors the soil salinity calibration points (shown in yellow in Figure 18) falling on the edge of one class, due to possible GPS or image georectification errors, could be contained in the next high or low class causing some over or underestimation of soil salinity for certain classes. To ensure proper classification, those points could be identified (by creating a small buffer around the class boundaries and selecting any points inside of these buffers) as outliers and then eliminating them.

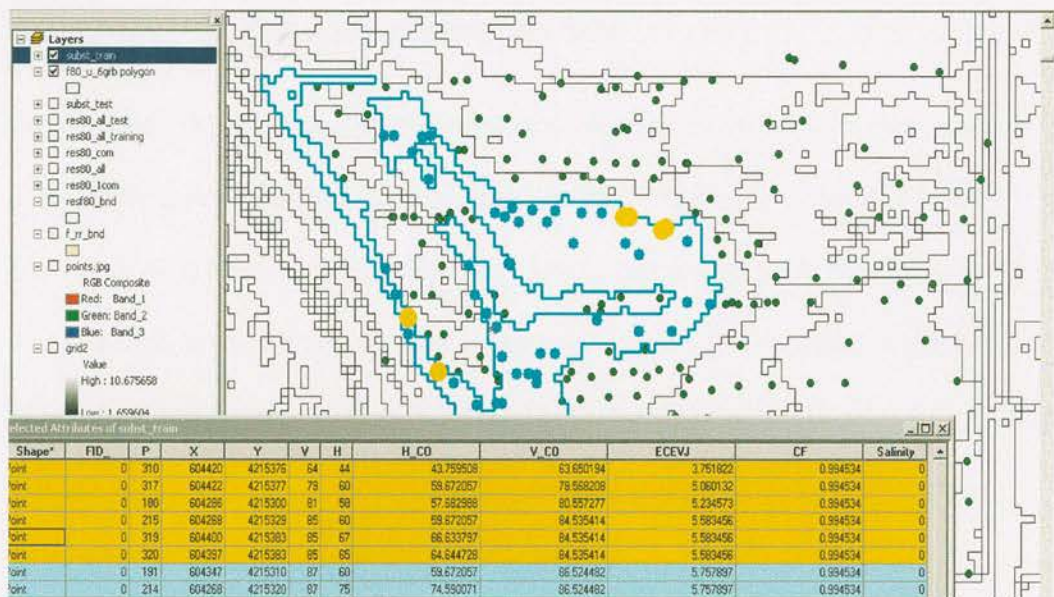


Figure 18. Soil salinity points falling in between classes

2.3.4 Advantages and Disadvantages of Methods Used to Detect Soil Salinity

Traditional Method

The traditional method for mapping soil salinity involves collecting soil samples from the field and analyzing them in the laboratory to determine the salinity levels in the soil. This method has changed slightly in recent years as handheld electromagnetic devices have come into use. Once calibrated, these devices can directly estimate the soil

salinity in the field, reducing the need to take samples to the lab (some soil samples might need to be collected to calibrate and/or validate the values obtained from the electromagnetic devices).

Disadvantages of the Traditional Method

- ***More labor***: Traditional methods, even using an electromagnetic device, consume substantial amounts of time and labor. The number of samples taken is often limited due to time and economic constraints. Consequently, the maps produced by the traditional method with these limited samples might not capture all the spatial variability of the soil salinity in the field.
- ***Inaccuracy***. When used, electromagnetic devices need to be calibrated properly to give good results, but even with calibration, electromagnetic devices might not give an accurate estimate of soil salinity levels because of certain field conditions. For example, if the field is too wet because of a previous irrigation or rainfall event, the EM-38 most likely would overestimate salinity levels, and if the field is too dry the EM-38 most likely would underestimate the salinity levels. These inaccuracies would result in misleading soil salinity maps.
- ***Accessibility and crop damage***. Mapping soil salinity using traditional methods might result in crop damage if data needs to be collected during the growing season; and for certain measuring methods such as the Veris system or the EM-38 when done using a trailer the accessibility is very limited during the growing season and samples have to be collected during the very early part of the growing season or the end of the growing season (after harvest).

Advantages of Traditional Methods

- With appropriate field conditions and well-calibrated instruments, soil salinity can be accurately estimated in the lab as well as in the field.
- Actual data is collected and a good idea of the field conditions is obtained by visiting each field.

Satellite Method

Disadvantages of the Satellite Method

- ***Inaccuracy.*** The satellite method is unable to differentiate between different salinity levels below a certain detection limit. However, since the purpose of this research is to estimate soil salinity levels that affect crops, lumping very low soil salinity into one level is normally not a problem. Likewise, the satellite method is unable to differentiate between high salinity and extreme salinity levels. Since the methodology depends on the crop biomass reflectance, if the crop is severely affected by a certain level of soil salinity, there is no way to estimate higher soil salinity levels since the crop is already severely affected. In addition, the satellite method is not accurate for small fields when using Landsat images which have 30m resolution, but most of the corn fields in the study area are large enough that this is not an issue.
- ***Unable to take into consideration special conditions.*** The satellite image is unable to identify the cause of the impact on crop growth. For instance, the satellite image is unable to differentiate between loss of biomass due to harvesting (alfalfa), irrigation stress, insect infestations or hail damage. However, in most cases, these situations are exceptions and not the norm.

- *Only certain levels of salinity can be detected in fields cultivated with salt tolerant crops.* Since the satellite image is evaluated for salinity on the basis of crop condition, if the crop is salt tolerant and thus is not affected by lower levels of soil salinity, the area in the satellite image planted with these types of crops will not be able to be evaluate for lower levels of soil salinity, only higher soil salinity levels would be able to be identified. These areas would need to be re-evaluated if the crop type changed to less salt tolerant crops.

Advantages of the Determining Soil Salinity Using Satellite scenes.

- Using satellite scenes can be very cost effective and it involves less effort than traditional methods. It also offers higher spatial resolution and greater consistency in estimation of soil salinity because it is not influenced by field conditions, like irrigations (impact that soil moisture has on the EM-38 readings). However, the main advantage of using satellite scenes may be its ability to cover a whole basin with considerably accuracy.

2.4 CONCLUSIONS

Soil salinity is identifiable and quantifiable using different satellite image types in conjunction with GIS and some GPS ground data. Images from satellites that offer higher spatial resolution offer the researcher the ability to detect soil salinity levels for small areas and more salt classes but the tradeoff is that the costs are significant when dealing with large areas (tens of thousands of hectares). Landsat imagery provides a larger area of coverage for less cost but did not allow us to separate the no loss areas from the slight crop loss areas. In spite of this, Landsat 7 imagery is considered to perform well since evaluating soil salinity depends mainly on the ability to separate and quantify critical

salinity classes (no/slight crop loss, moderate crop loss, severe crop loss). It is anticipated that results will be enhanced by using higher resolution imagery that might become available for commercial use in the near future.

3. SURFACE ENERGY BALANCE-BASED MODEL FOR ESTIMATING EVAPOTRANSPIRATION TAKING INTO ACCOUNT SPATIAL VARIABILITY IN WEATHER

3.1 ABSTRACT.

Reliable estimates of evapotranspiration (ET) from vegetation are needed for many types of water-resource investigations. How well models can estimate ET from vegetation varies depending on the capabilities of the model as well as the nature of the targeted vegetation. Model accuracy also depends heavily on the quality and quantity of data used. Information about the surface energy balance components derived from satellite imagery has been used by several models to estimate ET. This research introduces an enhanced surface energy balance-based model, the Remote Sensing of Evapotranspiration or ReSET model, for estimating ET. ReSET is an ET estimation model that takes into consideration the spatial variability in weather parameters, which makes it particularly applicable for calculating regional scale ET. ReSET also has the capability of interpolating between the available weather stations in time and space. The model's accuracy at daily and seasonal time scales is evaluated in several case studies.

3.2 INTRODUCTION

Recently, remote sensing algorithms have been widely used to estimate regional surface fluxes (e.g. evapotranspiration). Many of these surface energy balance models

were developed in the last decade (e.g., Kustas and Norman, 1996; Bastiaanssen et al., 1998a and b; Timmermans et al., 2004; Nagler et al., 2004; and Allen et al., 2005). These models use information derived from satellite imagery such as Landsat, AVHRR, ASTER, and MODIS to estimate ET (Nishida et al., 2003).

The remote sensing approach to estimating ET provides advantages over traditional methods. One of the most important advantages of the remote sensing approach is that it can provide regional estimates of ET. Most conventional methods are based on point measurements, limiting their ability to capture the spatial variability of ET. Another advantage of the remote sensing/surface energy balance ET models is that unlike most conventional methods which estimate a reference crop ET from meteorological data and apply crop coefficients to estimate the actual crop ET, remote sensing/surface energy balance models are able to estimate the actual crop ET directly. Satellites with high spatial resolution such as Landsat (30 m) and ASTER (15 m) give accurate estimates of ET with very high spatial resolution. Other satellites such as MODIS can be used for the same purpose, but the resolution is much coarser. Several models have been developed for estimating ET from satellite imagery, such as SEBAL (Bastiaanssen et al., 1998a and b) that uses Landsat 5 and Landsat 7 imagery and can be used with other image formats as well and METRIC that stems from SEBAL (Allen et al., 2005) but adds an internal calibration and a better method for calculating seasonal ET. METRIC uses the daily weather station reference ET as an index for interpolation between satellite image dates to produce seasonal ET estimates. Thus, METRIC is able to take into consideration the temporal variability in ET in the periods between satellite image dates. SEBS (Su, 2002) is yet another model that uses the same approach of the surface energy balance. SEBS

was tested using data obtained with the Thematic Mapper Simulator (TMS-NS001) and produced good estimates of ET for cotton and shrubs as well as grass. Other models, such as the Regional ET Estimation Model (REEM), uses ASTER scenes (Samani et al., 2005) and was developed for the purpose of evaluating evapotranspiration from riparian areas. Some of the models, such as TSEB (Kustas and Norman, 1999), use two approaches, coupling together the microwave-derived soil moisture and the radiometric surface temperature to estimate evapotranspiration using TIMS (Thermal Infrared Multi-spectral Scanner) and the L-band ESTAR (Electronically Scanned Thinned Array Radiometer). Another model for evaluating evapotranspiration that has yielded promising results is S-SEBI (Roerink et al., 2000). It uses Landsat-Thematic Mapper data and an approach that depends on the surface energy balance equation.

EVAPOTRANSPIRATION (ET)

ET is the sum of evaporation (water lost from the soil's surface) and plant transpiration; these processes occur simultaneously. The evaporation from an area where a crop is growing is mainly determined by the fraction of solar radiation that reaches the soil surface. This fraction decreases over the growing season as the crop develops and the crop canopy increasingly shades the ground. When the crop is small, water is predominantly lost by soil evaporation, but once the crop is well developed and completely covers the soil, transpiration becomes the dominant process.

ET estimates are used in addressing a number of different problems, and there has been extensive research on this topic, to accurately measure ET, it is necessary to use lysimeters. However, lysimeters are very expensive and are in use in only a few, select locations. Good estimates of ET can be derived from accurate measurements of various

weather parameters, but while weather networks have been widely implemented in the U.S., they only provide information at specific locations. Remote sensing models offer attractive new options for measuring ET and have the added advantage of providing information on the spatial variability of ET.

OBJECTIVE

The objective of this research is to obtain high resolution spatial ET information for a region or a river basin. It uses the energy balance methods based on Landsat and focused on enhancing the procedure of accounting for spatiotemporal variability. The model presented in this research builds on the approach used by Bastiaanssen et al. (1998a and b), but improves the approach's ability to deal with the temporal and spatial variability in ET estimates. The model is called Remote Sensing of Evapotranspiration (ReSET), and it has been applied using Landsat 5 and Landsat 7 imagery.

3.3 MODEL DEVELOPMENT

This section describes the development of a surface energy balance based model, ReSET, for estimating actual crop ET. ReSET is an enhanced ET estimation model based on the methodology implemented in the Surface Energy Balance Algorithm for Land or SEBAL (Bastiaanssen et al., 1998a and b). SEBAL allows the user to arrive at ET estimates using data from only one weather station. ReSET expands upon SEBAL and takes into consideration the spatial variability in weather parameters over a region by using data from multiple weather stations. The ReSET model has the ability to interpolate between the available weather stations in time and space taking into consideration the spatiotemporal variability of the available weather data by generating surfaces of wind

run and ET between weather stations. Consequently, ReSET represents an improved method for looking at ET at a larger scale such as a region or river basin scale.

The model's algorithm computes most of the essential hydro-meteorological parameters empirically from the satellite images. The only weather data it requires is wind run data at known locations (weather stations). In the model, the surface energy balance component, the sensible heat flux H , is solved iteratively, and the ET is derived as the closure term of the surface energy balance equation:

$$LE = (R_n - G) - H \quad (3.1)$$

where R_n = the net radiant energy exchange at the earth's surface, which is called net radiation; LE = the evapotranspiration expressed as latent heat flux density; H = the net surface-atmosphere flux of sensible heat; and G = the soil heat flux density.

The ReSET model is applied in this research to estimate ET using several Landsat 5 and Landsat 7 scenes. ET is computed for each pixel (the size of the pixel depends on the type of satellite image) in the satellite image for the instantaneous time of the image. The process is based on a complete energy balance for each pixel where ET is predicted from the residual amount of energy remaining from the classical energy balance: $ET = \text{net radiation} - \text{heat to the soil} - \text{heat to the air}$. The procedure for how ET can be estimated from satellite imagery is presented in detail in Bastiaanssen et al. 1998a; Bastiaanssen, 2000; Bastiaanssen et al., 2002; Allen et al., 2005; and Tasumi et al., 2005.

In ReSET the algorithm used to calculate the components of the surface energy equation from Landsat imagery can be summarized as follows: Landsat imagery contains visible bands (1, 2, 3), infrared bands (4, 5, 7), and a thermal infrared band (6). From the visible and infrared bands, surface albedo is derived. The Normalized Difference

Vegetation Index (NDVI) is derived from bands 3 and 4, and the surface temperature is derived from the thermal infrared band (band 6). These three components are combined with location parameterization (Digital Elevation Models (DEM) and surface roughness) to calculate the net radiation (R_n) based on a function developed by Bastiaanssen (2000). The soil heat flux (G) is calculated empirically using albedo, NDVI, surface temperature, and sensible heat flux.

The approach implemented in ReSET to estimate the latent heat flux (LE) that yields the instantaneous evapotranspiration relies on selecting two locations in the study region. The first location is called the wet or cold pixel. Water vapor at this location is assumed to be released based on the atmospheric requirement thus the vertical difference in temperature is down to the minimum. Under such conditions the sensible heat flux (H) goes to zero and components of the surface energy balance equation are reduced to net radiation R_n and soil heat flux G and latent heat flux LE ,

$$LE = (R_n - G) - 0 \quad (3.2)$$

The cold pixel represents one of the two extreme pixels used to solve the energy equation. The second extreme pixel is the dry or hot pixel at which ET is assumed to be zero meaning that the latent heat flux is assumed to be zero ($LE=0$). This assumption makes it possible to estimate the sensible heat flux at this location (H) since it is equal to:

$$H = R_n - G \quad (3.3)$$

Knowing the surface temperature at the two extreme pixels (dry and wet pixels), the difference in temperature between the near surface and the air (dt) at the wet (cold) pixel can be assumed to be zero since maximum evaporation conditions are assumed to exist, but for the dry (hot) pixel dt is calculated for air temperature of 20°C . With the

assumption that the dt at the wet pixel equals zero (i.e., $H_{wet} = 0$) the value of H at the dry pixel can be calculated, knowing the values of H at the two extreme pixels H can be calculated for the rest of the image

The first calculation of H is a preliminary estimate, and calculations for H must be repeated until H reaches stability. The instability is caused by the fact that air has three stability conditions (stable, unstable, and neutral). Stability conditions must be taken into consideration during the calculation of H since they affect the aerodynamic resistance to heat transport that directly affects the value of sensible heat flux (H). Once H reaches stability, the latent heat flux can be calculated using the energy balance equation (equation 3.1). The latent heat flux is then converted to estimate the instantaneous evapotranspiration. Assuming that the instantaneous evapotranspiration is constant over a whole day (24 hours) the instantaneous and day evapotranspiration can be calculated as follows:

$$ET_{inst} = LE / (R_n - G) \quad (3.4)$$

Where R_n , G , LE are all instantaneous, then the ET 24-hour is calculated by:

$$ET_{24} = 86,400 * ET_{inst} * (R_{n24} - G_{24}) / L \quad (3.5)$$

where ET_{24} is the 24-hour evapotranspiration, 86,400 is a time conversion from seconds to days, R_{n24} is the 24-hour net radiation, G_{24} is the 24-hour soil heat flux, L is the latent heat of vaporization that is used to convert the energy to millimeters of evaporation. L is based on the surface temperature and represents the energy needed to evaporate a unit mass of water as calculated by the following equation developed by Harrison (1963):

$$L = 2.501 - 0.00236(T_s - 2.73.16) * 10^6 \quad (3.6)$$

where T_s is the surface temperature in kelvin.

3.4 MATERIALS AND METHODS

3.4.1 Study Areas

The ReSET model was applied to two study regions: the lower Arkansas River Basin and the South Platte Basin in Colorado (Figure 19). The study regions have a large amount of irrigated agriculture. In both study regions a variety of crops are grown, but the most commonly crops are alfalfa and corn.

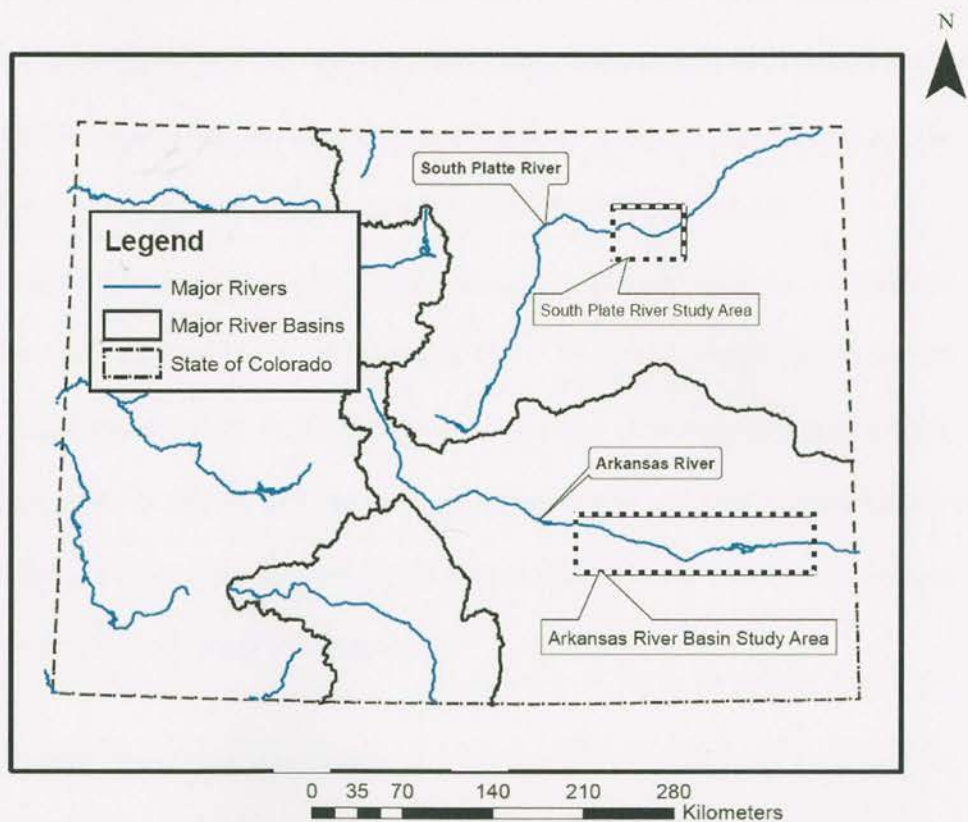


Figure 19. The lower Arkansas River Basin study region in Colorado

3.4.2 Satellite Imagery for the Lower Arkansas Study Region

Seven Landsat 7 scenes were used in this study region in order to cover the entire 2001 growing season, the dates of the scenes span from May 21, 2001 to September 26, 2001. The Landsat scenes were obtained in a raw National Landsat Archive Production

System (NLAPS) format. The images were processed using the ERDAS Imagine 8.7 software. Using the “layer stack” module in ERDAS, the eight separate bands of each image were stacked into one image file (.img) containing the eight bands resampled at a 15 m by 15 m resolution. This resolution matches the resolution of the highest resolution band of the Landsat 7 image, the panchromatic band.

In order to assure that the Landsat scenes were all spatially aligned correctly, they were orthorectified. This is a process by which an image is used as a reference and all other images are adjusted so that they spatially match that reference layer. For this work a USGS orthorectified Landsat image was used as the reference image. The other Landsat images were rectified using the polynomial rectification module in ERDAS.

Clouds affect the calculation of ET when using remote sensing. Even a thin layer of clouds will produce an error in the calculations, since the areas covered by clouds will reflect as cool areas which would be misclassified as actively growing areas with high ET values. The cloud cover in the seven Landsat scenes used in this research ranged from 0% to 14%. A cloud mask was created for each image to eliminate those areas of the images that were covered by clouds or cloud shadows.

3.5 RESET MODEL ENHANCEMENTS

The development of ReSET has focused on improving on other remote sensing of ET models in two ways: enabling the use of data from multiple weather stations and allowing for the calculation of a cumulative ET.

3.5.1 Spatial Interpolation Between Weather Stations

Most of the models that use remote sensing to estimate ET have relied on information from one weather station in the area of interest. Yet, due to spatial variability, using data from one weather station makes these models only appropriate for smaller or homogeneous areas. ReSET provides the advantage that it uses data from multiple weather stations. The ReSET model uses ground data in the form of wind run data to run the model and ET data for calibrating and validating the model. The model captures the spatial variability in ET over large areas by generating a surface for each parameter (wind run and ET) using interpolated values from all the weather stations that fall within the study region.

3.5.2 Temporal Interpolation Between Scenes

The second enhancement offered by the ReSET model is the ability to calculate the cumulative ET over time between the dates of the available Landsat scenes. Most remote sensing of ET models calculate the actual ET at the time when the satellite passes over the area of interest. This calculation is then extended to estimate the ET for that day. ReSET interpolates between available Landsat scenes dates by using a grid of ET values developed based on data from all the weather stations in the study region. In addition, the model calculates a ratio of the ReSET-determined ET (ET_{ReSET}) to the ET at the weather station (ET_{ws}) at the beginning (ET_{Rb}) and at the end of the interpolation period (ET_{Re}). Then, using the calculated ET from the weather stations for each day between the available Landsat scenes for all weather stations in the study area (ET_{d}), a grid of ET is generated that represents the weather station based ET for each day for the study region. The difference between ET_{Rb} and ET_{Re} is divided by the number of days between them

and used to develop a variable correction ratio grid for each day between the available Landsat scene dates. The correction ratio grid is multiplied by the weather station based ET for each day (ET_d) to produce the interpolated model ET for each day (ET_{dm}). The total ET for a given period is calculated as the sum of the daily ET grids (ET_{dm}) for the specified period of time. This technique is explained in greater detail later in this chapter. Figure 20 shows the ET that was calculated for a portion of the lower Arkansas Valley study region using the ReSET model.

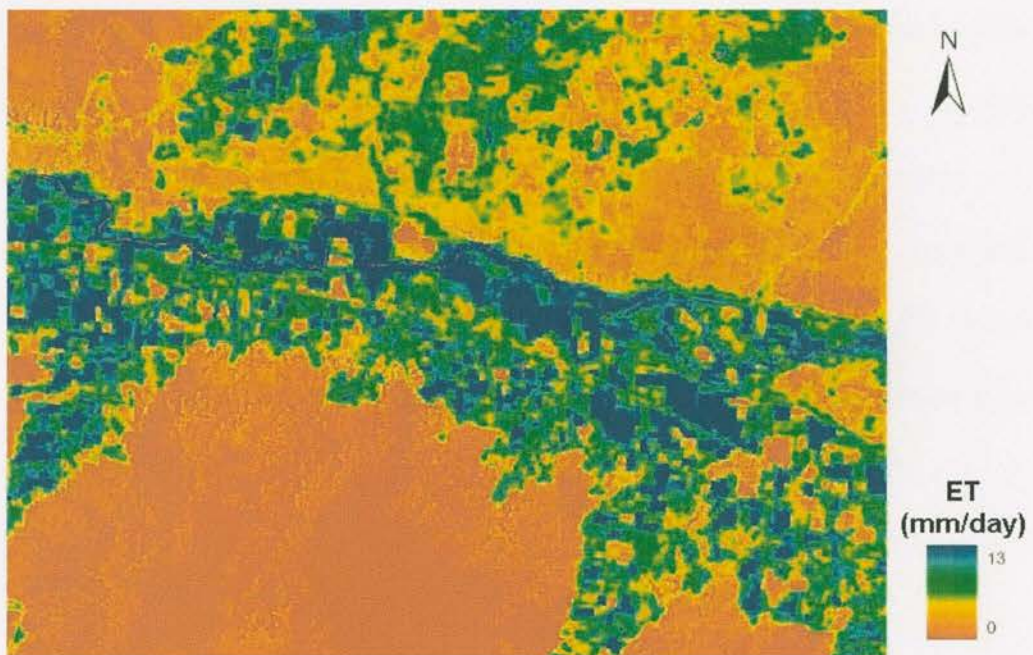


Figure 20. Estimated ET for a portion of the lower Arkansas River Basin in Colorado.

3.6 DATA PREPARATION

The data from the weather stations is used in the ReSET model in two phases. In the input phase, wind run is used as an input to the model. The second phase where the data is used is in producing the cumulative ET for a period of time. Daily ET values calculated from meteorological data measured at weather stations are used to interpolate

an ET grid for each available scene date. The weather station based ET grids are used to interpolate ET between consecutive scene dates. In order to provide the model with this data, a database that holds the raw weather station data was created. The database was developed using a number of SQL scripts that help retrieve the raw weather data from different weather station network websites. Currently, these scripts support downloading data from the following weather networks: the Colorado Agricultural and Meteorological (CoAgMet) network, the Northern Colorado Water Conservancy District Weather (NCWCD) network, the California Irrigation Management Information System and the Arizona Meteorological Network.

The weather data is imported into a consumptive use model: the Integrated Decision Support Group Consumptive Use Model (IDSCU) (Integrated Decision Support Group, 2004) which calculates the crop ET values (the user can select which ET method to use) for different crops and these crop ET values are then stored in the database along with the weather data.

3.7 GIS MODEL INTERFACE

In order to implement the model enhancements associated with taking into consideration the spatial and temporal variability of ET, a GIS module was created to handle the weather station data. The GIS module was integrated into ReSET using ESRI ArcMap 9.1.

The first function of the GIS is to use the locations of the weather stations and query the weather database to obtain the daily wind run at each weather station. The user then specifies a date, the date of the image being processed, and a cell size, and the GIS interpolates a raster layer using the daily wind run values at each weather station. The

result is a GIS raster layer where each cell holds a wind run value that is a result of interpolating between weather stations, the interpolation is carried out using ordinary kriging, the wind run raster layer is used as input to the ReSET model to account for the spatial variability in wind run instead of assuming a uniform wind run value for the whole area.

The second function of the GIS module is calculating the cumulative ET for a defined period of time. This is accomplished by selecting the weather station point theme and the ReSET processed scenes in the order that they occurred during the season. The output of this process is a raster layer of unique ET values (in millimeters) for each cell in the study region. The interpolation technique used in ReSET is similar to the one used in METRIC (Allen et al., 2005) except that METRIC uses only one weather station for interpolation. Consequently, METRIC is able to account for the temporal variation of ET, but ReSET, which uses multiple weather stations, is able to account for the temporal and spatial variability of ET.

The algorithm to calculate the cumulative ET value was developed by calculating the ET ratio at the beginning of the interpolation period as:

$$ET_{Rb} = ET_{ReSETb} / ET_{WSb} \quad (3.7)$$

ET_{Rb} is a grid of the ET ratio between the ReSET ET and the weather station ET at the beginning of the interpolation period between scene dates, ET_{ReSETb} is a grid of the ReSET ET and ET_{WSb} is a grid of the interpolated weather stations ET, for the beginning scene date. A similar ET ratio grid for the end of the interpolation period is calculated:

$$ET_{Re} = ET_{ReSETe} / ET_{WSe} \quad (3.8)$$

Then for each date between the scene dates a grid is generated using the weather station ET values for all weather stations in the study area to generate a grid (ET_{wsd}). The difference between ET_{Rb} (grid of the ratio at the beginning of the interpolation period) and ET_{Re} (grid at the end of the interpolation period) divided by the number of days between them is used to develop the first component of the correction ratio γ which captures the spatial variability of ET

$$\gamma = [(ET_{Rb}-ET_{Re})/N] \quad (3.9)$$

in which N is the number of days between the scenes for which data is being interpolated.

The interpolated ET changes for each day depending on where that day falls between the beginning and end of the interpolation period (T). The interpolated ET grid of weather station ET values (ET_{wsd}) for each day (d) is used to produce the modified ET grid for each day (ET_{dm}) between scene dates:

$$ET_{dm} = [ET_{Rb}-(T * \gamma)] * ET_{wsd} \quad (3.10)$$

The ET_{dm} grid changes from day to day depending on two variables, the first variable is T (location of interpolation date between the scene dates) and the second is the daily grid of interpolated weather station ET values (ET_{wsd}). The total ET for the period is the sum of daily ET grids (ET_{dm}) for all days between the scene dates (N):

$$ET_a = \sum_1^N ET_{dm} \quad (3.11)$$

The final product is a raster layer of the cumulative ET in millimeters for the days between the selected scenes.

3.8 APPLICATION OF THE RESET MODEL

ReSET was applied to two locations in Colorado (Figure 19). Weather station data were obtained for cross validating the model and estimating its relative accuracy.

To show the difference in the model results when using multiple weather stations instead of a single weather station as well as the spatial technique used to generate an ET grid for a region, the model was first applied to the Arkansas River Valley in southeast Colorado. A Landsat 7 scene from June 22, 2001 was used to calculate the daily ET values. The results of the ReSET model were compared to the daily ET values for alfalfa from the CoAgMet weather stations. Using seven Landsat 7 images for the lower Arkansas River Basin study area (May 21, 2001; June 6, 2001; June 22, 2001; July 8, 2001; July 24, 2001; September 10, 2001; and September 26, 2001) a seasonal ET was calculated for each cell and compared to the values from the weather stations.

A June 22, 2001 Landsat 7 image was processed using a single weather station located near the middle of the image: the Colorado State University, Rocky Ford weather station. The ET from this station was used to represent the weather station ET for the whole region. The ReSET model results are displayed in Figure 22. Another ET estimate using the ReSET model was generated using five weather stations located within the boundaries of the image, and it is shown in Figure 23.

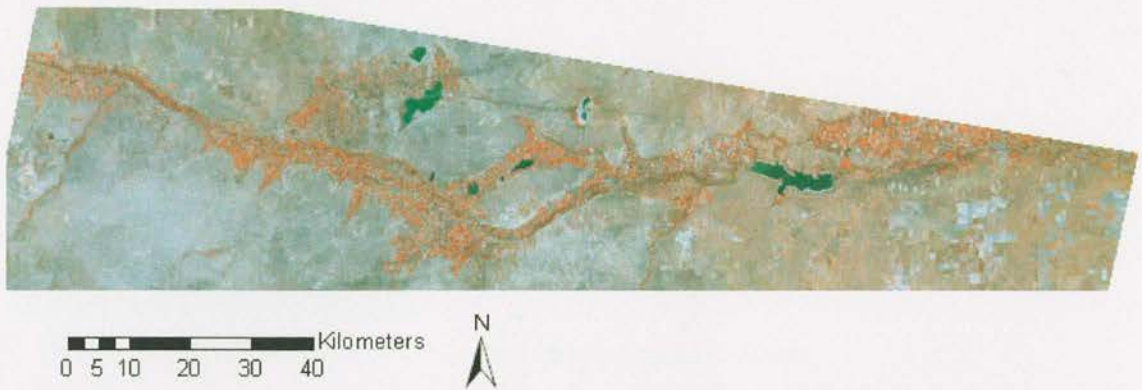


Figure 21. The satellite imagery for the study area on 6/22/2001.

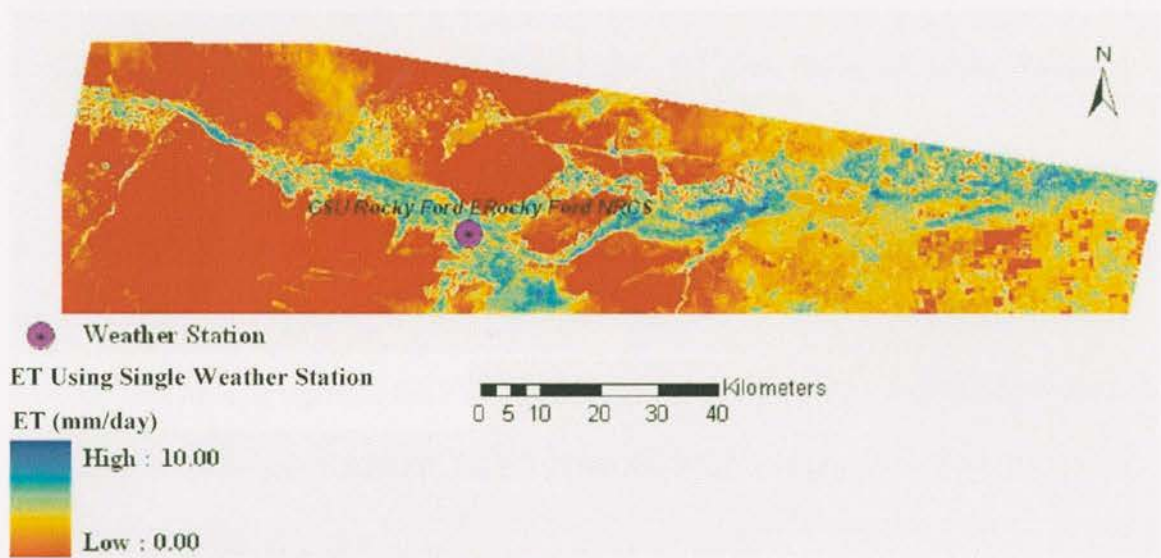


Figure 22. Colorado's Arkansas River Valley ET Grid Using a Single Weather Station on 6/22/2001.

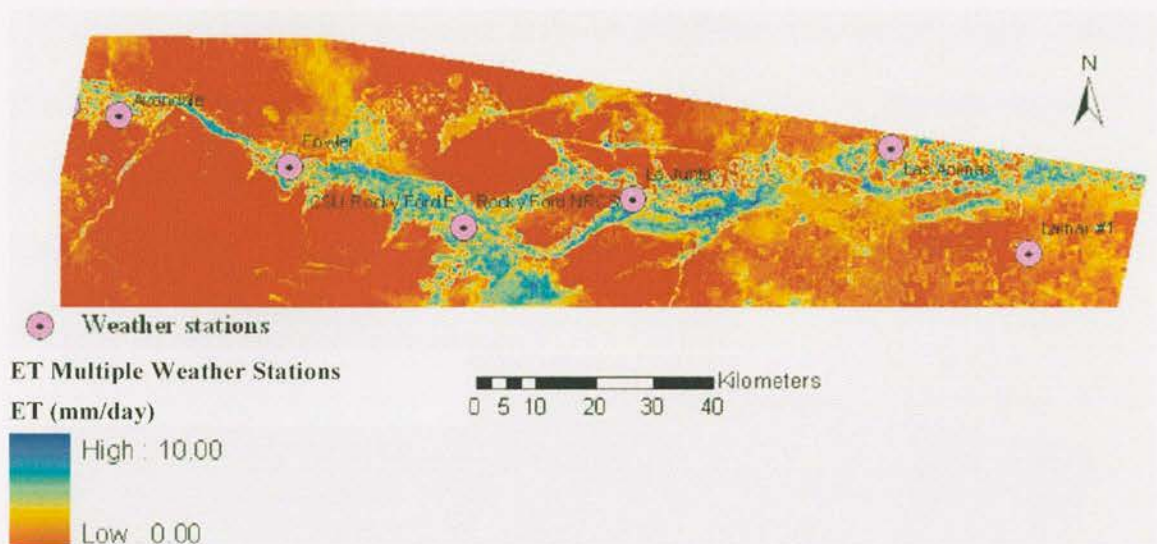


Figure 23. Colorado's Arkansas River Valley ET Grid Using Multiple Weather Stations on (6/22/2001).

To show the difference between the daily ET estimated using ground data from multiple weather stations (ET_{mws}) and the daily ET estimated using ground data from a single weather station (ET_{sws}), a wind grid generated for the study area (Figure 24) was used in the model to estimate the ET (ET_{mws}) with multiple weather stations. The satellite imagery that was used to estimate the ET (June 22, 2001) is shown in Figure 21.

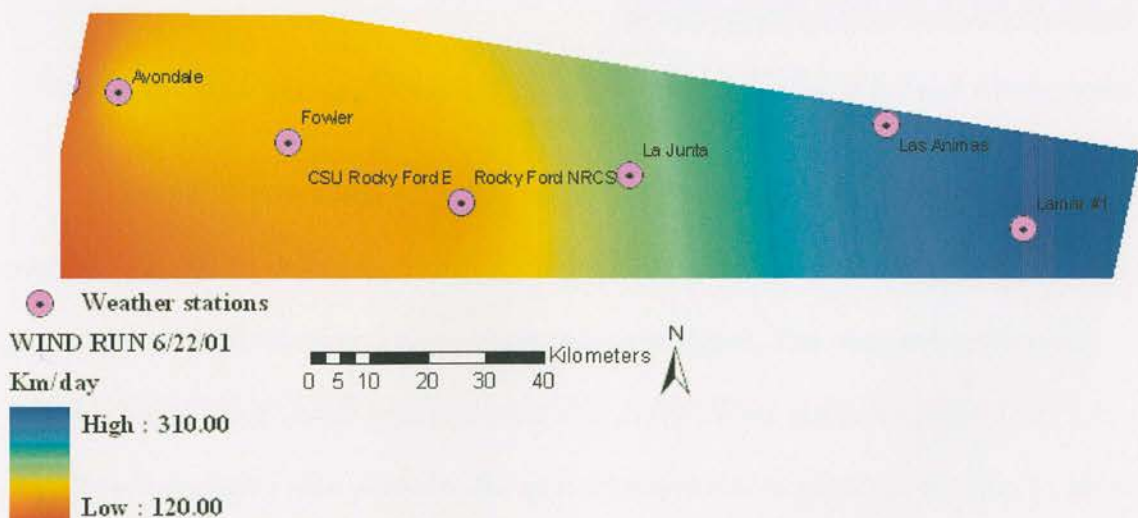


Figure 24 . Spatial distribution of wind run in the study area on 6/22/2001.

Figure 25 shows the difference in the ReSET ET between using a single weather station and multiple weather stations in this region ($ET_{mws} - ET_{sws}$). The same figure zooms in on an area to show the spatial variability of ET even inside some of the individual fields.

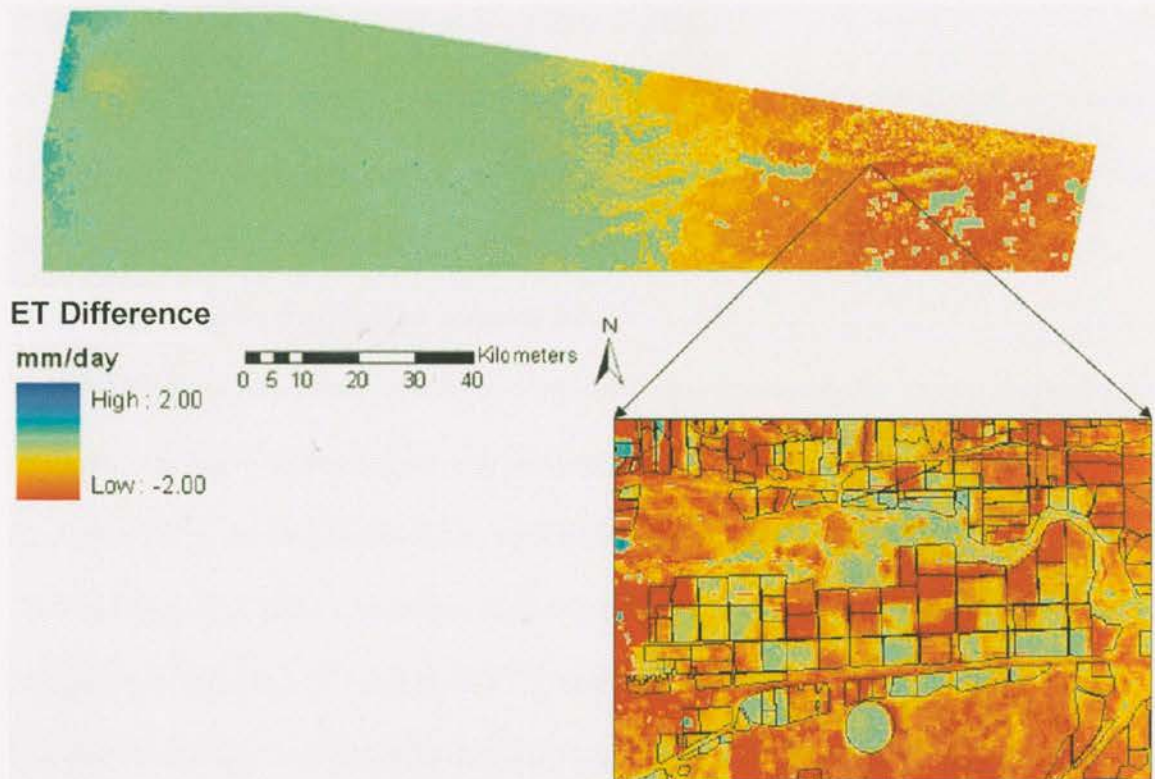


Figure 25. The difference in daily ReSET ET ($ET_{mws} - ET_{sws}$) for the whole study area and a zoomed area.

One of the major enhancements of the ReSET model is the use of multiple weather stations for obtaining wind run. Figure 24 clearly shows the variability in wind run within the 160 kilometers or so displayed in the figure. The wind run varied from 122.3 km/d to 273.53 km/d which is more than 220%. Wind run has a direct impact on ET. Therefore, being able to model the spatial variation in wind run over a region allows ReSET to capture the spatial variability of ET associated with it. For instance, the difference in ET estimated when using the June 22, 2001 Landsat 7 image in conjunction

with the wind run data obtained from only the station at the center of the image and from ET estimated using multiple weather stations amounts to ET of +/- 20 %. If not using the ReSET approach, the error can be reduced by selecting smaller areas around each weather station to be processed independently or using a grid of wind run developed using Thiessen polygons around each weather station.

The temporal resolution of Landsat is every 16 days which means that, assuming no cloud cover which would prevent the use of a scene, a remote sensing ET estimate can be obtained approximately every 2 weeks. However, daily ET estimates are needed in order to estimate monthly and/or seasonal ET.

Using the procedure previously described, the cumulative ET for the study area in the Arkansas River Valley region was generated and is shown in Figure 26. The CoAgMet ET at the Rocky Ford weather station (Figure 26) during the period from May 20, 2001 to June 6, 2001 sometimes varies significantly over a short period such as the changes between May 30th and June 2nd. During this four day period ET changed from less than 6 mm/day to over 9 mm/day, this is an increase of over 50%, such temporal variations strongly support the use of the weather station ET's as a daily correction ratio for interpolation between scenes rather than just using a linear interpolation.

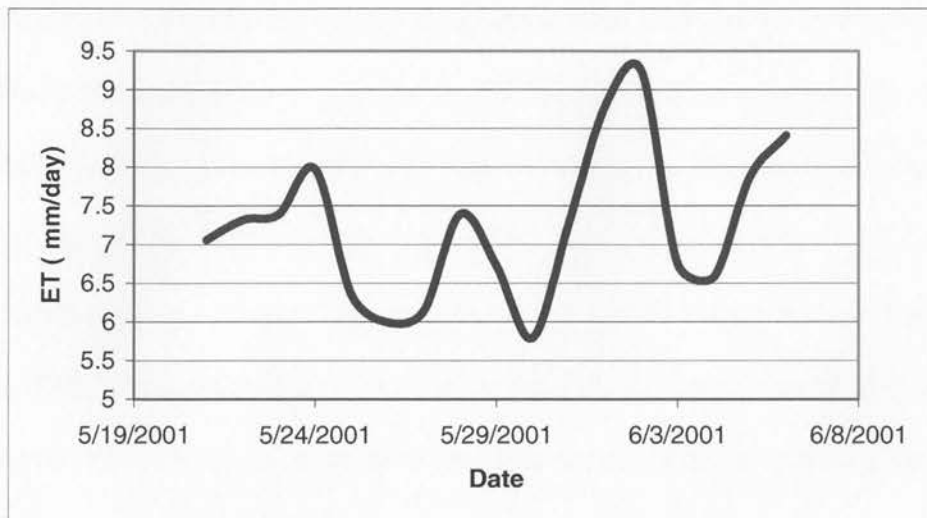


Figure 26. ET estimated at the CoAgMet CSU Rocky Ford weather station.

Crop growth can change dramatically during the vegetative growth stage. As a result, ET can increase significantly in a month of lush growth, and during senescence ET can decrease significantly. These changes in growth rates can introduce errors which may result in either overestimating or underestimating the cumulative ET in the time span between two satellite scenes, especially if only one satellite image is being used per month. Therefore using the modified interpolation method presented in this research will take into account such temporal and spatial variability in ET. This allows the model to adjust for changes in ET between scene dates and improves seasonal ET estimates.

An example from the South Platte Basin in Colorado (Figure 19) illustrates the advantage of calculating the seasonal ET using the proposed method that relies on the weather stations as an interpolation index versus using a simple linear interpolation between two scenes. This area has a denser network of weather stations than the study area in the Arkansas River Basin. Figure 27 shows the cumulative ET calculated using the ReSET approach and the cumulative ET calculated using the linear interpolation

approach. The two scenes used for this comparison were taken on 6/13/2004 and on 6/29/2004. When comparing the cumulative ET for this 16-day period, the linear interpolation approach produces ET estimates that are higher than the ReSET approach. The linear interpolation approach gives a total ET that is larger than the ReSET approach with as much as 60 mm (Figure 28), an estimate that is 50% higher than the ReSET estimate. This higher estimate is a result of the fact that the linear interpolation approach does not take into consideration the changes in the weather occurring during the 16-day period. Figure 29 shows that the NCWCD daily reference ET for this period varied between 1 mm and 8 mm at some of the weather stations. This temporal and spatial variation in ET significantly reduced the cumulative ET calculated by the ReSET model and created the difference between the ReSET estimate and the linear interpolation approach. This example shows the potential for significant errors when using linear interpolation versus taking into account the daily variation in ET during an interpolation period.

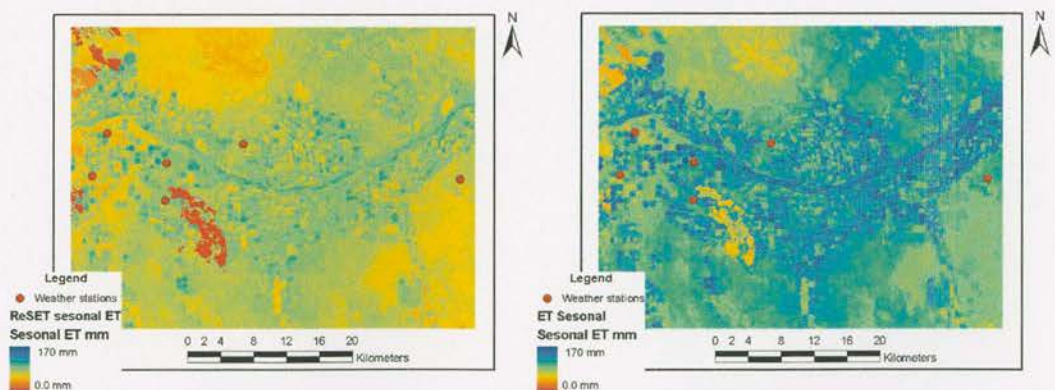


Figure 27. Cumulative ET calculated using ReSET and calculated using simple averaging.

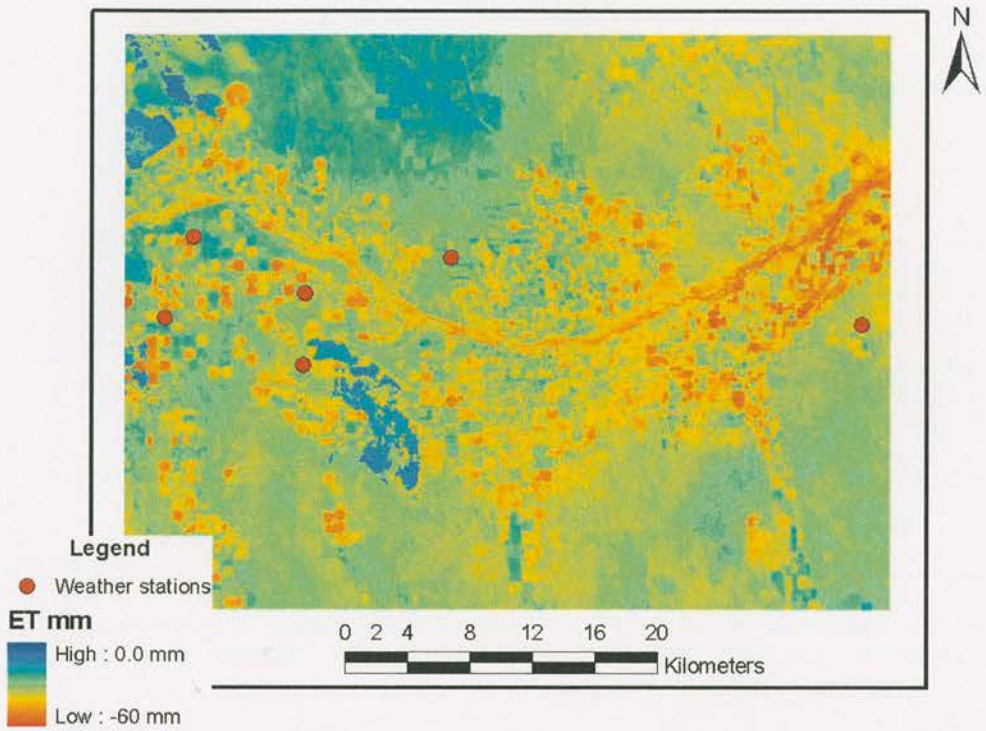


Figure 28. Difference in cumulative ET between ReSET and average.

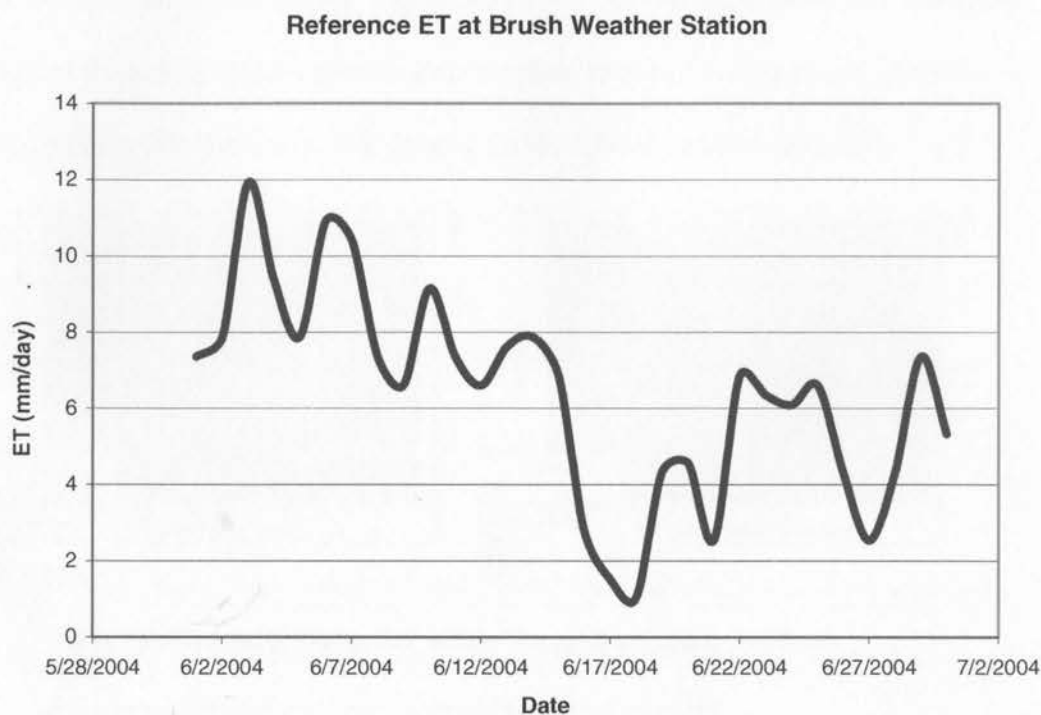


Figure 29. Variability in E_Tr at the Brush weather station over the interpolation period.

3.9 EVALUATING THE IMPACT OF REDUCING THE NUMBER OF WEATHER STATIONS

Using multiple weather stations when calculating cumulative ET for areas with significant spatial variation in ET makes a significant difference in the results. To compare the different outcomes obtained by using all available weather stations versus using fewer weather stations, we offer an example from the South Platte River Basin study area. The area contains six weather stations. ET estimates for a period of time were calculated using ReSET with all six weather stations and then using only three weather stations. Figure 30 shows the results of using all six weather stations as well as the results

when three weather stations are used. Figure 31 shows that the differences in cumulative ET estimates were mainly around the missing weather stations (as expected). The level of discrepancy between the estimates will depend on the spatial variability in ET.

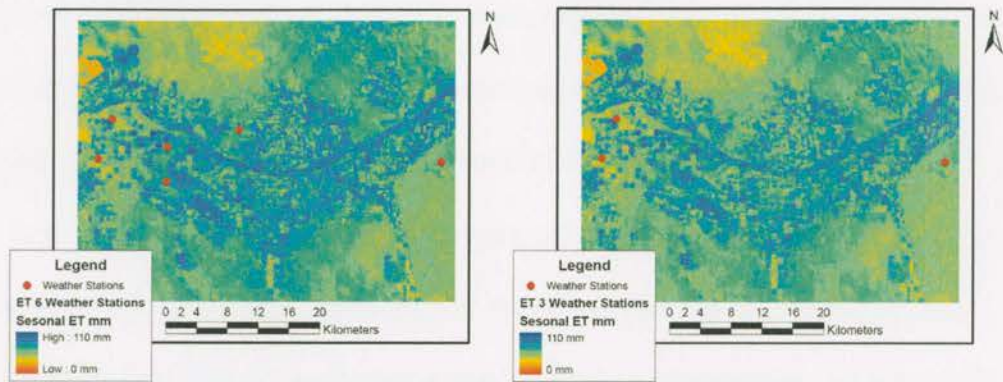


Figure 30. Cumulative ET using 6 and 3 weather stations.

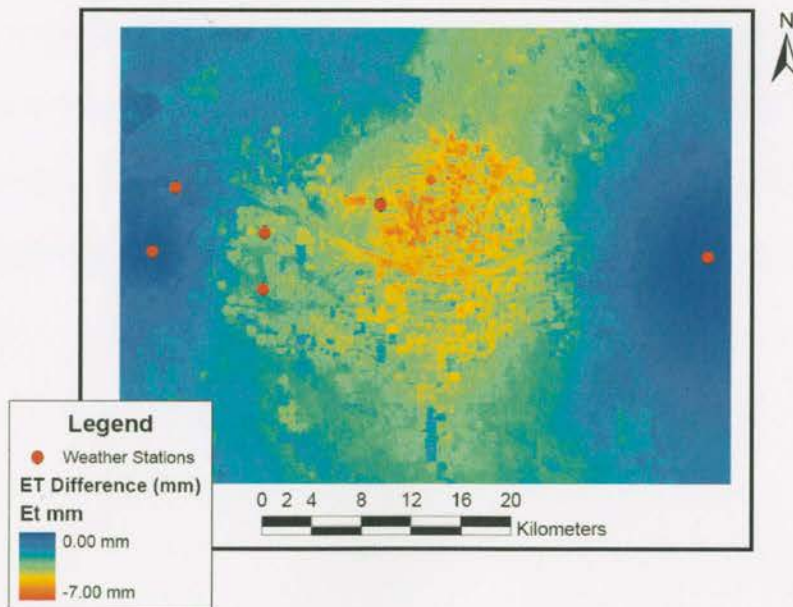


Figure 31. Difference in cumulative ET when using 6 weather stations versus 3 weather stations

3.10 CONCLUSIONS

Using wind run data from a single weather station to estimate aerial ET can introduce significant errors. In the cases presented in this chapter, these errors in the estimates of ET can be as much as 20%. Introducing the ability to use multiple weather stations in calculating the ET from remote sensing using the ReSET model enhanced the ET prediction and reduced this potential source of error.

Spatial and temporal variability between satellite scenes accounts for daily changes in ET which can affect seasonal ET estimates. Introducing the use of daily values of ET estimated from multiple weather stations as interpolation indexes result in estimates of seasonal ET that account for spatial variability. The model developed as part of this research, ReSET, uses a grid approach that utilizes multiple weather stations creating a surface that adapts to the spatial variability of weather conditions over a targeted area. The methodology and results presented here extend the application of remote sensing of ET to areas where significant spatial variation in weather data occurs.

4. A REMOTE SENSING - GIS APPROACH TO EVALUATE THE EFFECTS OF SOIL SALINITY ON EVAPOTRANSPIRATION

4.1 ABSTRACT

Evapotranspiration (ET) is assumed to be one of the processes important to crop production that is affected by soil salinity. This chapter describes the use of geographic information systems (GIS) and remote sensing techniques to investigate the relation between ET and soil salinity in agricultural areas. Soil salinity data was obtained from global positioning system-referenced ground measurements in several corn fields in the Arkansas River Basin in Colorado. Evapotranspiration was calculated using a remote sensing model named Remote Sensing of Evapotranspiration (ReSET) that is based on the concept of surface energy balance. Evapotranspiration values were regressed against the spatially corresponding soil salinity values to develop a relation between ET and soil salinity. The ET values correlate well with the soil salinity levels in the study region, with a correlation coefficient of up to 0.86.

4.2 INTRODUCTION

There are many factors that limit crop development and reduce crop yield in agricultural lands. These factors include soil salinity, poor land fertility, limited application of fertilizers, presence of hard or impenetrable soil horizons, plant diseases and pests, and poor soil management (FAO, 2005).

Salt concentrations rise when salts present in the soil and the surface and ground water accumulate in certain areas. Increases in salt concentration affect several processes important to plant growth including evapotranspiration (ET). ET is a vital process for plant growth and any perturbation in this process will affect plant growth and yield. High levels of salts in water available for plants affect the osmotic pressure that enables the plant to absorb water from the soil. The higher the level of salinity in the soil water, the harder plants must work to extract water from the soil. This leads to reduced amounts of water that can be used by the plant and hence a decrease in the plant's ET.

Extensive research has been conducted investigating the impacts of soil salinity on agriculture. Recently remote sensing and GIS have been used to evaluate the extent and impacts of soil salinity on agricultural lands (Peng, 1998). Applying remote sensing data and techniques has dramatically improved the ability to monitor or evaluate the efficiency of cropping production systems in saline areas (Poss et al., 2006). Remote sensing techniques have been used to diagnose general salinity problems (Everitt et al., 1977; Ripple et al., 1986). Stewart et al. (1976) concluded that the effect of salinity on yield is a direct result of reduced water uptake and transpiration. Other methods for calculating plant water uptake were examined by Cardon and Letey (1992a, 1992b, and 1992c). According to their findings, the most accurate representation of the effects of salinity on water uptake was achieved by using an empirical equation based on the soil water potential. The Food and Agriculture Organization (FAO) Irrigation and Drainage Paper 56 (Allen et al., 1998) presented a function that predicts the reduction in evapotranspiration caused by soil water salinity. They accomplished this combining yield-salinity equations from the FAO Irrigation and Drainage Paper 29 (FAO, 1985) and

yield-ET equations from FAO Irrigation and Drainage Paper 33 (FAO, 1979). The resulting equation provides an approximation of the reduction in evapotranspiration expected under a variety of salinity conditions. However, very few or no studies have used remote sensing and ET models to develop a direct relationship between soil salinity and ET.

In this research, remote sensing and GIS techniques were used to investigate the relationship between soil salinity and ET in a study area in the Arkansas River Basin in Colorado. As part of this research, regional surface fluxes (e.g. evapotranspiration) using remote sensing approaches were implemented and enhanced. The evapotranspiration estimates were calculated using a surface energy balance model. In the past decade a number of researchers have developed models that use this general concept (e.g. see Kustas et al., 1996; Bastiaanssen et al., 1998; Timmermans et al., 2004; and Allen et al., 2005). These models use satellite imagery, such as Landsat, AVHRR, ASTER and MODIS (Nishida et al., 2003) to generate estimates of ET.

For this study a remote sensing of ET model called ReSET was developed to explore correlations between soil salinity and ET. Both soil salinity and ET are spatially distributed over large areas, and using a remote sensing-GIS approach makes sense in dealing with data that is spatial in nature. Once the relationship between ET and soil salinity is developed, this knowledge can be used to quantify the impact of soil salinity on ET for certain crops. In this research, the crop that was selected was corn.

4.3 METHODOLOGY

The approach developed as part of this research is to generate an ET surface for each field in the study area using the surface energy balance-based model ReSET. The energy balance components are estimated using Landsat imagery. The ET values are then correlated with spatially collocated, field-collected soil salinity values. The soil salinity field data was collected at spatially referenced points. Each point was given an x-y coordinate using a global positioning system. A geographic information system was then used to generate the soil salinity coverage from the field soil salinity points. Once a set of points showing the ET and the soil salinity were obtained a regression line was developed between ET and soil salinity.

4.3.1 Selecting Fields to Study

Six corn fields located in Colorado's Lower Arkansas River Basin were selected to study the relationship between soil salinity and ET. Corn fields were selected for study because corn has a medium tolerance for soil salinity and has a fairly long growing season (over 110 days), making the effects of soil salinity on biomass and yield significant enough to be detected fairly easy. Corn shows the damaging effects of salinity when it is grown in soil with salinity levels as low as 2 dS/m. However, if gypsum is present in the soil, which is the case in the Lower Arkansas River Basin, corn does not begin to exhibit damage until higher salinity levels (maybe 3 dS/m) are reached. As salinity levels progress beyond this threshold, damage to the biomass and yield of corn plants increases. With soil salinity levels of 8 dS/m or greater, the crop starts to exhibit extreme damage.

Study fields were selected to be representative of soil salinity variability existing at the field scale. For example, a couple of the fields selected (fields 80 and RR) have the full spectrum of soil salinity levels (1 dS/m to 8 dS/m). The variability in these two fields provides a good opportunity to capture the correlation between ET and soil salinity over a large spectrum of values. Fields 6, 77 and 23 are homogenous fields that have low levels of soil salinity (under 4 dS/m). The impact of salinity on the corn crop in these fields is minor and almost invisible. Therefore, ET was largely unaffected by salinity in these fields. In contrast, field 40, which had a large range of soil salinity levels including areas where salinity levels were in excess of 12 dS/m, exhibited substantial problems. Parts of the field were barren, unable to sustain the crop.

By using satellite imagery as a data source, the impacts of soil salinity on the appearance and biomass of the plant can be detected; however, if the soil salinity level is low enough that it has very little impact on the crop, for instance, salinity levels of 3 dS/m or less, then the impact on the crop falls outside the lower detection limit of the satellite image. On the other hand, if the soil salinity level is too high (above 8 dS/m), to the point of being extremely damaging to the crop, these values fall outside the upper detection limit since in many instances very little or no crop actually grows in these areas. Therefore, no relation is developed to cover salinity levels outside the detection limits.

4.3.2 Estimating Evapotranspiration

ET is defined as the total water transferred into the atmosphere from the soil surface (evaporation) and from the surface of the vegetation (transpiration). When the crop is small, water is predominately lost by soil evaporation, but once the crop is well developed and completely covers the soil, transpiration becomes the main process.

ET is not easy to measure. Specific devices and accurate measurements of various physical parameters or the soil water balance from lysimeters are required to determine ET (Allen, et al., 1998). Most methods for determining ET are costly and require a great deal of accurate data which makes their application only practical for small areas. Recently, new methods of estimating ET using remote sensing-based models and an energy balance equation have been developed (Kustas et al., 1996; Bastiaanssen et al., 1998; Timmermans et al., 2004; and Allen et al., 2005). These methods are attractive because they tend to involve less field data collection and therefore save time and money.

4.3.2.1 Energy Balance and Microclimatological Methods

Evaporation of water requires energy, either in the form of sensible heat or radiant energy. That is why the evapotranspiration process is reliant on energy exchange at the vegetation surface and is governed by the amount of energy available at this surface. This concept makes it possible to predict the evapotranspiration rate using the surface energy balance: the energy arriving at the surface should equal the energy leaving the surface for the same time period. The equation for an evaporating surface can be written as:

$$\lambda ET = R_n - G - H \quad (4.1)$$

R_n is the net radiation, H is the sensible heat, G is the soil heat flux and λET is the latent heat flux.

In this research this energy balance approach is used to estimate ET. A remote sensing-GIS based model (ReSET) was developed for this purpose. ReSET is a model used to develop a surface energy balance algorithm based on reflectance information from Landsat satellite imagery. The model and processing of the imagery was carried out

using ERDAS Imagine 8.7. The model output is a raster layer that contains an estimate of the 24-hour ET value for each pixel of interest.

Image Georectification

The images were georectified using polynomial models. Ground-control points (GCPs), such as road intersections, canals, and field boundaries were needed for the georectification, and these points were provided by geographic information system shapefiles and GPS points.

Calculating the ET Surface

A Landsat 7 image for the study area taken on July 8th, 2001 was used to calculate ET. The Landsat 7 spectrum contains eight bands: three visible bands, a near infrared, an infrared, a thermal, and a panchromatic band. All the bands have a cell size of 30m by 30m except for the thermal band that has a cell size of 60m by 60m and the panchromatic band, which has a cell size of 15m by 15m. The July 8th Landsat image was selected for use because at that date the corn was almost at full cover and the image was almost free of cloud cover. The image was georectified and processed using the ReSET model to generate estimates of ET for each pixel.

4.3.3 Soil Salinity Data

Soil salinity data was collected as part of a project to study the impact of soil salinity and waterlogging on agriculture in the Lower Arkansas River Basin (Gates et al., 2006). The soil salinity was measured in the field using an electromagnetic device, an EM-38EE, connected to a differential GPS. The EM-38EE measures the electromagnetic conductivity (EC) of the soil. The EC values are then converted to salinity units (dS/m).

The EM-38EE usually measures the soil EC in two profiles, horizontal and vertical. The horizontal is the shallow soil profile (0.75 m) and the vertical is the deep soil profile (1.5 m). The coordinates of each sample point were recorded using a GPS, and these coordinates were used to generate a GIS point coverage for each field.

4.3.4 Combining the ET Surface and Soil Salinity Points

The output of the ReSET model is a raster layer for the whole study area with the calculated values of ET in millimeters/day for the 24 hour period of the date the image was acquired. The raster layers were then clipped to the boundaries of the selected fields. Each raster layer was converted to GIS polygons with each polygon retaining the model calculated ET value. GIS ET polygons were overlaid on the soil salinity points (Figure 32). Using a tool developed in ArcGIS the statistical mean of the soil salinity points within each ET polygon was calculated and saved in the table of attributes of the GIS ET polygon coverage. The table of attributes was then exported to a dbf file to develop a regression between the ET values and the corresponding soil salinity values.

4.4 RESULTS AND DISCUSSION

The analysis was first conducted at the field scale and then integrated over multiple fields.

Field Scale

Field 80

Field 80 is a corn field with an area of 113,400 square meters (28 acres). Figure 33 shows plan views of this field using a 4 m resolution Ikonos scene in (a) true color and (b) false color. The field has a full soil salinity spectrum which enables the monitoring of

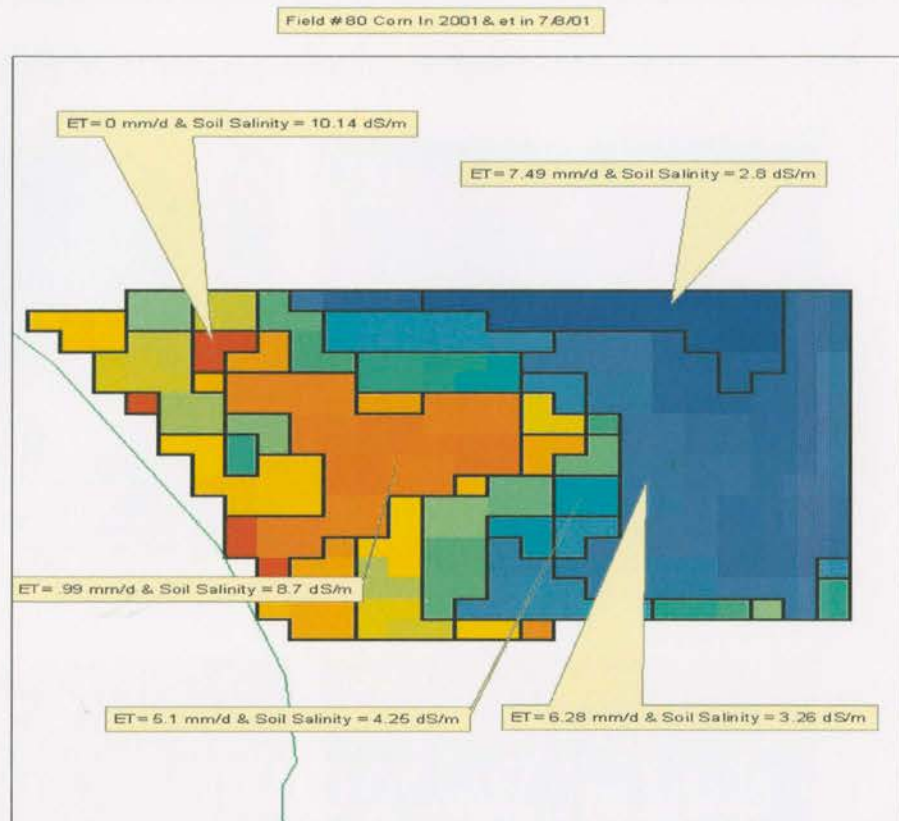


Figure 32. ET polygons with corresponding average soil salinity values for each polygon in field 80.

a smooth gradual decrease in ET corresponding to increases in soil salinity. In this field soil salinity levels increase from a low of 2.5 dS/m, which has no detectable effect on the crop, to a high of 8.7 dS/m, which has severe impacts on corn, reducing some planted areas to mostly bare soil.

Figure 33(c) shows a plan view of field 80 on a false color 30 m resolution Landsat 7 image. The Landsat 7 image was used as input to the ReSET model to estimate the ET values shown in Figure 33(d). Figure 33(d) shows low values of ET in the areas colored the yellow and orange, those areas which are most affected by soil salinity. The

ET values increase in the area less affected by soil salinity (light to deep blue colors). The values of soil salinity levels were regressed against the ET values in two ways. First,

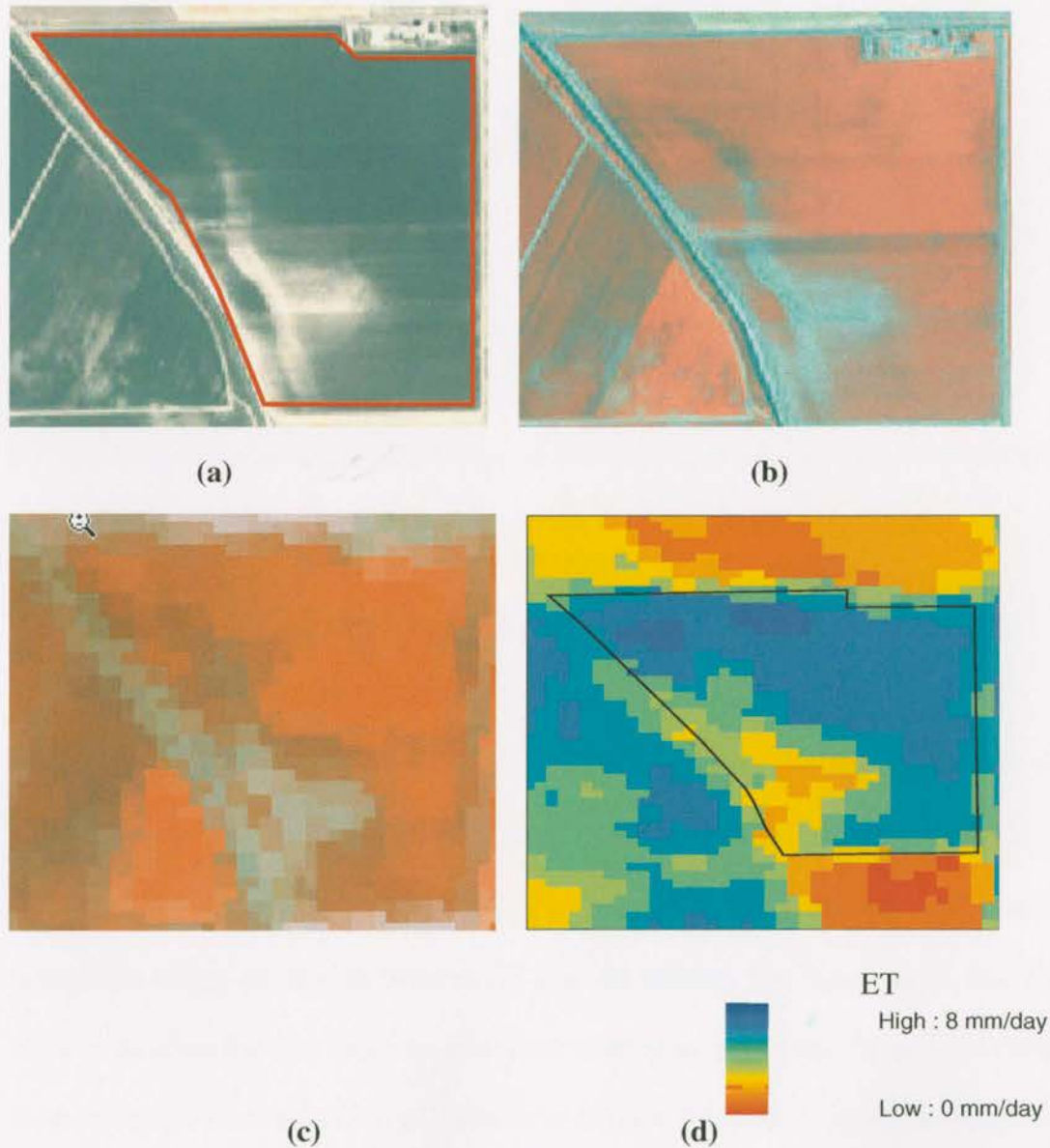


Figure 33. Plan view of field 80 from two different satellite scenes.

zonal regression was used: all the measured soil salinity points that fall in a zone are given one ET value that is represented by one point on the regression graph. The results of this analysis are shown in figure 34. Secondly, the regression for each salinity point was performed independently, meaning that each pixel from the evapotranspiration grid

was combined with the measured soil salinity point that falls within this pixel and represented by a point on the regression graph shown in figure 35.

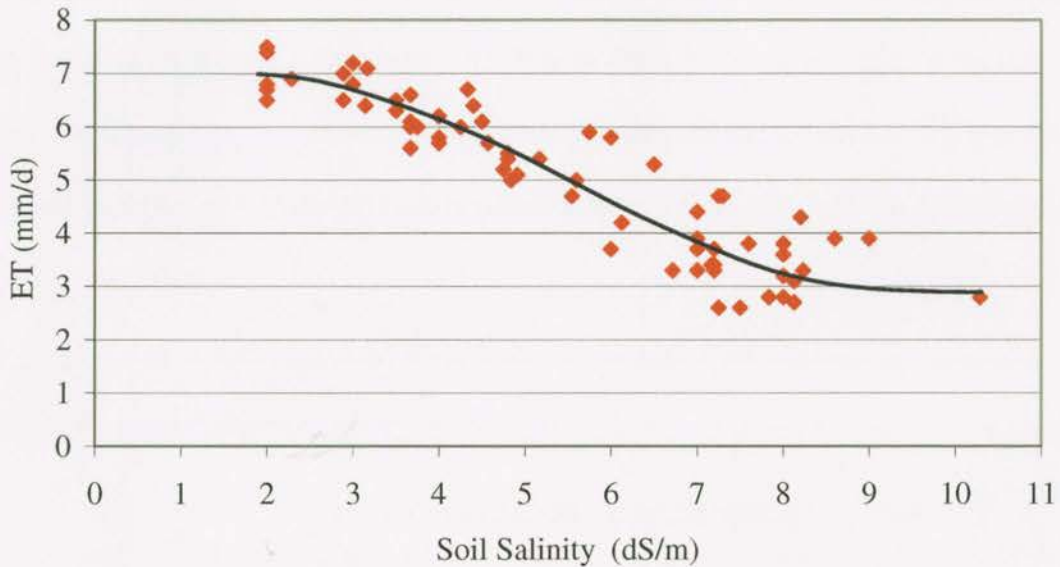


Figure 34. Soil salinity levels versus ET values in field 80 (zones to points).

The relation between the soil salinity and ET is indicated by the correlation coefficient (R). The correlation R statistic measures the linear correlation between two variables in figure 34 with an optimal value of 1.0. As shown in the figure, there is a clear correlation between soil salinity and ET. The correlation coefficient has a value of 0.86, implying a strong correlation between ET and soil salinity. The figure shows that the relation between the two variables is an inverse relation: a decrease in the ET corresponds to an increase in the soil salinity. The inverse relation for field 80 is expressed by the following equation:

$$ET = 0.0172(SS)^3 - 0.2806(SS)^2 + 0.7585(SS) + 6.448 \quad (4.2)$$

$$R^2 = 0.86$$

The same relation is also displayed in figure 35, the difference between figure 34 and figure 35 is that in figure 34 we are correlating the mean value of all salinity points

that fall in the same ET zone. An ET zone can consist of several pixels that have the same ET value. In figure 35, the mean value of the soil salinity points falling within one pixel are compared to the ET of this pixel. The pixel dimensions depend on the type of images used. In this case the pixel dimensions are 30m by 30m. In the two graphs, there is a higher correlation and less scatter when correlating soil salinity points to ET zones than when the mean value of the soil salinity points falling within one pixel are compared to the ET of the pixel.

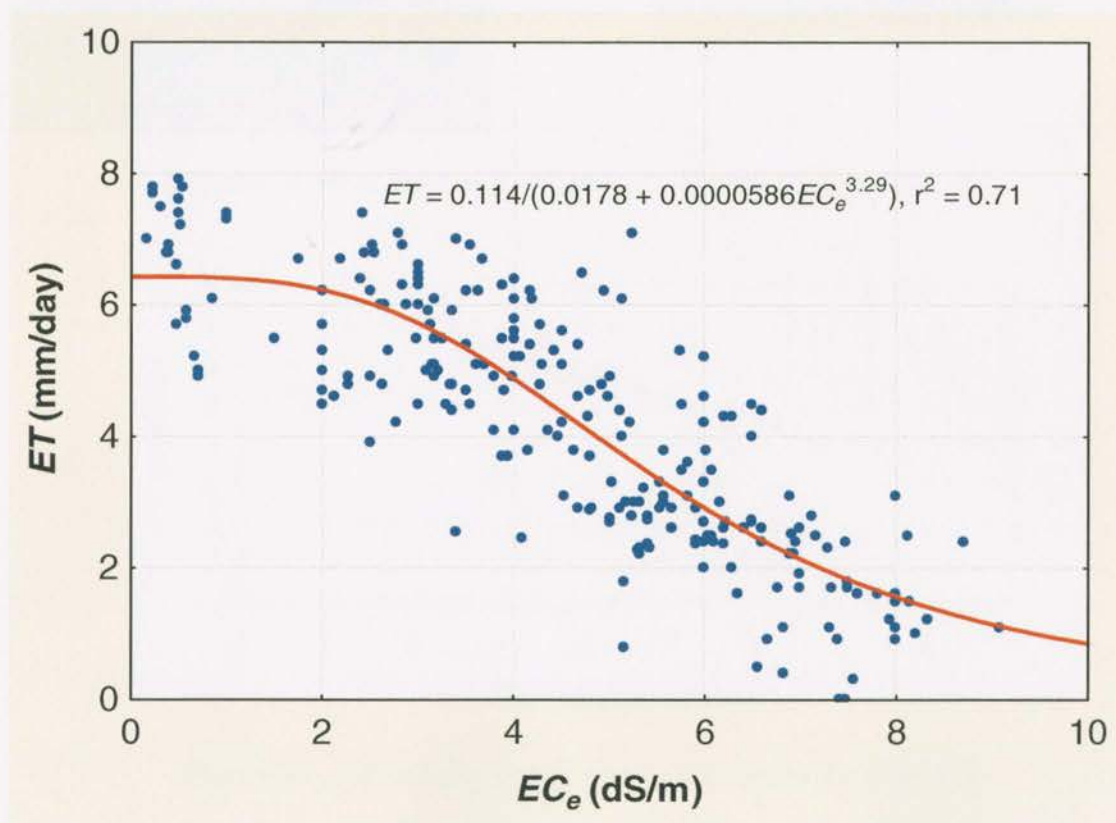


Figure 35. Soil salinity levels versus ET values in field 80 (pixel to point).

Field RR

Field RR is a corn field with an area of 60,750 square meters (15 acres). Like field 80, field RR displays a full spectrum of soil salinity values. A smooth gradual decrease in ET corresponding to an increase in soil salinity was monitored. In this field soil salinity

levels increase from a low of 2.6 dS/m, a level which has no detectable effect on the crop, to a high of 8.5 dS/m, which damages the corn crop reducing these areas to mostly bare soil.

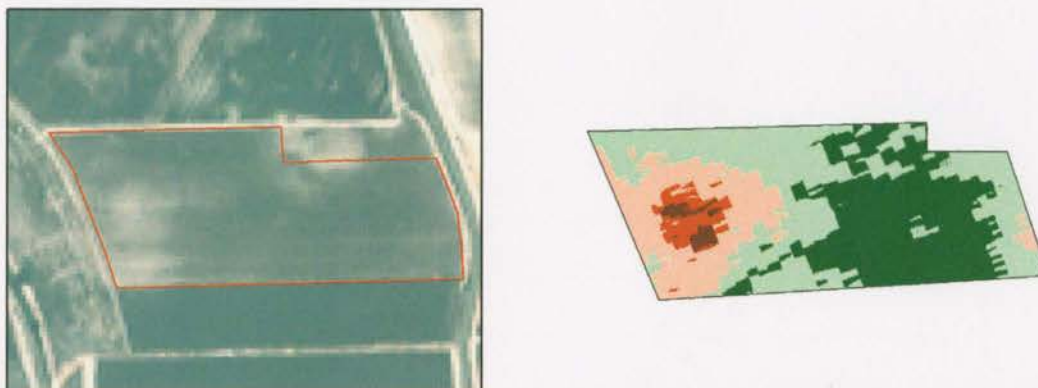


Figure 36. Plan view and soil salinity distribution in field RR.

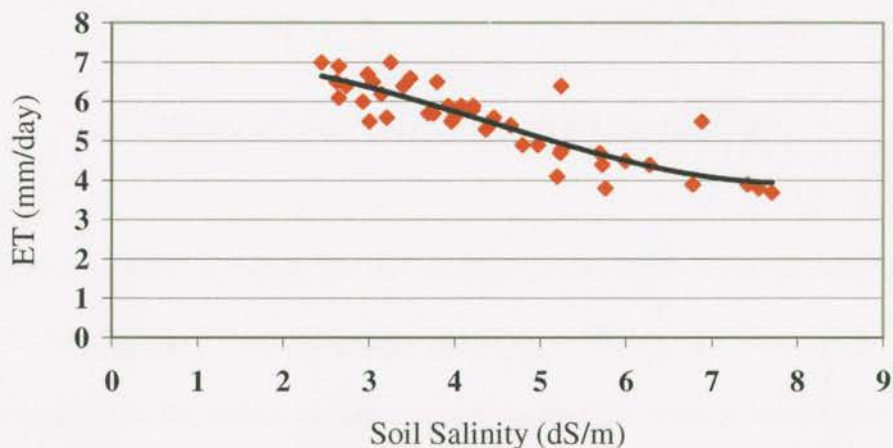


Figure 37. Soil salinity levels versus ET values for field RR.

$$ET = 0.0178(SS)^3 - 0.2339(SS)^2 + 0.3634(SS) + 6.9 \quad (4.3)$$

$$R^2 = 0.75$$

Field 40

Field 40 is a 101,171 square meter (25 acre) corn field. The full spectrum of soil salinity is represented in field 40. In addition in field 40, the soil salinity reaches

extremely high levels. All soil salinity points that had values higher than 8 dS/m had to be excluded because they exceeded the detection limit (no corn was present). However, the areas of field 40 that could be used still exhibited a good correlation between ET and soil salinity levels as shown in Figure 40.

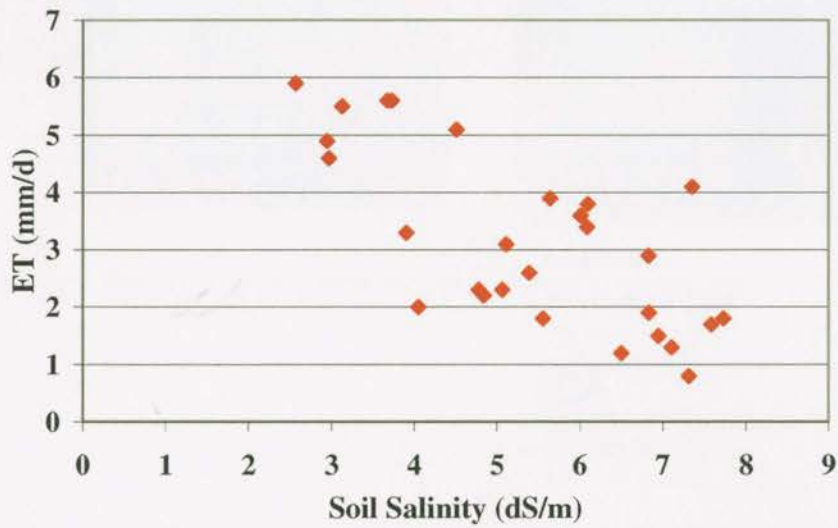


Figure 38. Soil salinity versus ET for field 40

Field 23

Field 23, shown in Figure 39, covers an area of 54,000 square meters (12.85 acres). The field has very low soil salinity resulting in almost no effect on ET. As the field is homogenous, the points are all clustered around the zone of low salinity and high ET (Figure 40). Therefore, although, this field does not display significant variability, field 23 does support the concept of the research by showing that low soil salinity has very little impact on ET.

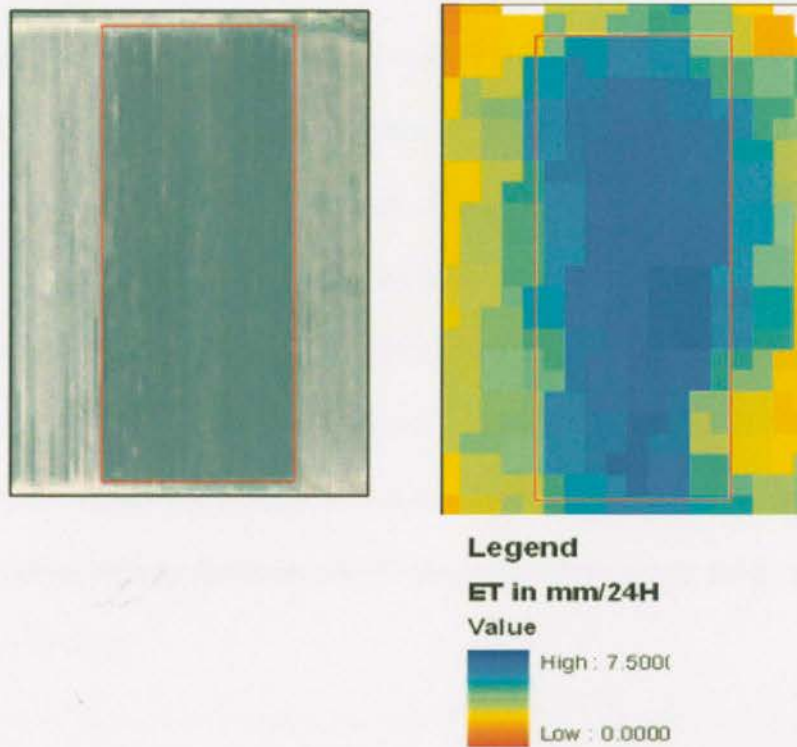


Figure 39. Plan view and soil salinity distribution in field 23

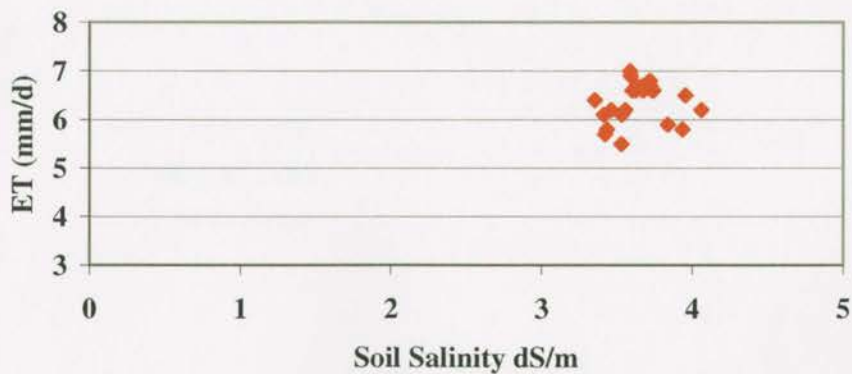


Figure 40. Soil salinity versus ET for field 23

Combined fields

To show the consistency of the relation between the soil salinity and ET in corn fields a combined graph was generated that contains two sets of points. The first set are points representing the relation between one grid (pixel) from the ET grid to the

georeferenced measured soil salinity point(s) that fall within that grid in field 80. The second set of points represents the relation between the average value of soil salinity points in one field and the average ET for the same field. The second set of points was created to show the relation between ET and soil salinity in the fields for which there are non-georeferenced soil salinity points. Due to the presence of non-georeferenced soil salinity points, the values of the soil salinity points and ET grid cells for each field were averaged to come up with one value of ET and soil salinity for each field. The results are presented in figure 41 and show that there is consistency in the two sets of points. This supports the idea that as salinity increases the ET decreases at the single point or as an average for the whole field.

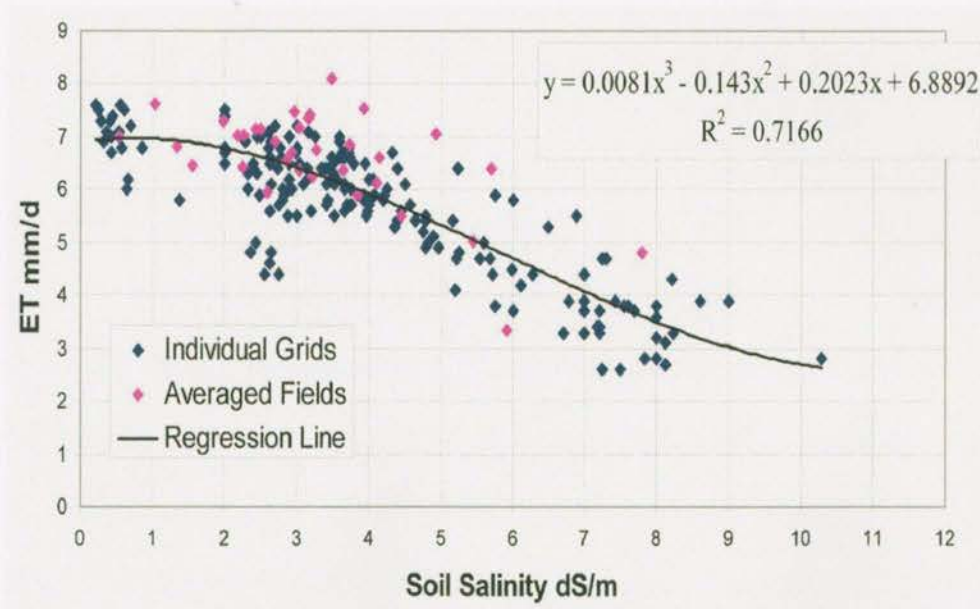


Figure 41. Soil salinity versus ET for individual grids as well as for whole fields

4.5 CONCLUSIONS

Evapotranspiration (ET) was used successfully as an indicator of soil salinity in corn fields. Strong correlation between ET and soil salinity was found in the corn fields

that have a wide variation of soil salinity levels. These correlations were used successfully in both detecting soil salinity levels as well as estimating the decline in the amount of ET caused by high soil salinity levels. However, the fields with soil salinity levels below the level at which the soil salinity starts to impact the crop's growth did not show a good correlation between ET and soil salinity as expected. If the soil salinity does not reach the level that hinders water uptake by the plant then ET will not be affected. These results show the potential for using this methodology to both detect levels of soil salinity in an area, if the crop type is known, as well as to help determine the impact that soil salinity has on the amount of ET when soil salinity is present.

5. SUMMARY AND CONCLUSIONS

5.1 SUMMARY OF WORK

Integrating remote sensing and geographic information systems techniques in agricultural applications is becoming more common. In this research a methodology was developed that maps soil salinity in agricultural areas producing several land cover classifications covering the whole spectrum of soil salinity levels. The methodology that was developed uses ground data in combination with satellite imagery to create soil salinity indices which relate ranges of reflectance in the satellite image to ranges in soil salinity, these indices are then used to predict soil salinity in other fields without the need to collect ground data. Validation of this methodology was done by comparing the predicted soil salinity values to ground data, the maximum error in predicting soil salinity levels was 10%. The larger detection errors fall in areas where salinity is known to be very high and therefore there is little vegetation which was used as the indicator for mapping soil salinity, the use of this methodology to map soil salinity has proven to be very efficient, saving significant field work and providing accurate salinity maps for large areas.

Evapotranspiration is another important factor in agriculture which is directly related to crop yield, models for remotely measuring evapotranspiration have been in use for some time, as part of this research a surface energy balance model was developed (ReSET), the ReSET model uses the Landsat 7 and Landsat 5 imagery for estimating

evapotranspiration from plants, the model was applied and validated in two locations in Colorado. ReSET is an enhanced ET estimation model that takes into consideration the spatial variability in weather parameters to enhance its applicability for regional scale use; RESET generates grid surfaces of wind run between available weather stations in time and space in order to merge the point data (weather stations) with the satellite scenes.

Evapotranspiration can be used as an indicator for the existence and severity of soil salinity. Using the ReSET model evapotranspiration maps were developed for selected fields on which soil salinity data had been collected, combining the soil salinity levels and the corresponding evapotranspiration data, several regressions were generated which demonstrate the relation between evapotranspiration and the soil salinity.

5.2 UNIQUE CONTRIBUTIONS

The primary contributions of this research are three-fold:

- (1) Using vegetation indices in mapping soil salinity: Many methodologies were previously developed for mapping soil salinity using satellite imagery, the majority of these methodologies target bare soil as an indicator for soil salinity and therefore they were not able to produce enough reflectance classes to cover the whole spectrum of soil salinity. The methodology developed as part of this research uses crop condition as an indicator of the existence and severity of soil salinity and it produced a large number of classes (9 classes for Landsat, and 16 classes for Ikonos) and therefore allowed for more accurate soil salinity maps to be generated.

(2) Develop an enhanced surface energy balance based model (ReSET) :

The first enhancement that was introduced in this model was using multiple weather stations for obtaining ground data needed to run and calibrate the model (wind run for running the model and ET for calibrating and validating the model), previously developed models mainly used ground data from one weather station. The second enhancement to the model is the calculation of the cumulative ET between the available scenes; since the actual ET is only calculated at best every 16 days (an most often less frequently than this) there is a need to estimate the ET for every day in the period between the scenes dates, the technique used in ReSET enhances the accuracy in interpolation in both space and time. In ReSET the temporal interpolation is done by calculating the ET difference ratio at the beginning and the end of the interpolation period, the ET from weather stations is calculated for all days for all weather stations in the study area as a layer that represents ET for each day. A variable correction ratio is calculated in the study area for each cell each day between scene dates, this correction takes into account the spatial and temporal variability of all the available weather station information.

(3) Using a surface energy model in demonstrating the impact of soil salinity on ET:

No study has used remote sensing to develop a relationship between soil salinity and ET. In this study remote sensing and GIS techniques were used to investigate the relation between soil salinity and ET in agricultural lands. ET was used successfully as an indicator of soil salinity in field planted with corn. A strong correlation between ET and soil salinity was found in fields planted with corn with a wide range of soil salinity levels. These correlations were used successfully in both detecting soil salinity levels in

fields planted with corn as well as estimating the decline in the amount of ET caused by high soil salinity levels.

6. RECOMENDATIONS FOR FURTHER WORK

6.1 DETECTING SOIL SALINITY

Detecting soil salinity can be enhanced by using higher spatial resolution satellite imagery. Using higher spatial resolution results in being able to more accurately delineate the cultivated areas and reduce the noise around the boundaries caused by roads and fallow areas, also high resolution imagery will yield more data to be used for estimating soil salinity. When using high resolution imagery, ground data should be collected on similar high resolution scale to match the imagery used, meaning that if imagery with resolution of 1 m by 1 m is used a point for each pixel should be collected to maximize the benefit of the higher resolution. The ground data collected should be geo-referenced using high accuracy GPS to minimize location errors.

6.2 RESET MODEL

The ReSET model can be modified to use different types of imagery other than Landsat 5 and Landsat 7, such as MODIS or ASTER which might be appropriate for certain applications. Since the theoretical basis of the ReSET model is the same as that of SEBAL it is expected that the accuracy of the ReSET model will be similar to SEBAL that was validated previously through several approaches by Bastiaanssen (1998a, 1998b). However, it would be a valuable contribution to compare the ET estimated by ReSET to actual ET measured using Lysimeters to ensure the accuracy of the ET

estimates. Seasonal ET can be validated through a detailed water balance for selected fields, this would be a valuable way to verify the seasonal ET estimates calculated by ReSET and will help to decide on the appropriate number of scenes to use for estimating the cumulative ET for a specific period of time.

6.3 SOIL SALINITY AND ET

Using evapotranspiration as an indicator for the levels of soil salinity is a new and unique approach that can be enhanced if more ground data is collected and additional research is conducted. Specifically it would be valuable to extend the application to other crops such as alfalfa and sorghum. More fields should be extensively surveyed for soil salinity using high accuracy GPS and continued soil salinity measurements to collect more data points per pixel to ensure that all the details on the ground are being captured in the survey and are located in the correct position which will lead to the development of enhanced relationships between soil salinity and evapotranspiration. By accumulating data collected for each crop from several regions, the relations between soil salinity and ET can be evaluated and if necessary individual relationships can be developed for each region, which can be used to enhance irrigation management in these regions.

7. REFERENCES

1. Abernethy, C. L., and G. R. Pearce. (1987). *Research Needs in Third World Irrigation*. Wallingford, England: Hydraulics Research Limited.
2. Abdel-Hamid, M. A. (1992). Detection of Saline Soils with Landsat Thematic Mapper, Multispectral Data from Bare and Vegetated Areas. Vol. 32, No.2, pp.307-318. Soil Science Department, Faculty of Agriculture, Cairo University Cairo, Egypt.
3. Abuzar, M., A. Mcallister, and M. Morris. (2001). Classification of seasonal images for monitoring irrigated crops in a salinity-affected area of Australia. *International Journal of Remote Sensing* 22(5): 717-726.
4. Allen, R. G., M. Tasumi, A. Morse, and R. Trezza. (2005). A Landsat-based energy balance and evapotranspiration model in western U.S. water rights regulation and planning. *Irrigation and Drainage Systems* 19(3-4): 251-268.
5. Allen et al., 1998 Allen, R.G., Pereira, L.S., Raes, D., Smith, M., (1998). Crop evapotranspiration. Guidelines for computing crop water requirements. FAO Irrigation Drainage Paper no. 56, FAO, Rome, Italy, 300 pp.
6. Ayers, R.S. and Westcot, D.W., (1985). Water Quality for Agriculture. FAO Irrigation and Drainage Paper 29 rev. 1, Rome, 174 pp

7. Bastiaanssen, W.G.M., M. Menenti, R.A. Feddes, A.A.M. Holtslag. (1998a). Remote sensing surface energy balance algorithm for land (SEBAL): 1. Formulation. *Journal of Hydrology* 212-213(1-4): 198-212.
8. Bastiaanssen, W.G.M., H. Pelgrum, J. Wang, Y. Ma, J.F. Moreno, G.J. Roerink, and T. van der Wal. (1998b). Remote sensing surface energy balance algorithm for land (SEBAL): 2. Validation. *Journal of Hydrology* 212-213(1-4) 213-229.
9. Bastiaanssen, W.G.M. (2000). SEBAL based sensible and latent heat fluxes in the irrigated Gedez Basin, Turkey. *Journal of Hydrology* 229(1-2):87-100.
10. Bastiaanssen, W.G.M.; M.U.D. Ahmad, Y. Chemin. (2002). Satellite surveillance of evaporative depletion across the Indus Basin. *Water Resources Research* 38(12): 91-99.
11. Cardon G.E., and J. Letey. (1992a) Evaluation of plant water uptake terms in soil-based models of water and solute movement. *Soil Sci Soc Am J.* 32:1876–1880.
12. Cardon G.E., and J. Letey. (1992b) A soil-based model for irrigation and soil salinity management. I. Tests of plant water uptake calculations. *Soil Sci Soc Am J.* 56:1881-1887.
13. Cardon G.E., and J. Letey. (1992c) A soil-based model for irrigation and soil salinity management. II. Test of water and solute movement calculations. *Soil Sci Soc Am J.* 56:1887-1892.
14. Csillag, F., L. Pasztor, and L.L. Biehl. (1993). Spectral band selection for the characterization of salinity status of soils. *Remote Sensing of Environment* 43(3) 231- 242.

15. Doorenbos, J. and Kassam, A.H. (1979). Yield response to water. FAO Irrigation and Drainage Paper 33, Rome, 193 pp.
16. Draeger, W. C. (1976). Monitoring irrigated level acreage using Landsat imagery: An application example .U.S. Geological Survey Open–File Report No.76-630. Sioux Falls, South Dakota.
17. Dwivedi, R.S. and Sreenivas, K. (1998). Delineation of salt-affected soils and waterlogged areas in the Indo-Gangetic Plains using IRS-1C LISS-111 data. *International Journal of Remote Sensing*. 19(14) 2739-2751.
18. Eldeiry, A. 2006. Spatil Modeling of Soil Salinity Using Remot Sensing, GIS, and Field Data. Ph.D. Dissertation. Colorado State University, Fort Collins.
19. Evans, F.H., P.A. Caccetta, R. Ferdowsian, H.T. Kiiveri, and N.A. Campbell. (1995). Predicting salinity in the Upper Kent River Catchment. *Report to LWRRDC*. Department of Agriculture Western Australia. Available at: <http://www.cmis.csiro.au/RSM/research/kent.pdf>.
20. Everitt, J.H., A.H. Gerbermann, and J.A. Cuellar. (1977). Distinguishing saline from non-saline rangelands with Skylab imagery. *Photogrammetric Engineering and Remote Sensing* 43(8) 1041-1047.
21. Ferdowsian, R. and K.J. Greenham. (1992). Integrated catchment management: Upper Denmark Catchment. Department of Agriculture Western Australia Technical Report 130.
22. Gates, T.K., J.P. Burkhalter, J.W. Labadie, J.C. Valient, and I. Broner, (2002). Monitoring and modeling flow and salt transport in a salinity-threatened irrigated valley. *Journal of Irrigation and Drainage Engineering*, 128(2): 87-99.

23. Gates, T.K, L.A. Garcia, and J.W. Labadie (2006). "Toward Optimal Water Management in Colorado's Lower Arkansas River Valley: Monitoring and Modeling to Enhance Agriculture & Environment". Colorado Agricultural Experiment Station, Technical Report TR-6-10.
24. Ghabour, T. K. and L. Daels. (1993). Mapping and monitoring of soil salinity of ISSN. *Egyptian Journal of Soil Science* 33(4) 355-370.
25. Harrison, L. P. (1963). Fundamental concepts and definitions relating to humidity. In: *Humidity and moisture. Vol. 3.*, Wexler, A., ed. New York, N.Y.: Reinhold Publishing Company.
26. Huston, D. M., and S. J. Titus. (1975). *An inventory of irrigated lands within the State of California based on lands and supporting aircraft data.* Space Sciences Laboratory Series, vol. 16 no. 56. Berkeley, California: University of California.
27. Integrated Decision Support Group. (2004). IDS Consumptive Use Model Version 3.1.1 User Manual. Fort Collins, C.O.: Colorado State University, Department of Civil and Environmental Engineering, Integrated Decision Support Group.
28. Joshi, M. D., and B. Sahai. (1993). Mapping of salt affected soils in Saurashtra Coast using Landsat satellite data. *International Journal of Remote Sensing* 14 (10): 1919- 1929.
29. Karale R. L. and K. Venugopal. (1970). Soil Survey of Ganges Plain in Meerut, Project Report, Indian Institute of Photointerpretation and Remote Sensing (Indian Institute of Remote Sensing). National Remote Sensing Agency, Hyderabad.

30. Kimes, D.S. and J. A. Kirchner. (1983). Diurnal-variations of vegetation canopy structure. *International Journal of Remote Sensing* 4(2): 257-271.
31. Kustas W. P., and J.M. Norman. (1996). Use of remote sensing for evapotranspiration monitoring over land surfaces. *Hydrological Sciences Journal-Journal des sciences hydrologiques* 41(4): 495-516.
32. Kustas W.P., and J.M. Norman. (1999). Evaluation of soil and vegetation heat flux predictions using a simple two-source model with radiometric temperatures for partial canopy cover. *Agricultural and Forest Meteorology* (1): 13-29.
33. Massoud, F. I. (1977) "The use of satellite Imagery in detecting and delineating salt- affected soils" *Pedologie Teledetection AISS_ISSS*, Rome.
34. Massoud, F. L., (1977) Basic principal for prognosis and monitoring of salinity and sodicity. *Proceedings of the International Conference on Managing Saline Waters, for Irrigation*, Texas Technical University Lubbock, Texas, pp. 432-454.
35. Mongkolsawat, C. and Thirangoon, P. (1990). A Practical Application of Remote Sensing and GIS for Soil Salinity Potential Mapping in Korat Basin, Northeast Thailand, Technical Report Series No. 8, Remote Sensing and Water Management in Northeast Thailand, Khonkaen. pp.290-297.
36. Myers, V. I., D. L. Carter, and W. J. Rippert, W.J. (1966). Remote sensing for estimating soil salinity. *Journal of the Irrigation and Drainage Division, ASCE* 92:59.
37. Nagar, S. C. and Singh, D. (1979). Semi-detailed Soil Survey of Part of District Hardoi, Uttar Pradesh, Project Report Indian Photo-interpretation Institute (Indian Institute of Remote Sensing). National Remote Sensing Agency,

Hyderabad.

38. Nagler, P.L., R.L. Scott, and C. Westenburg, J.R. Cleverly, E.P. Glenn, and A.R. Huete. (2005). Evapotranspiration on western U.S. rivers estimated using the Enhanced Vegetation Index from MODIS and data from eddy covariance and Bowen ratio flux towers. *Remote Sensing of Environment* (3): 337-351.
39. Nishida, K., R.R. Nemani, J.M. Glassy, and S.W. Running. (2003). Development of an evapotranspiration index from Aqua/MODIS for monitoring surface moisture status. *IEEE Transactions on Geoscience and Remote Sensing* 41(2): 493-501.
40. Peng, W. L. (1998). Synthetic analysis for extracting information on soil salinity using remote sensing and GIS: A case study of Yanggo Basin in China. *Environmental Management* 22(1): 153-159.
41. Rahman, S., G. F. Vance, and L. C. Munn. (1994). Detecting salinity and soil nutrient deficiencies using SPOT satellite data. *Soil Science* 158(1): 31-39.
42. Rao, B. R. M., T. R. Sankar, R. S. Dwivedi, S. S. Thammappa, L. Venkataratnam, R. C. Sharma, and S. N. Das. (1995). Spectral behavior of salt-affected soils. *International Journal of Remote Sensing* 16(12): 2125-2136.
43. Richards, L. A., editor (1954). *Diagnosis and Improvement of Saline and Alkali Soils*. US Department of Agriculture, Agricultural handbook No 60. US Government Printing Office, Washington DC, USA.
44. Ripple, W. J., B. J. Schrumph, and D. L. Isaacson. (1986). The influence of observational interdependence on spectral reflectance relationship with plant and soil variables. *International Journal of Remote Sensing* 7(2): 291-294.

45. Roerink G.J., Z. Su, and M. Menenti. (2000). S-SEBI: A simple remote sensing algorithm to estimate the surface energy balance. *Physics and Chemistry of the Earth Part B: Hydrology Oceans and Atmosphere* 25(2): 147-157.
46. Samani, Z., R. Skaggs, and M. Bleweiss. (2005). "Regional ET estimation from satellites." 31st International Symposium on Remote Sensing from Satellite, June 20-24, St. Petersburg, Russia.
47. Savige, C., Western, A., Walker, J. P., Kalma, J. D., French, A. and Abuzar, M., (2005). Obtaining Surface Energy Fluxes from Remotely Sensed Data. In A. Zerger and R. M. Argent (Eds), MODSIM 2005 International Congress on Modelling and Simulation. Modelling and Simulation Society of Australia and New Zealand, December 2005, 2946-2952.
48. Serageldin, I. (1995). Water resources management: A new policy for a sustainable future. *Water International* 20(1): 15-21.
49. Su, Z. (2002). The Surface Energy Balance System (SEBS) for estimation of turbulent heat fluxes. *Hydrology and Earth System Sciences* 6(1): 85-99.
50. Steven, M. D. (1993). Satellite remote sensing for agricultural management: Opportunities and Logistic constraints. *Photogrammetry and Remote sensing* 48(4): 29-34.
51. Szabolcs, I. (1992) Salinization of soil and water and its relation to desertification. *Desertification Control Bulletin*, No.21, pp.32-37
52. Tasumi M., R.G. Allen, R. Trezza and J.L. Wright. (2005). Satellite-based energy balance to assess with in-population variance of crop coefficient curves. *Journal of Irrigation and Drainage Engineering-ASCE* 131(1): 94-109.

53. Thiruvengadachari, S. (1981). Satellite sensing of irrigation patterns in semiarid areas: An Indian study. *Photogrammetric Engineering and Remote Sensing* 47(10): 1493-1499.
54. Thiruvengadachari, S. (1996). Use of satellite remote sensing in irrigation system management. In Symposium on Management Information Systems in Irrigation and Drainage: Sixteen Congress on Irrigation and Drainage. New Delhi: International commission on Irrigation and Drainage.
55. Thomas, J. R., and C. L. Wiegand. (1970). Osmotic and matric suction effects on relative turgidity, temperature and the growth of cotton leaves. *Soil Science* 109(2): 85-92.
56. Timmermans, W.J., A.S.M. Gieske, W.P. Kustas, P. Wolski, A. Arneeth and G.N. Parodi. (2004). "Determination of water and heat fluxes with MODIS imagery: Maun, Botswana." Proc. of the SPIE conference: 10th International remote sensing meeting: Remote sensing for agriculture, ecosystems, and hydrology: 8-12 September 2003 Barcelona. / ed by. V. Manfred Owe, Guido D'Urso, Jose F. Moreno, Alfonso Calera. SPIE, p. 444-455.
57. Wall, S. L., (1979). California's irrigated lands. Paper presented at the Symposium on Identifying Irrigated Lands Using Remote Sensing Techniques: State of the Art, Nov. 15-16 1979 at U.S. Geological Survey EROS Data Center, Sioux Falls, South Dakota, USA.
58. Wiegand, C. L., and A. J. Richardson (1990). Use of spectral vegetation indices to infer leaf area evapotranspiration and yield: I. Rationale. *Agronomy Journal* 82(3): 623- 629.